UNIVERSITA' VITA-SALUTE SAN RAFFAELE

CORSO DI DOTTORATO DI RICERCA INTERNAZIONALE

IN MEDICINA MOLECOLARE

CURRICULUM IN GENE AND CELL THERAPY

INTRACELLULAR IRON OVERLOAD AFFECTS HSC METABOLISM BY IMPAIRING MITOCHONDRIAL FITNESS IN β-THALASSEMIA

DoS: Prof. Giuliana Ferrari

Second Supervisor: Prof. Cristina Lo Celso

Tesi di DOTTORATO DI RICERCA di Silvia Sighinolfi

Matr. 015521

Ciclo di dottorato XXXV

SSD BIO/13

Anno Accademico 2021/2022

UNIVERSITA' VITA-SALUTE SAN RAFFAELE

CORSO DI DOTTORATO DI RICERCA INTERNAZIONALE
IN MEDICINA MOLECOLARE

CURRICULUM IN GENE AND CELL THERAPY

INTRACELLULAR IRON OVERLOAD AFFECTS HSC METABOLISM BY IMPAIRING MITOCHONDRIAL FITNESS IN β-THALASSEMIA

DoS: Prof. Giuliana Ferrari

Second Supervisor: Prof. Cristina Lo Celso

Tesi di DOTTORATO DI RICERCA di Silvia Sighinolfi

Matr. 015521

Ciclo di dottorato XXXV

SSD BIO/13

Anno Accademico 2021/2022

I	Silvia Sighinolfi
Registration number	015521
Born at	Vignola
On	01/12/1994

Author of the PhD Thesis titled:

INTRACELLULAR IRON OVERLOAD AFFECTS HSC METABOLISM BY IMPAIRING MITOCHONDRIAL FITNESS IN β-THALASSEMIA

☐AUTHORIZES the public release of the thesis

☒DOES NOT AUTHORIZE the public release of the thesis for 36 months

From the PhD thesis date, specifically

From 01/12/2022 To 01/12/2025

Because:

☐The whole project or part of it might be subject to patentability;

☒Parts of the thesis have been or are being submitted to a publisher or are in press;

☐The thesis project is financed by external bodies that have rights over it and on its publication.

Copyright the contents of the thesis in whole or in part is forbidden

Date Signature

28/10/22 Silvia Sighinolfi

DECLARATION

This thesis has been:

- composed by myself and has not been used in any previous application for a degree. Throughout the text I use both "I" and "We" interchangeably.
- has been written according to the editing guidelines approved by the University.

Permission to use images and other material covered by copyright has been sought and obtained. For the following images (Introduction, figures 1 and 10), it was not possible to obtain permission and are therefore included in thesis under the "fair use" exception (Italian legislative Decree no. 68/2003).

All the results presented here were obtained by myself, except for:

1. RNAseq data (Results, chapter 1, figure 1 B-C, figure 3A; chapter 2, figure 5; chapter 3, figure 9A; chapter 4 figure 10) were obtained by Annamaria Aprile, Project Leader, Gene Transfer into stem cells Unit, TIGET, Milan, Italy in collaboration with Ivan Merelli, PhD, and Stefano Beretta, PhD, from the SR-TIGET Bioinformatic Core, TIGET, Milan, Italy.

2. Transmission Electron Microscopy (TEM) specimens (Results, chapter 2, figure 6B) were processed by Dr. Mariacarla Panzeri, Alembic, Experimental Imaging Centre, San Raffaele Scientific Institute, Milan, Italy.

3. Formalin-Fixed Paraffin-Embedded (FFPE) specimens (Results, chapter 6, figure 18-19A) were processed by Dr Amleto Fiocchi, Animal Histopathology Facility, San Raffaele Scientific Institute, Milan, Italy.

All sources of information are acknowledged by means of reference.

Parts of the chapter 3.1, introduction have been published in: https://pubmed.ncbi.nlm.nih.gov/35631417/

Where specified in Figure legends, graphical elements from Biorender are used and acknowledged as per license of Ospedale San Raffaele – SR Tiget's Plan active at the time of submission.

ABSTRACT

Mitochondrial activity and metabolism significantly control hematopoietic stem cell (HSC) function and fate. HSCs change the metabolic state in response to stress signals, such as reactive oxygen species (ROS), which drive HSC entry into cell cycle accompanied by increased mitochondrial oxidative phosphorylation (OXPHOS) and glycolysis. However, excessive accumulation of ROS results in oxidative damage of cellular organelles, including mitochondria. Iron is one of the sources of ROS and HSCs can uptake iron but little is known about the effects of iron on HSC metabolism.

Recently, we demonstrated an impaired function of HSCs in β-Thalassemia (BThal), a condition of systemic iron overload (IO). We also observed that IO reduces the hematopoietic supportive capacity of BThal BM mesenchymal stromal cells. However, there is no evidence of the direct effect of IO on HSCs in BThal. We hypothesized that IO and the resulting oxidative stress could alter HSC metabolism and function.

We found a positive enrichment of iron homeostasis genes in HSCs from thalassemic *th3* mice, suggesting increased iron uptake and storage. Consistently, we detected high levels of free reactive iron in the cytoplasm and in mitochondria of *th3* HSCs, correlating with high ROS levels. As a result, mitochondria are impaired, with low mass and activity. Interestingly, *th3* multipotent progenitors inherited dysfunctional mitochondria since the rescue of mitochondrial activity occurred in the transition to more committed progenitors. In line with mitochondrial dysfunction, *th3* HSCs had reduced OXPHOS-derived ATP and relied on glycolysis. *In vivo* reduction of mitochondrial ROS rescued mitochondrial activity and metabolism, and increased *th3* HSC frequency and quiescence, thus indicating that oxidative stress is the cause of mitochondrial dysfunction and potentially HSC defects. Importantly, *in vivo* administration of iron dextran to wt mice generated intracellular IO and mitochondrial oxidative stress and decreased mitochondrial activity in HSCs, indicating that IO alone is sufficient to impair mitochondria.

Our study unveils that IO directly impacts on HSC metabolism by inducing oxidative stress and mitochondrial dysfunction. Alterations in mitochondrial activity and metabolic profile, in response to IO, are expected to alter HSC function. This research will add novel insight about the role of iron in regulating HSC metabolism and provide clues for improving clinical conditions associated to IO, such as BThal.

TABLE OF CONTENTS

ACRONYMS AND ABBREVIATIONS

2NBDG = 2-[N-(7-nitrobenz-2-oxa-1,3-diazol-4-yl)amino]-2-deoxy-D-glucose
Acetyl-CoA = acetyl coenzyme A
AECs = arteriolar endothelial cells
ALL = acute lymphoblastic leukemia
ALT = alanine aminotransferase
ANGPT1= angiopoietin 1
AST = aspartate aminotransferase
ATM = ataxia telangiectasia mutated
BM = bone marrow
BMD = bone mineral density
BP = biological process
BThal = β-thalassemia
CAR = CXCL12-abundant reticular
Cat = catalase
CFU-Fs = colony-forming unit fibroblasts
CLPs = common lymphoid progenitors
CMPs = common myeloid progenitors
CRISPR = clustered regularly interspaced short palindromic repeat
Cx43 = connexin-43
CXCL12 = C-X-C motif chemokine ligand 12
DAMPs = damaged-associated molecular patterns
ddPCR = droplet digital PCR
DEG = differentially expressed genes
DFO = deferoxamine
DFP = defiprone
DFX = deferasirox
Drp1 = dynamin-related protein 1
ECs = endothelial cells
EPO = erythropoietin
ERFE = erythroferrone
ETC = electron transport chain
$FADH_2$ = flavin adenine dinucleotide
FAO = fatty acid oxidation
Fe^{2+} = ferrous iron
Fe^{3+} = ferric iron
FeAS = ferrous ammonium sulfate
Fe-S = iron sulphur
FGF1 = fibroblast growth factor 1
FPN = ferroportin
FT = ferritin
Fth1 = ferritin heavy chain 1 gene
Ftl1 = ferritin light chain 1 gene
Gapdh = glyceraldehyde-3-phosphate dehydrogenase
GO = gene ontology
Gpx = glutathione peroxidase
GSEA = gene set enrichment analysis

Gsr = glutathione reductase
GVHD = graft-versus-host-disease
H^+ = proton
H_2O_2 = hydrogen peroxide
Hb = hemoglobin
HCT = hematocrit
HIF1α = hypoxia-inducible factor 1 alpha
Hmox1 = heme oxygenase 1 gene
HSCs = hematopoietic stem cells
HSCT = hematopoietic stem cell transplantation
HSPC = hematopoietic stem and progenitor cell
ICT = iron chelation therapy
IE = ineffective erythropoiesis
IFNs = interferons
IL-7 = interleukin 7
IMM = inner mitochondria membrane
IO = iron overload
IRE = iron responsive element
IRP = iron regulatory protein
ko = knock-out
LCR = locus control region
LDH = lactate dehydrogenase
LEPR = leptin receptor
LIC = liver iron concentration
Lin^- = lineage negative cells
LIP = labile iron pool
MAPK = mitogen-activated protein kinase
MFI = mean fluorescent intensity
MKs = megakaryocytes
MMP = mitochondrial membrane potential
MPPs = multipotent progenitors
MRI = magnetic resonance imaging
MSCs = mesenchymal stromal cells
MTG = mitotracker-green
mTOR = mammalian target of rapamycin
mtROS= mitochondrial reactive oxygen species
Mφs = macrophages
NADH = nicotinamide adenine dinucleotide
NOX = NADPH oxidase
NTBI = non transferrin-bound iron
NTDT = non transfusion-dependent thalassemia
O_2 = molecular oxygen
O_2^- = superoxide anion
OBs = osteoblasts
OC = osteoclast
OH^- = hydroxyl radical
OMMs = mitochondrial outer membranes
OPN = osteopontin

OXPHOS = oxidative phosphorylation
PAMPs = pathogen-associated molecular patterns
PDH = pyruvate dehydrogenase
PDKs = pyruvate dehydrogenase kinases
PK/Pklr = pyruvate kinase
pO_2 = partial pressure of oxygen
Prdx = peroxiredoxins
PRRs = pattern recognition receptors
PS = phosphatidylserine
PTH = parathyroid hormone
PαS = PDGFRα$^+$ Sca1$^+$
RBCs = red blood cells
RNAseq = RNA sequencing
ROS = reactive oxygen species
RT = reverse-transcription
SCD = sickle cell disease
SCF = stem cell factor
scRNAseq = single cell RNA sequencing
SECs = sinusoidal endothelial cells
SIC = serum iron concentration
Slc40a1 = ferroportin gene
SNS = sympathetic nervous system
SOD = superoxide dismutase
TCA = tricarboxylic acid cycle
TDT = transfusion-dependent thalassemia
TEM = transmission electron microscopy
TF = transferrin
TFR1 or TFRC = transferrin receptor 1
Th3 = Hbb$^{th3/+}$ thalassemic mice
TMRE = tetramethylrhodamine ethyl ester
TMRM = tetramethylrhodamine methyl ester
TNFs = tumor necrosis factors
Tpi1 = triosephosphate isomerase 1
TPO = thrombopoietin
Tregs = regulatory T cells
Txn = thioredoxin
UMI = unique molecular identifiers
UTR = untranslated region
Wt = wild-type
ZFNs = zinc finger nucleases

LIST OF FIGURES AND TABLES

INTRODUCTION

1 – Hematopoietic Stem Cell

The blood system is one of the most regenerative tissues in mammals, with billions of cells arising daily in adults. Given that mature blood cells are short-lived, a restricted pool of HSCs continuously sustains blood-cell formation throughout lifetime. This is achieved by the capacity of HSCs to self-renew, which is the ability to regenerate themselves long-term, and differentiate, giving rise to progenitor cells that in turn proliferate and differentiate into mature blood cells (Laurenti & Gottgens, 2018). At steady state, adult HSCs are maintained quiescent in the BM and divide rarely to maintain blood homeostasis avoiding the exhaustion of the stem cell pool. However, they can reversibly exit from dormancy after exposure to stressors, such as oxidative stress and inflammatory signals, to replenish the hematopoietic system.

HSCs are functionally defined by their ability to reconstitute long-term the entire blood system in lethally irradiated mice (Notta *et al*, 2011) . On the contrary, progenitors have low self-renewal capacity, restricted lineage differentiation potential and fail to engraft long-term after transplantation.

Historically, hematopoiesis was thought to be a stepwise process, in which HSCs, at the apex of hematopoietic hierarchy, progressively lose their self-renewal ability and acquire lineage-specific potential (Akashi *et al*, 2000). According to this classical model, HSCs directly differentiate into multipotent progenitors (MMPs), which in turn give rise to common myeloid progenitors (CMPs) or common lymphoid progenitors (CLPs). The earliest myelo-lymphoid split is followed by further branching steps, progressively moving from multi- to unipotent progenitor cells.

However, recently single-cell RNA sequencing and *in vivo* cell tracking challenged this classical hierarchy roadmap, showing HSC heterogeneity in terms of molecular signature, metabolism and lineage differentiation output. The discovery of lineage-biased HSCs (Beerman *et al*, 2010; Dykstra *et al*, 2007; Gekas & Graf, 2013; Sanjuan-Pla *et al*, 2013) and distinct subpopulations of MPPs (Pietras *et al*, 2015) pointed out that lineage segregation occurs at early stage during hematopoiesis. The differentiation is a continuous process, during which some lineage-specific genes, already expressed in primitive HSCs,

are suppressed whereas others are activated concurrently (Fig. 1) (Laurenti & Gottgens, 2018).

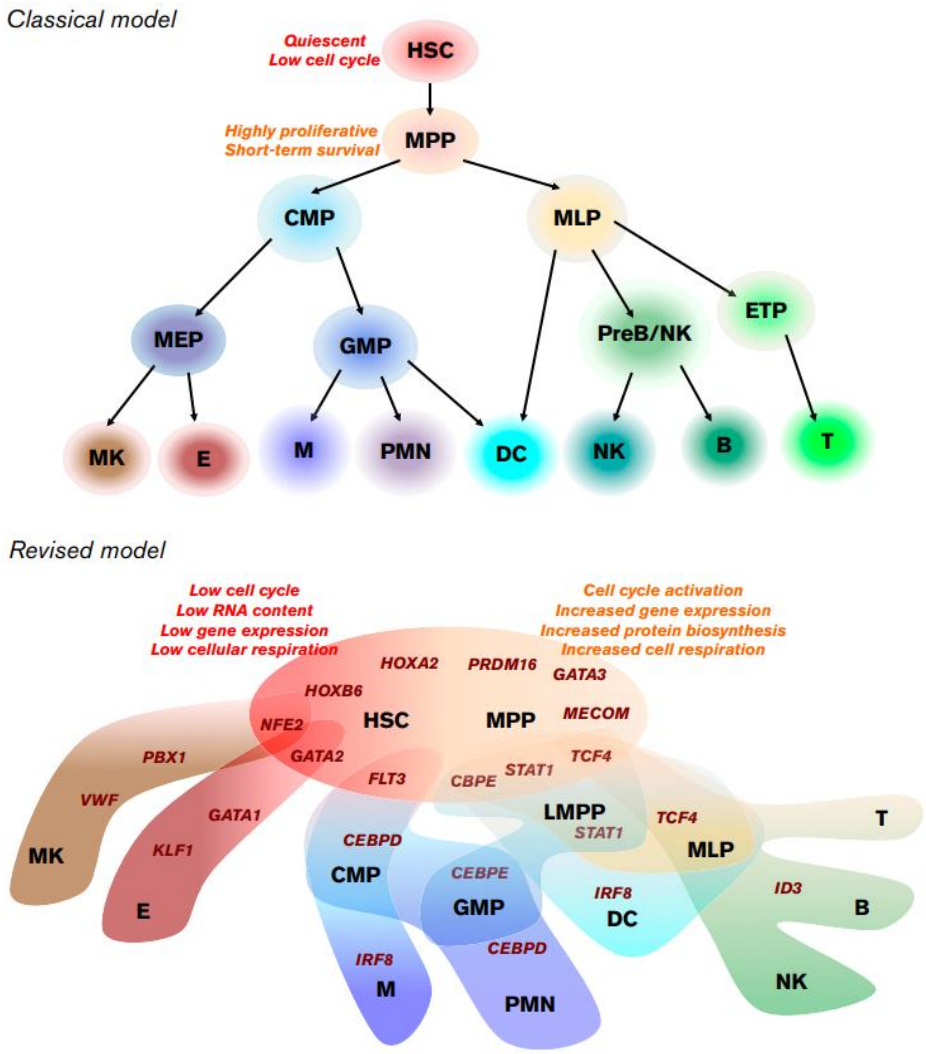

Figure 1. Models of hematopoiesis. *The classical hierarchical model (at the top) vs the new model (at the bottom) proposing hematopoiesis as a continuous process (From Scala & Aiuti, 2019).*

Murine HSCs are phenotypically defined as Lin^{-} $ckit^{+}$ $Sca1^{+}$ $CD48^{-}$ $CD150^{+}$, whereas murine MPPs are Lin^{-} $ckit^{+}$ $Sca1^{+}$ $CD48^{-}$ $CD150^{-}$ (Oguro *et al*, 2013).
Human HSCs are phenotypically defined as Lin^{-} $CD34^{+}$ $CD38^{-}$ $CD45RA^{-}$ $Thy1^{+}$ Rho^{lo} $CD49f^{+}$, whereas human MPPs are Lin^{-} $CD34^{+}$ $CD38^{-}$ $CD45RA^{-}$ $Thy1^{-}$ Rho^{lo} $CD49f^{-}$ (Notta *et al*., 2011).

Adult HSCs reside in a specialized microenvironment in the BM, termed niche. The HSC niche is a complex local microenvironment that directly maintains and regulates

HSC self-renewal, proliferation and differentiation, thus ensuring hematopoietic homeostasis (Morrison & Scadden, 2014). HSC behaviour is governed by the complex interaction with different cellular component of the BM niche, soluble factors and physical cues (Pinho & Frenette, 2019).

The BM is encased in the central cavities of long and axial bones. The periosteum covers the outer surface of the bone, whereas the endosteum lining the inner surface of the bone cavities is at the interface between bone and BM. Numerous blood vessels enter the BM to enable efficient delivery of nutrients, oxygen and growth factors, while allowing the removal of waste products. Arteries carrying oxygenated blood branch to give rise to small, thin-walled arterioles, that preferentially localize close to the endosteum. On the contrary, sinusoids carrying deoxygenated blood are distributed through the BM cavity (Fig. 2).

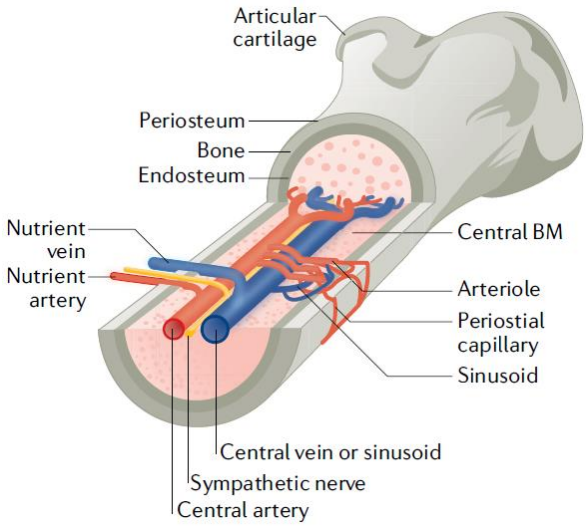

Figure 2. Microarchitecture of murine BM in the femur. *The periosteum surrounds the outer surface of the bone, whereas the endosteum encloses the BM. Arterioles (in red) and sinusoids (in blue) form a dense network, allowing the transport of nutrients and the removal of waste products. Sympathetic nerves (in yellow) wrap arterioles forming the "neuro-reticular complex" (From Pinho & Frenette, 2019).*

High-resolution imaging studies in mouse BM revealed that HSC niche includes endosteal niches, near the bone surface, and perivascular niches, that can be further divided, on the basis of the proximity to arterioles or sinusoids, into arteriolar and sinusoidal respectively (Adams & Scadden, 2006). However, histologic analysis cannot resolve the position of HSCs over time. Recently, *in vivo* time-lapse imaging showed that the most quiescent HSCs reside close to both sinusoids and endosteum, whereas activated

HSCs become more motile, moving away from the endosteum. In particular, active HSCs were found in a subset of BM cavities with high bone-remodelling activity, but not in cavities with low bone-resorbing activity (Christodoulou *et al*, 2020). HSC localization in the BM niche also changes during lineage commitment suggesting that local cues in the BM impact the spatial organization of definitive blood cell differentiation (Zhang *et al*, 2021). Stress signals alter HSC spatial localization in the BM thus negatively affecting their function. Aged HSCs were reported to localize further away from the endosteum as compared to young HSCs (Kohler *et al*, 2009).

2 – HSC regulation in the BM niche

Excessive differentiation or reduced self-renewal of HSCs cause the depletion of the stem cell pool, on the contrary insufficient differentiation or uncontrolled self-renewal can give rise to leukaemia. Therefore, HSC activity need to be tightly regulated. HSC behaviour is governed by a complex network of cell-extrinsic factors from the BM microenvironment, including regulatory signals secreted from other BM cell populations, biochemical factors and physical cues; and cell-intrinsic factors, such as metabolic state (Pinho & Frenette, 2019).

A wide range of Insults can perturb HSC function directly through the accumulation of toxic molecules or reduced nutrient availability, as well as indirectly by altering the crosstalk between HSCs and other BM niche components. Understanding the relative contributions of cellular and molecular players to the regulation of HSC activity is fundamental to gain a more complete picture of the HSC niche, thus offering new therapeutic opportunities (Batsivari *et al*, 2020).

2.1– HSC regulation by niche cells

(Parts of the chapter 3.1 have been published in: https://pubmed.ncbi.nlm.nih.gov/35631417/)

Conditional deletion of various cell types, depletion of niche factors along with advanced BM imaging in mouse models allowed the identification of the cellular players of the HSC niche. BM populations are intimately connected with each other and alterations of a specific niche or depletion of specific factors could negatively affect other

niche components, thus impairing HSCs. Several non-hematopoietic and hematopoietic cell types have been identified (Fig. 3).

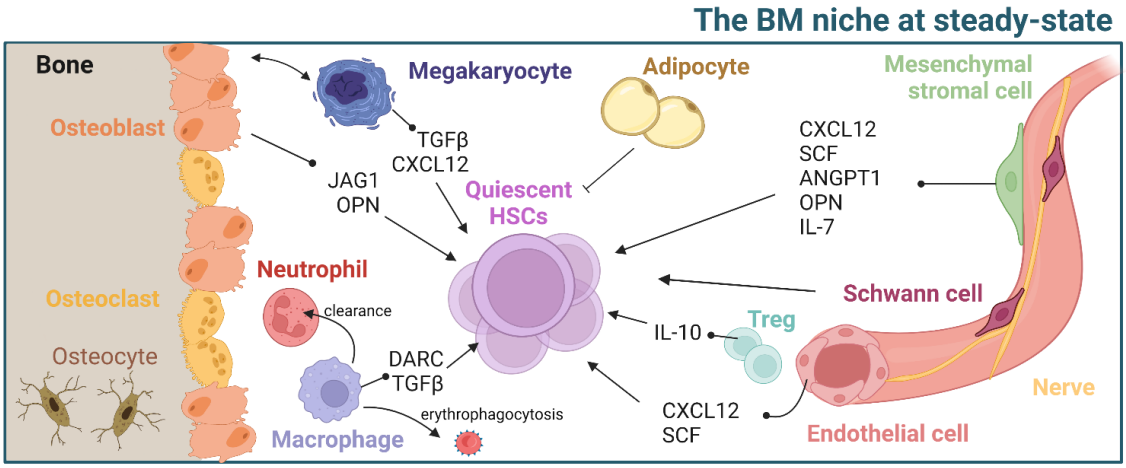

Figure 3. The BM niche. *Various stromal (osteoblasts, mesenchymal stromal cells, endothelial cells, adipocytes, sympathetic nerves and Schwann cells) and hematopoietic (megakaryocytes, macrophages, neutrophils and regulatory T cells) cell types and niche factors modulate HSC activity (Modified from Aprile et al, 2022).*

2.1.1 – Stromal BM cells

BM stromal components, such as osteolineage cells, mesenchymal stromal cells (MSCs) and endothelial cells (ECs), provide physical support and control HSC homeostasis.

Osteolineage cells, covering the endosteum, were the first population to be associated with HSC function. Early studies showed that human osteoblasts (oBs) induce HSC differentiation towards myeloid lineages *in vitro* (Taichman & Emerson, 1994). Moreover, oBs purified from murine long bones increase HSC engraftment in co-transplantation setting *in vivo* (El-Badri *et al*, 1998). oBs are activated by the parathyroid hormone (PTH) and PTH-stimulated oBs are increased in number and induce HSC expansion through the activation of Notch signaling (Calvi *et al*, 2003).

Several growth factors and cytokines are produced by oBs, e.g. Osteopontin (OPN), C-X-C motif chemokine ligand 12 (CXCL12), stem cell factor (SCF), thrombopoietin (TPO) and Angiopoietin1 (ANGPT1). However, recent evidence suggest that these cells do not directly regulate HSCs. Indeed, loss of OB-derived CXCL12 or SCF, has little effect on HSC number (Ding *et al*, 2012; Greenbaum *et al*, 2013). Also the contribution of the OB-derived TPO and ANGPT1 is controversial since hepatocytes were shown to be the major functional source of TPO for HSC maintenance (Decker *et al*, 2018),

whereas hematopoietic cells and stromal cells seem to be the main sources of ANGPT1 (Zhou *et al*, 2015). Although these studies challenged the essential role of oBs for HSC activity, recently *in vivo* live-imaging suggested that HSC localization and function is tightly dependent on bone turnover. HSC expansion was found only in bone cavities with both OB and osteoclast (OC) activity, whereas bone cavities with low OC activity do not host HSCs (Christodoulou *et al.*, 2020).

MSCs are a rare population in the BM near the blood vessels, that have the ability to differentiate into bone, fat and cartilage. Human MSCs $CD146^+$ generate colony-forming unit fibroblasts (CFU-Fs) *in vitro* and heterotopic ossicles *in vivo*. Moreover, upon serial transplantation they generate a compartment of perivascular stromal cells with similar phenotype and properties as the originally explanted cell, indicating self-renewal ability *in vivo* (Bianco *et al*, 2013; Sacchetti *et al*, 2007; Mendez-Ferrer *et al*, 2010). In mice, different MSC population were identified using transgenic mouse models, including $Nestin^+$ perivascular cells, CXCL12-abundant reticular (CAR) cells, leptin receptor $(LEPR)^+$ cells and $PDGFR\alpha^+$ $Sca1^+$ (PαS) cells (Ding *et al.*, 2012; Mendez-Ferrer *et al*, 2010; Morikawa *et al*, 2009; Sugiyama *et al*, 2006). But it is now widely recognised that there is overlap between these stromal populations.

MSCs modulate HSC activity directly by N-cadherin-mediated physical interaction (Wein *et al*, 2010). Nevertheless, MSCs mainly control HSCs indirectly through the secretion of SCF and CXCL12 as well as other regulatory factors, such as ANGPT1, OPN and interleukin 7 (IL-7). Moreover, MSCs preserve HSC function under stress signals, such as oxidative stress and infections. Excessive reactive oxygen species (ROS) alter HSC quiescence and function and MSCs neutralize ROS, thus protecting HSCs from myeloablation-induced oxidative damage (Taniguchi Ishikawa *et al*, 2012). Inflammatory signals induce HSC proliferation, differentiation and loss of self-renewal. Mitochondrial transfer has been reported in various tissue as a mechanism to rescue injured cells (Gomzikova *et al*, 2021), for instance HSCs acquire mitochondria from BM MSCs in response to acute bacterial infection thus resulting in rapid leukocyte expansion (Mistry *et al*, 2019). Also, mitochondrial transfer from MSCs to acute lymphoblastic leukemia cells (ALL) prevents therapy-induced apoptosis in ALL cells (Burt *et al*, 2019).

BM ECs, lining the surface of blood vessels, maintain vascular homeostasis, thus regulating HSC trafficking and function. Two different EC populations have been

identified on the basis of their localization and the differential expression of surface markers: arteriolar endothelial cells (AECs) and sinusoidal endothelial cells (SECs). The permeability of arterioles and sinusoids modulates ROS levels in adjacent HSCs and BM niche populations. On the one hand, less permeable arterioles maintain low ROS levels preserving HSC quiescence, on the other, leaky sinusoids increase ROS levels in HSCs, resulting in their activation and mobilization into the bloodstream (Itkin *et al*, 2016).
Notch signaling in BM ECs promotes osteogenesis (Ramasamy *et al*. 2014) and HSC expansion by inducing EC proliferation, arteriole formation and their coverage by PDGFRβ^{+} MSCs (Kusumbe *et al*. 2016). Moreover, ECs provide soluble factors, including CXCL12 and SCF, that maintain HSC self-renewal and promote hematopoietic regeneration after injury (Ding & Morrison, 2013; Doan *et al*, 2013; Winkler *et al*, 2012).

Adipocytes and the sympathetic nervous system (SNS) also control HSC function. While adipocytes are negative regulators of HSCs (Naveiras *et al*, 2009), the SNS, that innervates both the bone and the BM, modulates HSC mobilization into the circulation and protects them against genotoxic stress (Mendez-Ferrer *et al*, 2008; Park *et al*, 2015). Moreover, non-myelinating Schwann cells, adjacent to sympathetic nerves, contribute to HSC quiescence (Yamazaki *et al*, 2011).

2.1.2 – Hematopoietic BM cells

HSC progeny, including megakaryocytes (MKs), macrophages (Mφs), neutrophils and regulatory T (Tregs) cells play a key role in HSC maintenance.

Initial studies revealed that HSCs are located adjacent to MKs in a non-random fashion and MK depletion leads to HSC proliferation (Bruns *et al*, 2014). During homeostasis, MKs directly preserve HSC quiescence by secreting specific factors, such as CXCL4 and TGFβ (Bruns *et al.*, 2014; Zhao *et al*, 2014). However, after chemotherapeutic stress, MKs stimulate HSC regeneration through fibroblast growth factor 1 (FGF1) signaling (Zhao *et al.*, 2014). Furthermore, MKs control HSC function indirectly through the interaction with osteolineage cells. Of note, oBs cultured with MKs showed increased proliferation by a mechanism that requires cell-to-cell contact (Lemieux *et al*, 2010), whereas oCs cultured with MKs display a reduction in number (Bord *et al*, 2005).

Mφs are a heterogenous population with phagocytic activity present in all tissues, where they act as immune sentinels for pathogens and scavengers for senescent and

damaged cells. They are characterized by the expression of several molecular markers, including F4/80, Gr-1, CD115 and CD169. In response to different environmental signals, Mφs can adopt distinct functional characteristics, polarizing to M1 (classically activated or pro-inflammatory) or M2 (alternatively activated or anti-inflammatory) phenotype. The former protects from infections and cancer by activating the inflammatory cascade, the latter promotes tissue repair and regeneration by secreting anti-inflammatory cytokines (Seyfried *et al*, 2020a). BM Mφs directly regulate HSC quiescence and self-renewal by physical interaction and cytokine secretion (Hur *et al*, 2016; Ludin *et al*, 2012). M2 macrophages induce HSC self-renewal, while M1 macrophages exert an opposite role (Luo *et al*, 2018). In addition, BM Mφs indirectly regulate HSC location by inducing the expression of HSC retention factor by MSCs and promoting HSC mobilization through neutrophil clearance (Casanova-Acebes *et al*, 2013; Chow *et al*, 2011). The homeostatic clearance of erythrocytes also affects HSCs. Mφs play a crucial role in iron homeostasis and host defence by recycling senescent erythrocytes through a process named "erythrophagocytosis" (Korolnek & Hamza, 2015). In humans, iron derived from erythrophagocytosis is the main source of iron influx in the body, exceeding iron absorption form the diet and iron stored in hepatocytes. Iron is an essential element, involved in many biological processes, such as oxygen transport, energy metabolism, DNA synthesis and cell signaling (Muckenthaler *et al*, 2017); and recently iron was found to play a key role in regulating HSC function and metabolism (Kao Y-R, 2021; Muto *et al*, 2017). BM Mφs erythrophagocytosis provide iron to HSCs during hematopoietic stress to fuel HSC differentiation (Zhang *et al*, 2022). In addition, during infection and inflammation, Mφs sequester iron from the microenvironment to limit the growth of pathogenic microbes (Ganz, 2012).

The differentiated hematopoietic cells that regulate HSC mobilization and quiescence also include neutrophils and Tregs (Fujisaki *et al*, 2011; Hirata *et al*, 2018; Kawano *et al*, 2017).

2.2 – Metabolic regulation of HSCs

HSCs remain quiescent for the most of their lifetime to preserve the stem cell pool and divide only when required to give rise to all blood lineages. During HSC quiescence,

proliferation and differentiation, specific metabolic pathways are required to meet their energetic and biosynthetic demands. Therefore, metabolism is a key regulator of HSC fate (Bartram & Filippi, 2022).

Changes in cell cycle and functional state determine metabolic adaptations; vice versa, metabolism controls HSC cell cycle and function. Indeed, stress signals, such as ROS, can directly modify HSC metabolism by altering metabolic enzymes and mitochondria fitness, thus affecting HSC function.

Understanding the metabolic need of HSC functional states and the extrinsic regulators of HSC metabolism is crucial for providing new therapies for hematological disorders and optimizing HSC expansion *ex vivo* (Kumar & Geiger, 2017; Morganti *et al*, 2022).

2.2.1 – HSC quiescence

Quiescent HSCs rely on anaerobic glycolysis and maintain a low mitochondrial metabolic activity in the hypoxic BM niche.

Glycolysis is a ten-step process that breaks down glucose into pyruvate within the cytosol. During anaerobic glycolysis, pyruvate is converted to lactate by lactate dehydrogenase (LDH) instead of being transported into mitochondria where, once converted to acetyl coenzyme A (acetyl-CoA), fuels OXPHOS during aerobic glycolysis. The metabolism of glucose to lactate produces only 2 molecules of ATPs per molecule of glucose, however it is sufficient to meet the low metabolic requirements of quiescent HSCs and their need of limiting generation of ROS, as a byproduct of active mitochondria (Kohli & Passegue, 2014) (Fig. 4).

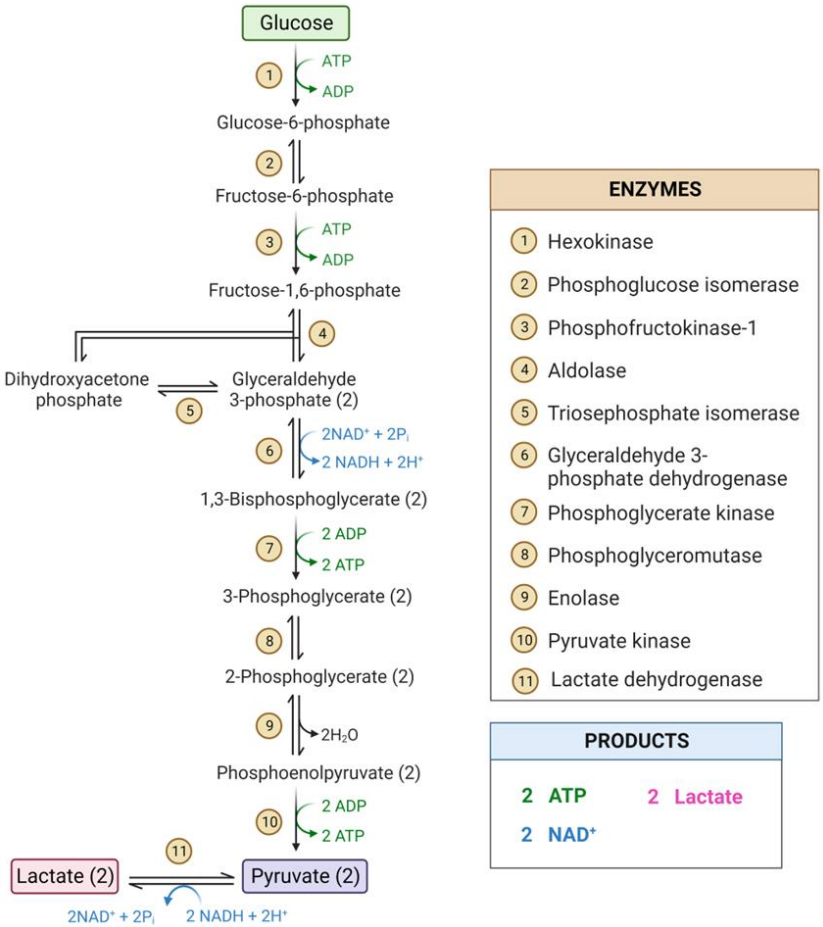

Figure 4. Anaerobic glycolysis pathway. *Per each molecule of glucose, 2 ATPs, 2 lactate and 2 NAD^+ are produced. Enzymes catalysing glycolysis steps are shown in the table (created with BioRender.com).*

Quiescent HSCs uptake high levels of glucose from the microenvironment and express glycolytic enzymes, thus resulting in increased production of pyruvate and lactate but low ATP as compared to progenitors and differentiated cells (Schonberger *et al*, 2022; Simsek *et al*, 2010; Takubo *et al.*, 2013). Of note, quiescent HSCs specifically activate glycolysis and suppress influx of glycolytic metabolites into mitochondria by expressing high levels of pyruvate dehydrogenase kinases (*Pdks*), which inhibit the pyruvate dehydrogenase (PDH)-mediated conversion of pyruvate to acetyl-CoA. Loss of *Pdks* reduces glycolysis and increases mitochondrial activity, thus resulting in decreased HSC quiescence and self-renewal (Takubo *et al.*, 2013). Moreover, quiescent HSCs express high levels of *Hif1α*, which senses low oxygen rates of the BM niche and is one key activator of glycolysis (Takubo *et al.*, 2010). Deletion of *Meis1*, the transcriptional activator of *Hif1α*,

causes HSC dysfunction through increased mitochondrial metabolism and consequent ROS generation (Kocabas *et al*, 2012).

To preserve quiescence, HSCs carry high number of mitochondria, which are mostly inactive (de Almeida *et al*, 2017; Takihara *et al*, 2019). While ETC complex II is highly expressed in HSCs, ATP synthase is not, thus resulting in high MMP, which cannot be used by ATP synthase (Morganti *et al*, 2019). As a consequence, quiescent HSCs, despite high mitochondrial mass and MMP, generate low ATP and ROS.

However, a limited mitochondrial activity is essential for HSC function. Indeed, loss of mitochondrial metabolism in ko mouse model, lacking specific mitochondrial enzymes, reduces HSC quiescence and impairs their differentiation (Anso *et al*, 2017; Yu *et al*, 2013).

Also vitamin metabolism is essential for HSC quiescence. Recently, treatment with vitamin B3 was found to improve the function of aged HSCs by reducing mitochondrial metabolism (Sun *et al*, 2021). Moreover, vitamin A/retinoic acid signaling preserves HSC quiescence and self-renewal (Schonberger *et al.*, 2022).

Finally, lysosomes have emerged as critical regulators of HSCs since high number of lysosomes with slow activity, including sluggish clearance of mitochondria, preserves HSC quiescence by limiting the release of toxic molecules, such as ROS (Liang *et al*, 2020).

2.2.2 – HSC differentiation requires metabolic rewiring

The transition from quiescence to proliferation and differentiation requires higher energy inputs, thus HSCs enhance the more energetic OXPHOS (Nakamura-Ishizu *et al.*, 2020).

During OXPHOS, pyruvate, generated from glucose, is shuttled to the mitochondrial matrix and converted to acetyl-CoA, which enters the tricarboxylic acid cycle (TCA). Subsequent enzymatic reactions of the TCA produce the reduced cofactors nicotinamide adenine dinucleotide (NADH) and flavin adenine dinucleotide ($FADH_2$), which transport their electrons to the ETC complexes, thus fueling OXPHOS (Baldwin & Krebs, 1981). The electron transfer through the ETC protein complexes I-IV provides the energy to pump protons out of the matrix and generate a proton gradient across the IMM, which in turn allows the flow of protons back in the mitochondrial matrix at the level of complex

V ATP synthase, thus producing ATP. The total force driving protons is a combination of both the MMP (Δψm, a charge or electrical gradient) and the mitochondrial pH gradient. OXPHOS generates 36 molecules of ATPs per molecule of glucose (Berg J. M., 2015) (Fig. 5).

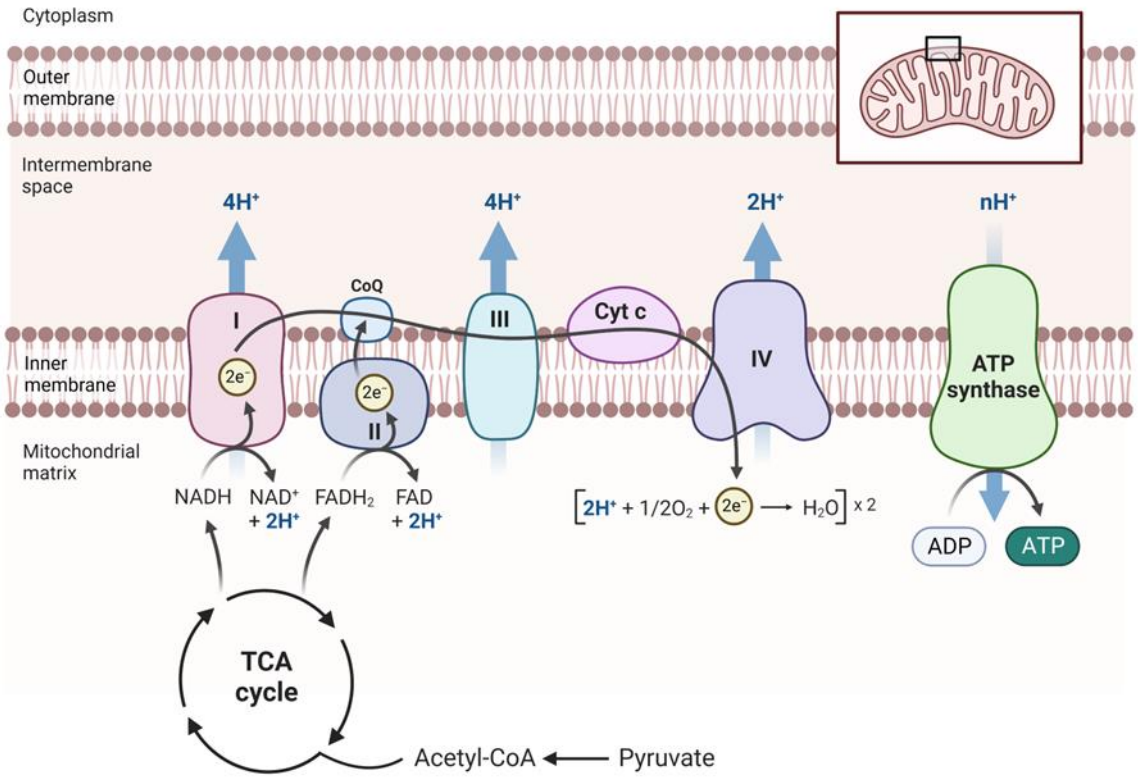

Figure 5. TCA cycle and OXPHOS. *Acetyl-CoA derived from pyruvate enters the TCA cycle in the mitochondrial matrix and generates NADH and $FADH_2$, which transfer their electrons to the ETC complexes in the IMM. The electron flow through ETC creates an electrochemical proton gradient across the IMM, which is coupled to ATP production by ATP synthase (created with BioRender.com).*

HSC differentiation is accompanied by increased OXPHOS, resulting in high ATP but also ROS generation, as shown by initial works exploiting ko mouse models of metabolic regulators (Chen *et al.*, 2008; Maryanovich *et al*, 2015). Moreover, i*n vitro* culture of HSCs in presence of differentiation stimuli and FCCP, that uncouples the electron transport from ATP production, decreases mitochondrial area and function, thus blocking HSC differentiation (Vannini *et al*, 2016).

Recently, the development of advanced metabolomic approaches and single-cell RNA sequencing (scRNAseq) allowed the identification of the key metabolic intermediates and molecular players regulating HSC functional state. The transition from HSCs to MPPs

involves the upregulation of genes encoding for TCA and ETC enzymes and TCA-related metabolites are enriched in MPPs (Schonberger *et al.*, 2022).

Moreover, HSCs can be classified based on MMP as MMP^{high} and MMP^{low}, with high and low mitochondrial activity respectively, using potentiometric dyes, such as tetramethylrhodamine ethyl ester (TMRE) and tetramethylrhodamine methyl ester perchlorate (TMRM). These positively charged dyes accumulate in the negatively charged mitochondrial matrix in proportion to the MMP (Perry *et al*, 2011). While MMP^{low} HSCs are mostly quiescent, MMP^{high} HSCs are primed towards differentiation, as shown by reduced quiescence, increased cell division and positive enrichment of genes involved in DNA replication and cell cycle progression (Liang *et al.*, 2020; Qiu *et al*, 2021). However, active MMP^{high} HSCs also express at high levels glycolytic genes, such as the glucose transporter *Glut1*, and display higher glucose uptake than MMP^{low} HSCs. In addition, glycolysis inhibition reduces only MMP^{high} HSC viability *in vitro,* thus suggesting that active HSCs increase both glycolysis and OXPHOS to meet their high energy demands (Liang *et al.*, 2020).

Fatty acid oxidation (FAO) breaks down long fatty acid chains in the mitochondria to generate acetyl-CoA, which in turn fuels TCA cycle and OXPHOS, thus sustaining HSC proliferation and differentiation. Moreover, FAO preserves HSC pool by promoting asymmetric instead of symmetric differentiation (Ito *et al*, 2012; Schonberger *et al.*, 2022) (Fig. 6).

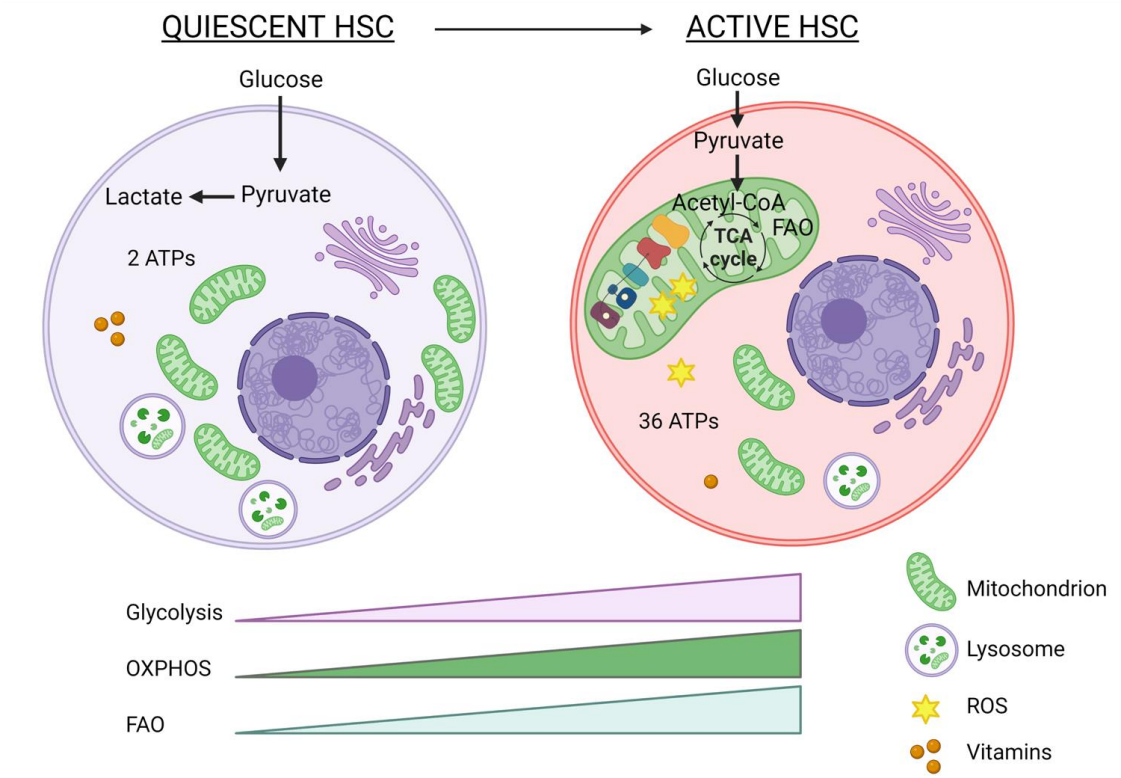

Figure 6. Metabolism of quiescent and active HSCs. *Quiescent HSCs rely on low energetic glycolysis, although they have high number of mitochondria and low mitochondrial activity is required to preserve function. Moreover, slow clearance of mitochondria by lysosomes and the metabolism of vitamins maintain HSC quiescence. On the contrary, active HSCs require high energy inputs and upregulate OXPHOS, glycolysis and FAO to produce high ATP but also ROS (created with BioRender.com).*

2.2.3 – Mitochondria as key regulators of HSC metabolism

Since mitochondria are the "powerhouse" of the cell, containing the major enzymes that oxidize carbohydrates, proteins and lipids to produce ATP, they are crucial regulators of HSC fate and function.

Active mitochondria are elongated with numerous folds of the IMM, named cristae, that host the ETC complexes and form a compact network. Conversely, inactive mitochondria are small and round with low number of cristae (Liang *et al.*, 2020; Qiu *et al.*, 2021).

Mitochondrial network is continuously remodeled through cycles of biogenesis of new mitochondria, fusion, fission and degradation by mitophagy, thus affecting HSC metabolism.

Increased mitochondrial biogenesis in HSCs, as shown by high expression of key biogenesis regulators *Pgc1a* and *Tfam*, correlates with high mitochondrial activity and subsequent HSC differentiation (Nakamura-Ishizu *et al*, 2018). By contrast, inhibition of mitochondrial biogenesis maintains HSC quiescence (Hu *et al*, 2018).

Fusion is a two-step process consisting in the fusion first between the mitochondrial outer membranes (OMMs) and then between the IMMs of two mitochondria, thus leading to increased mitochondrial size and more compact mitochondrial network. On the contrary, fission results in smaller mitochondria and fragmented mitochondrial network. DRP1 is the cytosolic fission regulator and, once it is recruited on mitochondrial surface by the binding with its receptors FIS1, MFF, MIEF1 and MIEF2, it constricts mitochondrion (Mishra & Chan, 2014).

Although the role of fusion is still largely unexplored in HSCs, it was found to maintain HSCs with extensive lymphoid potential (Luchsinger *et al*, 2016). Moreover, it could promote complementation between damaged mitochondria, thus acting as a first line of defense before mitophagy activation (Youle & van der Bliek, 2012).

Recently, the effects of mitochondrial fission on HSCs gained attention. Loss of fission by genetic deletion or pharmacological inhibition of DRP1 causes mitochondrial dysfunction in HSCs, resulting in impaired HSC repopulating ability. In addition, active dividing HSCs have reduced mitochondrial fission and seem to keep dysfunctional mitochondria as a mechanism of divisional memory (Hinge *et al*, 2020).

Mitophagy is a specific form of autophagy that selectively removes dysfunctional or damaged mitochondria, preventing accumulation of defective mitochondria. During PINK1-dependent mitophagy, PINK1 localized in the OMM recruits the E3 ubiquitin ligase parkin, which ubiquitinates mitochondrial proteins and recruits autophagy receptors to activate a cascade of ubiquitination, thus resulting in autophagosome formation and mitochondrial degradation (Bingol & Sheng, 2016). Besides *Pink1* and parkin, other key mitophagy players include *Ulk1*, *Optn*, *Sqstm1*, *Map1lc3b* and *Gabarapl1* and they are all expressed by HSCs (Ito *et al*, 2016). Mitophagy preserves HSC stemness and loss of mitophagy in ko mouse models for mitophagy genes impairs HSC self-renewal and regenerative potential (Ho *et al*, 2017; Ito *et al.*, 2016). Vice versa, hyperactivation of mitophagy reduces mitochondrial number and results in aberrant differentiation of HSCs (Hashimoto *et al*, 2021; Jin *et al*, 2018) (Fig. 7).

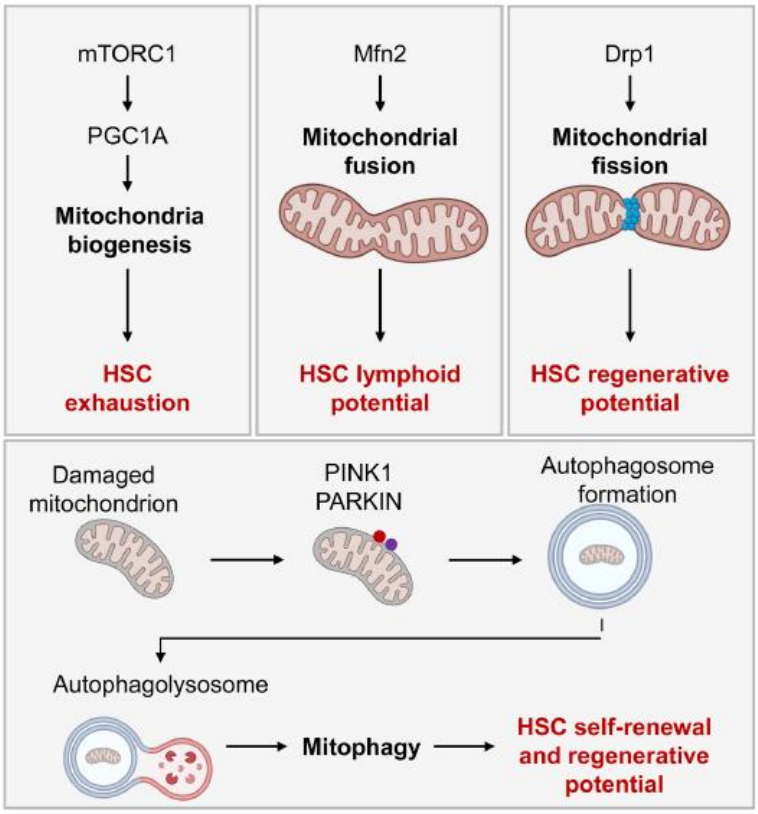

Figure 7. HSC regulation by mitochondrial dynamics. *Key players of mitochondrial biogenesis (e.g. Pgc1a), fusion (e.g. Mfn2), fission (e.g. Drp1) and mitophagy (e.g. Pink1, parkin) were found to regulate HSC homeostasis by affecting their differentiation and self-renewal (From Morganti et al., 2022).*

During mitophagy, lysosomes fuse to damaged mitochondria to form the autophagosome, thus lysosome function is fundamental for adequate clearance of mitochondria. Indeed, the sequestration and slow degradation of dysfunctional mitochondria into lysosomes maintains HSC quiescence, whereas activation of lysosomes with toxin release induces HSC differentiation (Liang *et al.*, 2020).

2.3 – HSC regulation by soluble factors

HSCs respond to several soluble factors in the microenvironment, including oxidative stress, iron, variation in the partial pressure of oxygen (pO_2) and inflammatory signals, by switching their metabolic state and cell cycle, thus shifting the balance between self-renewal and differentiation (Mendelson & Frenette, 2014). These factors can act directly on HSCs or indirectly by altering other BM niche cells.

2.3.1 – ROS

ROS are highly reactive molecules due to the presence of unpaired electrons in the outer valence shell. Intracellular ROS typically include: superoxide anions (O_2^-), hydrogen peroxide (H_2O_2) and hydroxyl radicals (OH^-), which are generated from the reduction of molecular oxygen (O_2) during a series of redox reactions. H_2O_2 is the main ROS encountered intracellularly as a consequence of its longer half-life and its higher ability to diffuse across cellular membranes (Holmstrom & Finkel, 2014).

Mitochondria and NADPH oxidase (NOX) are the primary source of ROS within the cell. Mitochondria produce ROS, as a result of the activity of the electron transport chain (ETC). The electron flow through the ETC protein complexes I-IV in the inner mitochondria membrane (IMM) generates the proton motive force, that pumps protons (H^+) into the mitochondrial intermembrane space against their concentration gradient. The combination of the electric gradient, mitochondrial membrane potential (MMP), and the mitochondrial pH gradient drives ATP synthesis via oxidative phosphorylation (OXPHOS). During this process, O_2 is reduced to H_2O by complex V ATP synthase. However, O_2 can undergo aberrant reduction at complexes I and III, thus generating O_2^-. Therefore, mitochondria are key modulators of cellular redox homeostasis (Murphy, 2009).

NOX family was first described in neutrophils as enzymes responsible for ROS production during host defence (Hampton *et al*, 1998). In particular, NOX generate O_2^- through the reduction of NADPH to $NADP^+$ (Fig. 8).

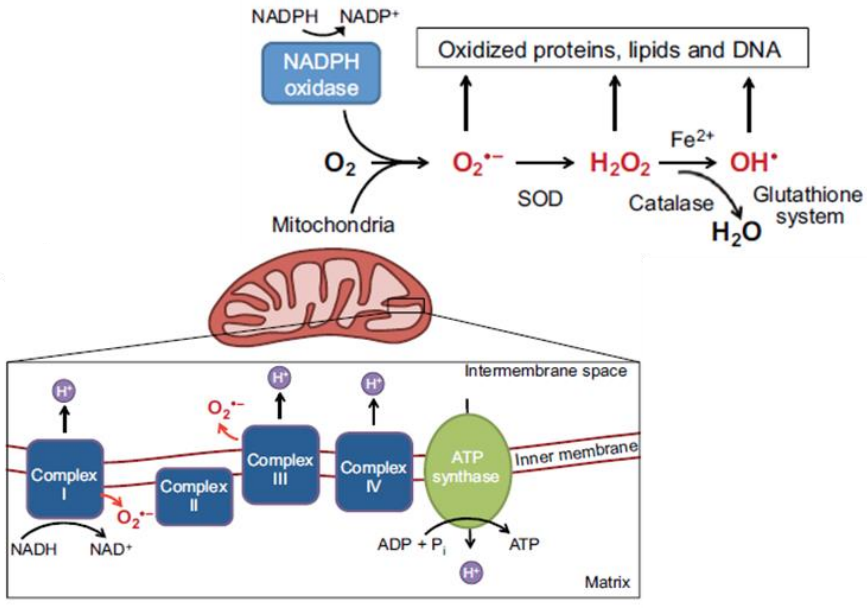

Figure 8. Generation of intracellular ROS. *ROS, including superoxide anions (O_2^-), hydrogen peroxide (H_2O_2) and hydroxyl radicals (OH^-), are mostly generated from the ETC in mitochondria and NAPDH oxidase (Modified from Bigarella et al, 2014).*

ROS can be generated also from free reactive iron via the Fenton and Haber-Weiss reactions (Kajarabille & Latunde-Dada, 2019), thus cellular iron levels need to be tightly regulated. Also variation in oxygen levels and inflammatory signals can affect both mitochondrial activity and NOX and, consequently, modulate intracellular ROS content (Mittal *et al*, 2014; Takubo *et al*, 2013).

In physiological context, ROS are important signaling molecules, regulating HSC quiescence, proliferation, differentiation and self-renewal by direct modulation of redox-sensitive enzymes and transcription factors (Bigarella *et al.*, 2014). ROS act as second messengers by oxidizing at specific amino acid residues, typically cysteine and methionine, target proteins (redox sensors), which in turn undergo conformational changes that affect their function, stability and localization. However, abnormal accumulation of ROS causes oxidative damage of DNA, lipids and proteins, impairing organelles, especially mitochondria, with further ROS generation (Tan & Suda, 2018). Therefore, stem cells, including HSCs, evolved strategies to manage ROS levels and counteract oxidative stress.

ROS scavenger, such as superoxide dismutase (SOD), catalase, glutathione peroxidase, peroxiredoxin and thioredoxin, are antioxidant enzymes that detoxify ROS by accepting electrons from them. SOD reduces O_2^- to H_2O_2, which in turn is rapidly converted into water by catalase or glutathione peroxidase, whereas OH^- is neutralized by the glutathione system (Murphy, 2012). However, when ROS levels outpace the efficiency of the antioxidant enzyme system, an excessive accumulation of ROS occurs, leading to intracellular oxidative stress.

HSCs maintain a low basal level of ROS, which preserves stem cell quiescence and self-renewal. On the contrary, a physiological increase of ROS is required for cell proliferation and differentiation (Jang & Sharkis, 2007). ROS directly modulate key regulators of HSC function, such as the protein kinases ataxia telangiectasia mutated kinase (ATM), p38 mitogen-activated protein kinase (MAPK) and mammalian target of rapamycin (mTOR). Specific deletion of ATM in mice results in ROS elevation followed by the activation of p38 MAPK, thus reducing HSC quiescence and repopulating ability

and inducing senescence (Ito *et al*, 2006). mTOR increases mitochondrial biogenesis and activity, promoting ROS generation and, as a consequence, HSC proliferation and differentiation (Chen *et al*, 2008). During aging, HSCs increase in number but have reduced repopulating ability, and myeloid-biased differentiation (Geiger *et al*, 2013). Moreover, aged HSCs display increased OXPHOS and ROS generation, and mitochondrial stress, that compromise their functions (Morganti & Ito, 2021). Reduction of mitochondrial ROS (mtROS) by *in vivo* administration of the antioxidant Mito-Q to middle-aged and aged mice can prevent or restore mitochondrial dysfunction and HSC defects, thus indicating that mtROS cause HSC functional decline in aging (Mansell *et al*, 2021).

The accumulation of ROS in HSCs can be the result of increased ROS generation but also impaired antioxidant defence system. FOXO are transcription factors critical for the regulation of antioxidant enzymes and loss of FOXO3 enhances ROS levels, leading to impaired HSC self-renewal due to p38 MAPK activation (Miyamoto *et al*, 2007; Yalcin *et al*, 2008). In addition, lack of the regulator of redox homeostasis sirtuin 1 (SIRT1) causes ROS accumulation in HSCs, accompanied by DNA damage and reduced repopulating ability (Rimmele *et al*, 2014).

ROS reduction under basal levels as well as excess ROS are detrimental to HSCs. Knock-out (ko) mice for AKT1 and AKT2 have reduced ROS, resulting in HSC cell cycle arrest in G0 and impaired differentiation (Juntilla *et al*, 2010). On the contrary, when intracellular ROS levels are extremely high, DNA and cellular organelles are irreversibly damaged and cell death occurs (Ito *et al.*, 2006) (Fig. 9).

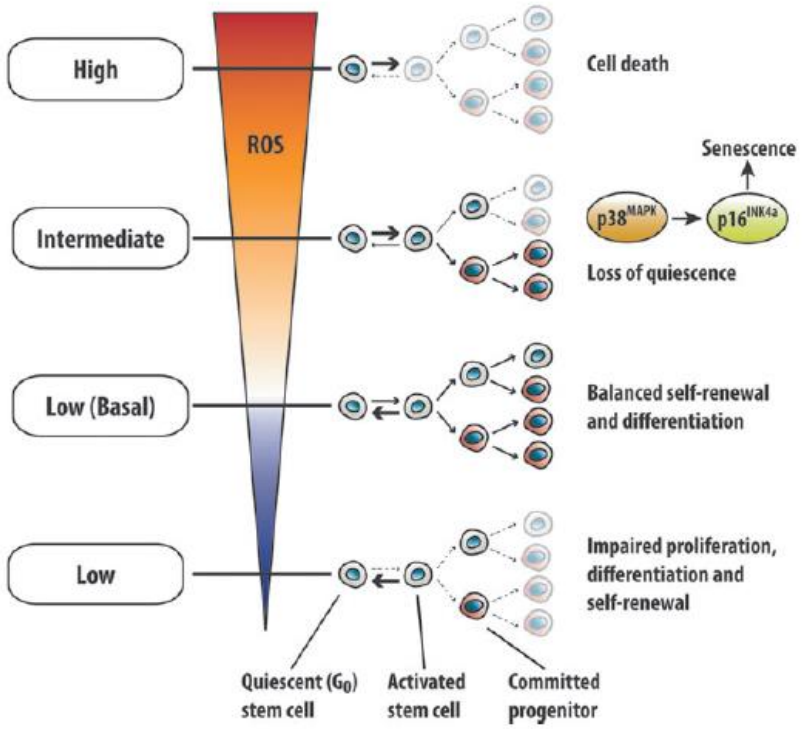

Figure 9. HSC response to different levels of intracellular ROS. *At steady-state ROS are maintained low to preserve the stem cell pool (basal), whereas a physiological increase of ROS drives HSC proliferation and differentiation (intermediate). Both lower and higher intracellular ROS alter HSC function: when ROS are under the basal threshold HSCs are maintained quiescent with differentiation blockade; when ROS greatly exceed the basal threshold cell death occurs (From Tan & Suda, 2018).*

BM niche cells control intracellular ROS levels in HSCs thus regulating their function. In particular, stromal cells import ROS from HSCs through Connexin-43 (Cx43) gap junctions. Loss of Cx43 in HSCs leads to ROS accumulation followed by senescence due to their inability to transfer ROS to BM stromal cells (Taniguchi Ishikawa *et al.*, 2012).

Other soluble factors, such as iron, O_2 and inflammatory cytokines regulate HSC function by modulating intracellular ROS levels. Given the central role of mitochondrial metabolism in ROS generation, HSCs can change their metabolic state to manage ROS accumulation (Nakamura-Ishizu *et al*, 2020).

2.3.2 – Iron

Iron is an essential element involved in several cellular processes, including oxygen transport, metabolism, DNA synthesis and repair, and cell signaling. Iron carries out these functions due to its ability to accept and donate electrons, constituting the prosthetic group of many proteins in the form of heme or iron sulphur (Fe-S) cluster (Wang & Babitt,

2019). In particular, heme is present in hemoglobin and myoglobin, where it regulates oxygen transport, mitochondrial enzymes, where it participates in energy generation, antioxidants and other enzymes, thus constituting more than 95% of total iron in humans (Chiabrando *et al*, 2014).

While a small amount of iron is required for cellular homeostasis, excessive iron accumulation is toxic. Indeed, free iron, in the form of ferrous ion (Fe^{2+}) and ferric ion (Fe^{3+}) can participate in Fenton and Haber-Weiss reactions, thus generating ROS, which in turn damage cellular components (Kajarabille & Latunde-Dada, 2019) (Fig. 10).

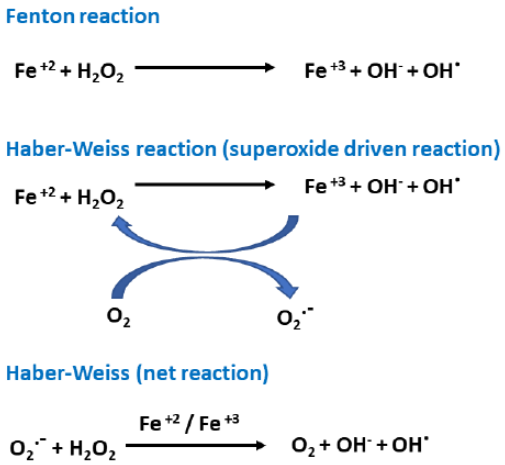

Figure 10. Fenton and Haber-Weiss reactions. *Iron toxicity is due to its involvement in harmful ROS-generating reactions (From Kajarabille & Latunde-Dada, 2019).*

Iron-derived ROS can induce the peroxidation of lipid in membrane bilayers, culminating in ferroptosis, an iron-dependent form of cell death morphologically, biochemically and genetically distinct from apoptosis, necrosis and autophagy (Jiang *et al*, 2021). Ferroptosis was initially discovered in RAS mutant tumor cells in which cell death was reverted only by treatment with antioxidants and iron chelators (Dixon *et al*, 2012).

Given the fundamental role of iron in cellular functions and its potential harmful effects, plasma iron levels as well as intracellular iron deposits need to be tightly modulated. Iron metabolism is regulated both at systemic level and at cellular level to avoid iron deficiency and IO, which are detrimental to cell survival.

Plasma iron levels depend on dietary iron absorption and iron recycling by macrophages. Duodenal enterocytes absorb only 1-2 mg of dietary iron per day, corresponding to less then 10% of iron needs, to compensate for iron losses (Hentze *et al*, 2010; Wang & Babitt,

2019). The rest of iron derives from macrophages that phagocytize and degrade damaged and senescent erythrocytes to recycle iron from hemoglobin (Korolnek & Hamza, 2015). Iron is then released from enterocytes and macrophages in the bloodstream through the iron exporter ferroportin (FPN). Circulating iron (Fe^{3+}) is bound to transferrin (TF) and is mainly delivered to the BM where it is uptaken by erythrocytes for hemoglobin synthesis after binding to the membrane-bound TF receptor 1 (TFR1). However, since TFR1 is ubiquitously expressed, all cells can uptake iron from the circulation. The human body has no pathway to excrete iron and unused iron is stored in the liver, which also play a key role in regulating systemic iron homeostasis by the secretion of hepcidin (Muckenthaler *et al.*, 2017). Hepcidin inhibits the release of iron into the bloodstream by binding to FPN and mediating its degradation via proteasome (Sangkhae & Nemeth, 2017) (Fig. 11).

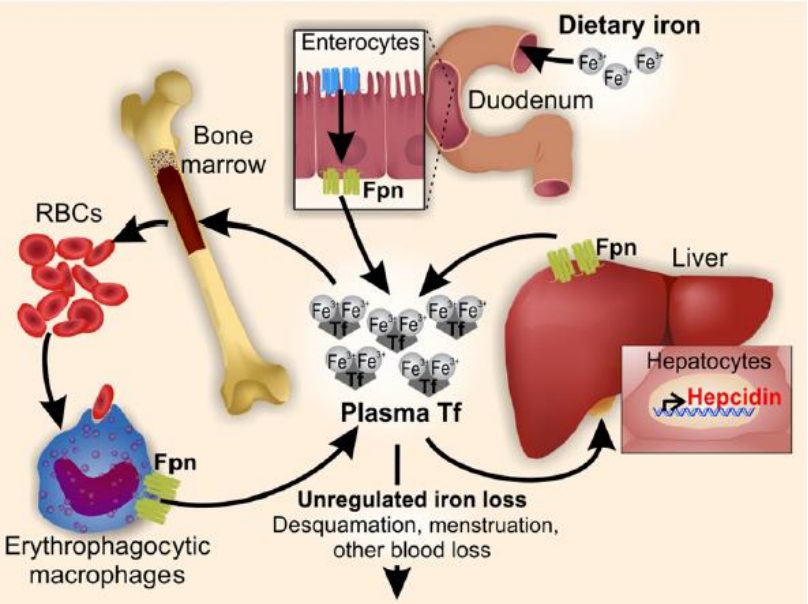

Figure 11. Systemic iron homeostasis. *Circulating iron derives from iron absorption by duodenal enterocytes and iron recycling by macrophages. Iron is mostly used in the BM for hemoglobin synthesis, whereas the unused iron is stored in the liver. The hepatic hormone hepcidin is the central regulator of systemic iron homeostasis (From Sangkhae & Nemeth, 2017).*

Cells control iron uptake, utilization, intracellular transport and detoxification to ensure adequate iron supply and avoid iron toxicity (Hentze *et al.*, 2010). Transferrin-bound Fe^{3+} binds to TFR1 and the complex is then internalized by receptor-mediated endocytosis. pH acidification within the endosome leads to the dissolution of the complex, followed by the recycling of TF and TFR1 and the release of Fe^{3+}. Fe^{3+} is then

reduced to Fe^{2+} by the metalloreductase STEAP3 and transported into the cytosol by DMT1, where it constitutes the labile iron pool (LIP) readily available for cellular use. Since free Fe^{2+} in the LIP is extremely reactive, most of it is delivered to mitochondria (Paul *et al*, 2017), whereas excess Fe^{2+} is converted to Fe^{3+} and stored in ferritin (FT) or exported in the circulation by FPN.

Mitochondria are major hubs of iron utilization and accumulation and mitochondrial iron is mainly utilized for heme synthesis and Fe-S cluster assembly (Muhlenhoff *et al*, 2015). Therefore, iron perturbations can negatively impact on mitochondria function and metabolism, thus affecting cell viability (Paul *et al.*, 2017) (Fig. 12).

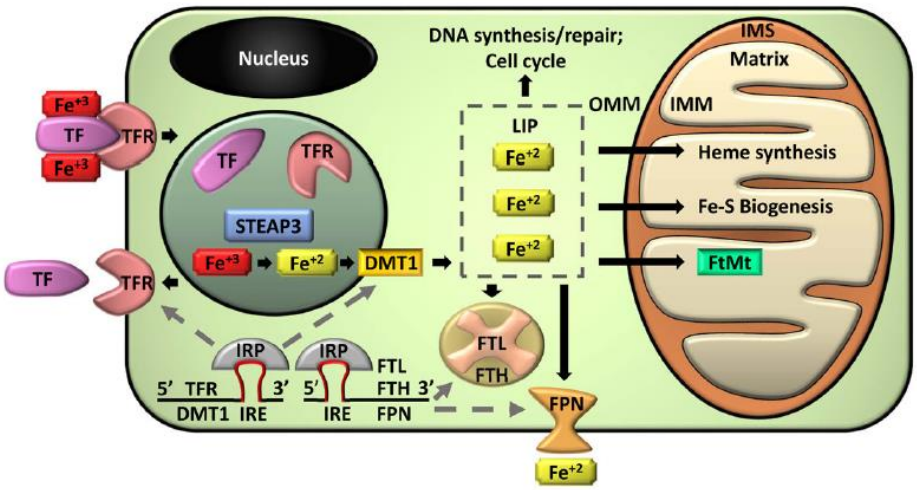

Figure 12. Cellular iron homeostasis. *Key molecular players involved in iron uptake, intracellular trafficking and release from the cell are shown. Plasma iron (Fe^{3+}) is internalized after the binding of transferrin (TF) to its receptor (TFR). Once in the endosome, Fe^{3+} is converted to Fe^{2+} and released in the cytosol, where it constitutes the labile iron pool (LIP). Iron is mainly used for heme and Fe-S cluster synthesis in the mitochondria, whereas excess iron is stored in ferritin (FT) or is released in the circulation through ferroportin (FPN) (From Paul et al., 2017).*

Cellular iron homeostasis is maintained by the iron regulatory protein (IRP) 1 and 2 system. In iron deficient cells, IRPs binds to the iron responsive element (IRE) in the untranslated regions (UTR) of mRNA encoding key players of iron metabolism. In particular, the binding of IRPs to the 5' UTR of *Ft* and *Fpn* blocks their translation, conversely the binding of IRPs to the 3' UTR of *Tfr1* results in mRNA stabilization. As a result, iron storage and export are inhibited, whereas iron uptake is increased. When cells display intracellular IO, IRP1 acquires enzymatic function and IRP2 is degraded via proteasome after binding to FBXL5 to limit iron uptake and enhance iron export in the circulation (Hentze *et al.*, 2010) (Fig. 13).

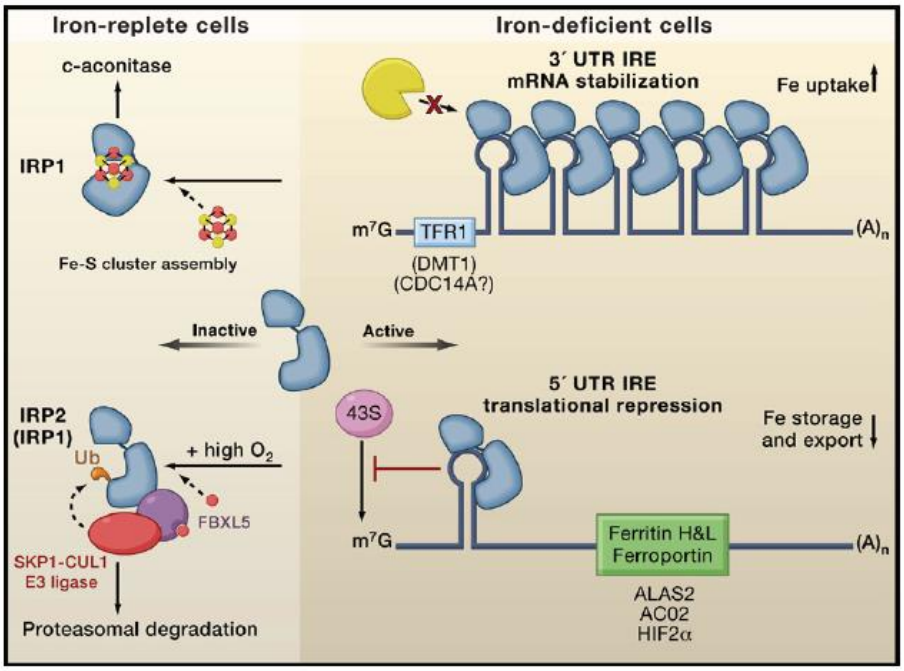

Figure 13. Regulation of cellular iron homeostasis by IRPs. *In iron deficient cells, IRPs binds to IRE in the mRNA of iron homeostasis genes thus regulating their translation to increase intracellular iron levels. On the contrary, in iron-overloaded cells the IRP system is inactivated (From Hentze et al., 2010).*

HSCs express the key regulators of iron uptake, transport and storage thus they can import iron from the microenvironment and accumulate it, participating in the regulation of iron homeostasis. HSCs contain lower amounts of free iron as compared to other hematopoietic cells (Kao Y-R, 2021) and fluctuation of iron levels regulates HSC function through ROS generation (Muto *et al.*, 2017; Zhang *et al.*, 2022). Initial studies in wild-type (wt) mice treated with high iron dose *in vivo* showed ROS accumulation in the BM and decreased levels of hematopoietic regulatory factors, such as CXCL12, SCF and TPO, resulting in reduced HSPC repopulating ability (Okabe *et al*, 2014). Moreover, *in vitro* treatment with high concentration of ferrous ammonium sulfate (FeAS) induces HSPC apoptosis through ROS-activated p38 MAPK. Of note, FeAS also impairs cytokine secretion by stromal cells in culture (Tanaka *et al*, 2019). *In vivo* and *in vitro* administration of iron chelators, which sequester and neutralize excess iron, restores HSPC function (Chai *et al*, 2015; Lu *et al*, 2013). Thus, IO in the BM can negatively impact HSPCs both directly and indirectly by affecting other BM niche cells.

Intracellular IO as well as intracellular iron deficiency are detrimental to HSC stemness. Loss of FBXL5 results in IRP hyperactivation and increased LIP in HSCs, thus reducing

their frequency and impairing their self-renewal capacity (Muto *et al.*, 2017). Similarly, intracellular iron deficiency in TFR1-ko HSCs impairs their differentiation and reduces their repopulating ability (Wang *et al*, 2020), thus suggesting that adequate iron uptake mediated by TFR1 is essential for HSC function. These findings were recently confirmed by two other works showing the importance of limiting intracellular iron levels, without resulting in iron deficiency, during regeneration and cell division (Kao Y-R, 2021; Zhang *et al.*, 2022). The gut microbiota was found to regulate HSC function by controlling macrophage erythrophagocytosis and, consequently, iron availability in the BM. Under stress conditions, microbiota or BM macrophages depletion induce iron deficiency in the BM and low intracellular iron in HSCs, which, in turn, leads to reduced HSC quiescence and repopulating ability. In addition, wt animals fed with deficient iron diet displayed impaired HSC repopulating ability, suggesting that iron could regulate HSC self-renewal independent of the microbiota. Indeed, *in vitro* very low iron concentrations decreases the survival of wt HSCs, whereas low basal iron preserves their stemness (Zhang *et al.*, 2022). Interestingly, low intracellular iron content in HSCs seems to activate the IRP-mediated limited iron response during cell division, which enhances their repopulating ability. Therefore, intracellular iron limitation could be required to sustain HSC cell division and function (Kao Y-R, 2021).

2.4 – The interplay between iron, ROS and HSC metabolism

In the last few years, the analysis of the BM niche in clinical conditions characterized by IO revealed the effects of IO on different BM populations, although still poorly characterized. In hemoglobinopathies, such as β-thalassemia (BThal) and sickle cell disease (SCD), mutations in the β-globin gene impair the survival of red blood cells (RBCs). Haemolytic anemia triggers a cascade of events, including increase of iron and heme in the circulation (Aprile *et al*., 2022). Free heme and iron were found to induce oxidative stress in BThal and SCD MSCs and affect their ability to maintain HSCs (Crippa *et al*., 2019; Tang *et al*., 2019). Moreover, circulating iron was shown to alter SCD Mφ phenotype toward a proinflammatory state (Vinchi *et al*., 2016). In both diseases HSCs are impaired but the direct contribution of IO to HSC dysfunction in these conditions has not been proved.

Since the vast majority of iron is metabolized or stored in mitochondria, IO and iron deficiency can negatively affect mitochondrial fitness and bioenergetic, thus impairing HSCs. Indeed, IO in mouse liver causes mitochondrial dysfunction through ROS generation (Moroishi *et al*, 2011). In addition, tumor cells which undergo ferroptosis exhibit smaller and fragmented mitochondria with reduced number of cristae (Dixon *et al.*, 2012).

Recently, limited intracellular iron content was found to promote mitochondrial FAO, resulting in increased HSC division, thus suggesting that iron can affect mitochondria also in HSCs (Kao Y-R, 2021). However, further investigations are required in order to understand how intracellular iron levels affect the metabolic and transcriptional programs underlying HSC function and fate. In this view, studies in hematological diseases characterized by dysregulated iron homeostasis will help to unravel the link between iron, ROS and HSC metabolism.

3 – β-Thalassemia

Thalassemias are rare autosomal recessive disorders characterized by reduced or absent synthesis of adult hemoglobin (Hb). Hb is a tetramer made of four polypeptide chains containing heme prosthetic group, and different combinations of globin chains are assembled during embryonic, fetal and adult life. Adult Hb is composed of two α-globin chains and two β-globin chains (HbA, $\alpha_2\beta_2$). Defects in α-globin chains give rise to α-thalassemia, whereas alterations in β-globin chains cause β-thalassemia (BThal).

It has been estimated that 1-5% of the world population are carriers of thalassemia mutations (Taher *et al*, 2018). Since thalassemia mutations confer resistance to malaria infection, the prevalence of thalassemia is highest in the Mediterranean area, sub-Saharan Africa, Middle Est, India and Southeast Asia. Moreover, due to population migrations, it has spread in non-endemic regions, such as North America and Europe, thus evolving into a global health issue (Kattamis *et al*, 2022).

3.1 – BThal pathophysiology

BThal is caused by mutations in the β-globin gene on human chromosome 11. More than 350 mutations have been identified and they include silent mutations, mild mutations leading to reduced synthesis of β-globin chains (β^+) and severe mutations causing complete absence of β-globin chains (β^0). BThal can be classified based on the severity of the clinical phenotype as BThal minor (heterozygote carrier), intermedia (patients $\beta^+\beta^+$) or BThal maior ($\beta^0\beta^0$ and $\beta^0\beta^+$) (Taher *et al*, 2021).

Impaired production of β-globin chains causes an imbalance between α and β-globin, and the accumulation of α-globin tetramers in red blood cells (RBCs). α-globin chains are unstable and precipitate, releasing iron and ROS, thus blocking the maturation and inducing premature death of erythroid precursors in the bone marrow (BM) (ineffective erythropoiesis, IE) and outside the BM (peripheral hemolysis). As a result, chronic hemolytic anemia occurs and impacts on multiple organ viability. Indeed, anemia and the resulting hypoxia stimulate the kidney to produce the hormone erythropoietin (EPO), which increases the proliferation of RBCs and IE. The enhanced production of RBCs in the BM is accompanied by BM expansion and subsequent bone defects. Bone diseases, including osteopenia and osteoporosis, are common complications of BThal patients (Taher *et al*, 2008). Moreover, to compensate for increased cell death, multiple sites of hematopoiesis are activated outside the BM, mainly in the spleen and liver, resulting in splenomegaly and hepatomegaly respectively. The exposure of senescent signals, such as phosphatidylserine (PS), in the membrane of RBCs during IE increases their pro-coagulant potential and, together with endothelial damage, and platelet, monocyte and granulocyte activation, induces hypercoagulability, leading to thrombotic events and pulmonary hypertension (Taher *et al.*, 2008). Finally, IE dysregulates iron homeostasis by increasing iron absorption and release from stores, resulting in iron overload (IO) and organ damage (Taher *et al.*, 2018) (Fig. 14).

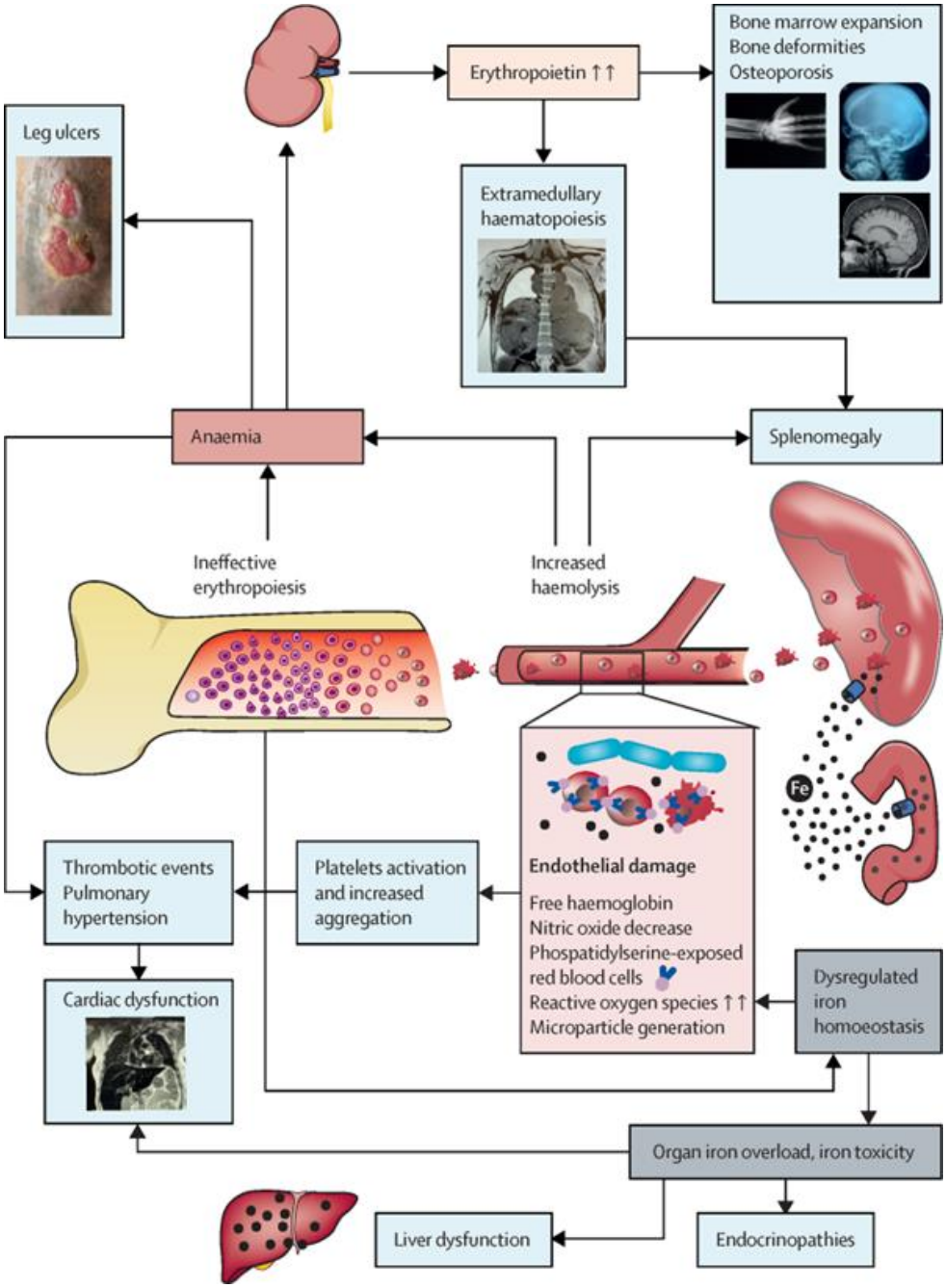

Figure 14. Pathophysiology of BThal. *The α/β chain imbalance results in IE, with compensative erythropoietic expansion in the BM and extramedullary hematopoiesis, chronic hemolytic anemia, hypercoagulability, and IO, resulting in multi-organ complications (From Kattamis et al., 2022).*

3.1.1 – Pathological effects of iron and ROS dysregulation

In BThal, as in other hemolytic disorders, the premature death of erythroid precursors releases iron and ROS, and promotes the production of new RBCs in the BM and in extramedullary sites. Increased erythropoiesis requires high iron for hemoglobin

synthesis and, as a consequence, enhances intestinal iron absorption and iron mobilization from the stores. During IE, high EPO levels stimulate the synthesis of the hormone erythroferrone (ERFE) by erythroid precursors. ERFE is a potent suppressor of hepcidin production, that leads to hyperabsorption of iron from the diet and high iron efflux from macrophages and hepatocytes into the circulation, thus resulting in primary IO. Vice versa, IO can contribute to IE further worsening the clinical picture. Moreover, iron intake from transfusion, the mainstay treatment for BThal, leads to secondary IO. Patients transfused with 2-4 units of blood per months usually intake 0.3-0.6 mg/kg iron per day, that accumulates in various organs due to the absence of a physiological mechanism to excrete excess iron (Taher *et al.*, 2021) (Fig.15).

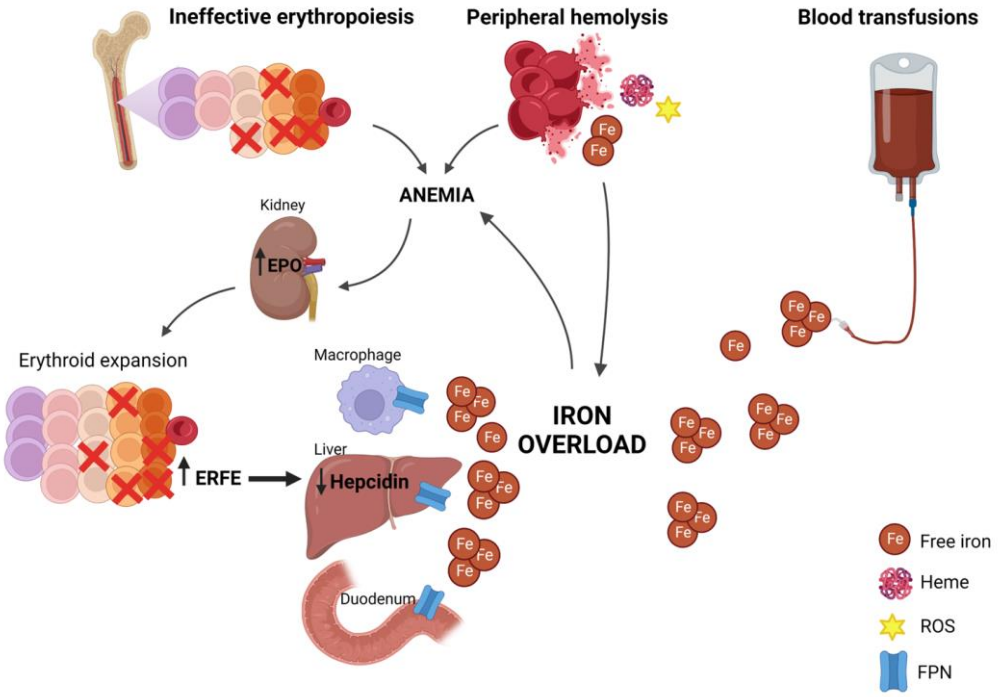

Figure 15. Causes of IO in BThal. *IE and peripheral hemolysis, hallmark of BThal pathophysiology, and therapeutic blood transfusions generate IO (created with BioRender.com).*

Excess plasma iron exceeds the iron-carrying capacity of transferrin (TF) and free non TF-bound iron (NTBI) is toxic due to its ability to induce extracellular and intracellular oxidative events. Excess ROS in the circulation might generate chronic sterile inflammation thus promoting endothelial dysfunction, platelet activation and aggregation with further ROS generation (Voskou *et al*, 2015). Moreover, NTBI can enter specific cells, such as hepatocytes, cardiomyocytes, pancreatic β cells and BM cells, causing oxidative damage of DNA, proteins and lipids ultimately resulting in cell death (Coffey

& Ganz, 2018). Observational studies conducted in non-transfused vs regularly transfused patients showed that both primary and secondary IO mainly affect the liver leading to higher liver iron concentration (LIC), but only secondary IO involves cardiac iron loading (Taher *et al*, 2010) (Fig. 16A, B).

A **B**

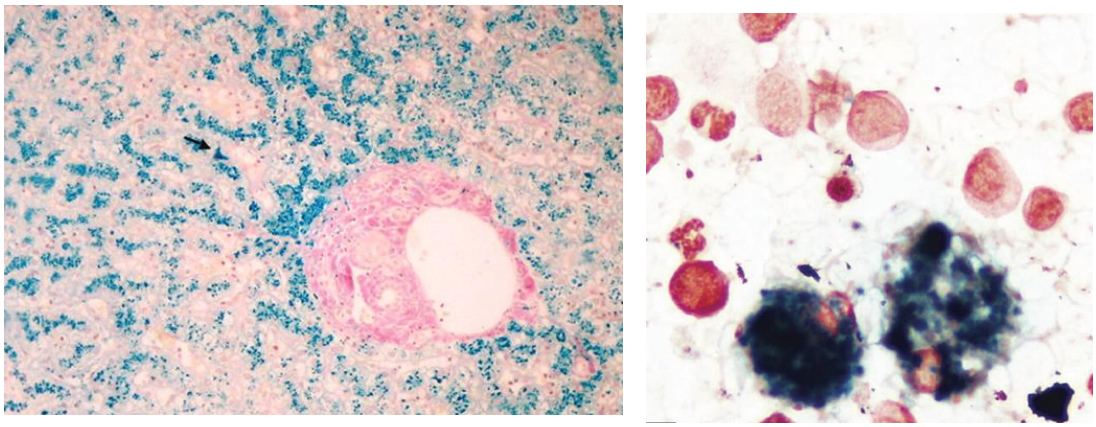

Figure 16. Tissue IO in BThal. *A) Perl's staining of the liver of BThal patient. Black arrow indicates iron deposit in blue (From Origa et al, 2007). B) Perl's staining of BM aspirates of BThal patient (From Ali M., 2020).*

Iron accumulation in different organs gives rise to different clinical complications: IO in the liver results in fibrosis, cirrhosis, that can lead to hepatocellular carcinoma, whereas cardiac IO causes cardiac siderosis, which is at the origin of arrythmias and heart failure. Moreover, endocrine dysfunction, such as hypogonadism, hypothyroidism and hypoparathyroidism, bone diseases and BM alterations can be the result of IO (Taher & Saliba, 2017). IO in the BM generates excess ROS, which impair the proliferation and differentiation of stromal cells (Crippa *et al*, 2019). Moreover, IO might affect hematopoietic stem cells (HSCs) but nothing is known in BThal (Chai *et al.*, 2015; Muto *et al.*, 2017). The quantification of IO historically relied on the analysis of serum ferritin levels and serum ferritin levels ≥800/1000 ng/ml are associated with clinically relevant IO. However, serum ferritin levels vary in response to inflammation and other stress conditions, thus limiting its reliability for the analysis of IO. On the contrary, magnetic resonance imaging (MRI) is an international reproducible technique for the non-invasive quantification of LIC and cardiac iron concentrations. LIC ≥5 mg/g indicates increased risk for morbidities linked to IO (Taher & Saliba, 2017).

3.2 – Murine models of BThal

The murine adult hemoglobin is a tetramer formed by two α-globin chains and two β-globin chains. Unlike humans, two β-globin genes, b1 (β^{major}) and b2 (β^{minor}) are expressed and the $\alpha_2\beta_2^{major}$ constitute 80% of murine hemoglobin, whereas $\alpha_2\beta_2^{minor}$ only 20% (Whitelaw *et al*, 1990).

Several mouse models recapitulating the main features of BThal have been exploited (Casu *et al*, 2020; McColl & Vadolas, 2016; Shehee *et al*, 1993; Skow *et al*, 1983). Among them, $Hbb^{th3/+}$ (*th3*) mice lacking both β^{major} and β^{minor} genes, show a more severe phenotype but they don't require blood transfusions to survive. While homozygous die perinatally, heterozygous *th3* mice display IE and anemia with dramatically reduced RBC counts, hemoglobin and hematocrit, increased reticolocytes and extramedullary hematopoiesis (Yang *et al*, 1995). In addition, they have bone abnormalities, including osteoporosis (Vogiatzi *et al*, 2010), and increased risk of thrombotic events reminiscent of those in humans (Kalish *et al*, 2015). Finally, *th3* mice exhibit high ERFE production and subsequent decreased expression of hepcidin, resulting in iron accumulation especially in the spleen. Thus, *th3* mice is a useful model to study primary IO (Yang *et al*., 1995).

3.3 – Therapeutic options for BThal

The mainstay treatment for severe BThal consists in regular blood transfusions to suppress IE and increase Hb concentration, along with iron chelation therapies to reduce iron burden. BThal patients are categorized based on transfusion requirements into transfusion-dependent thalassemia (TDT) or non-transfusion-dependent thalassemia (NTDT). While TDT patients need transfusions to survive, NTDT patients can require transfusions occasionally but not for their entire lifetime (Taher *et al.*, 2018). Recently, new therapeutic agents that ameliorate anemia and IO have been proposed (Cappellini *et al*, 2020). However, the only curative options are allogeneic HSC transplantation (HSCT) or autologous transplantation of genetically corrected cells upon gene therapy (Caocci *et al*, 2017; Lidonnici & Ferrari, 2018).

3.3.1 – Iron chelation therapy

Iron chelation therapy (ICT) counteracts excess iron loading from the diet and from blood transfusions, thus limiting downstream pathophysiological complications.

Three iron chelators, used alone or in combination, have been approved by regulatory agencies for ICT: deferoxamine (DFO), deferiprone (DFP) and deferasirox (DFX), that differ for administration route, targeted organs, efficacy and safety. ICT is still an organ-based approach: DFX monotherapy or in combination with DFO is the strategy of choice for TDT patients with severe cardiac and hepatic IO, whereas DFP monotherapy or in combination with DFO is recommended for TDT patients with lower hepatic iron burden (Taher & Saliba, 2017). Therefore, adequate quantification of IO before ICT is required to appropriately determine chelation regimen and continuous monitoring of iron levels during ICT is necessary for proper dose adjustment avoiding overchelation. In addition, adherence to treatments is essential for successful ICT.

Although ICT improved patient survival, BThal patients still display IO and related complications (Angelucci & Pilo, 2016). Moreover, iron chelators show several side effects, including bone defects, renal dysfunction and hepatic failure (Kattamis *et al.*, 2022). Therefore, a better understanding of systemic and intracellular iron regulation in BThal will improve current ICTs and ameliorate patients' quality life.

3.3.2 – Strategies to improve anemia and IO

Novel pharmacological agents can reduce IE and ameliorate anemia. Among them, two twin molecules Luspatercept and Sotatercept bind to TGFb and promote erythroid maturation. Luspatercept has been reported to reduce of at least 33% blood transfusion requirements in 21% of TDT patients and induce transfusion independence in 11% of TDT patients (Cappellini *et al.*, 2020). Mitapivat, a pyruvate kinase (PK) activator, was found to ameliorate IE and anemia by enhancing the metabolism of RBCs in *th3* mice (Matte *et al*., 2021).

Strategies aimed to increase hepcidin levels have shown beneficial effects on IE in preclinical and clinical studies. As first proof of principle, the upregulation of hepcidin mediated by TMPRSS6 deletion was reported to normalize serum iron concentration (SIC) and LIC, and increase Hb (Nai *et al*, 2012). Then,39inihepcidinss, small peptides that act as the endogenous hepcidin, suppressing intestinal iron absorption and iron

release from the stores, were shown to reduce IO and improve IE and anemia in *th3* mice (Casu *et al*, 2016).

Moreover, the oral ferroportin inhibitor Vamifeport (VIT-2763) ameliorates IE and anemia in *th3* mice (Nyffenegger *et al*, 2021) and reduces serum iron and transferrin saturation in NTDT patients (Taher, 2022).

3.3.3 – Allogeneic hematopoietic stem cell transplantation and gene therapy

The only definitive cure for BThal patients consists in the replacement of impaired RBCs with those differentiating from normal donor HSCs after HSCT.

Allogeneic HSCT requires HLA-matched donor and children transplanted from HLA-matched sibling donor show a disease-free survival exceeding 80% (Angelucci *et al*, 2014). However, only few patients have HLA-matched siblings and alternative donors for HSCT can be HLA-matched unrelated donor or haploidentical but in both contexts overall survival of transplanted patients is lower due to high risk of graft failure and graft-versus-host-disease (GVHD) (Lucarelli *et al*, 2012). Moreover, positive outcome of HSCT correlates with patient age, thus, according to current guidelines allogeneic HSCT is recommended for patients younger than 14 years old and with a suitable HLA-matched donor.

Autologous HSCT after gene therapy is a promising therapeutic strategy feasible for a large number of patients, including those lacking an HLA-matched donor (Lidonnici & Ferrari, 2018). Autologous hematopoietic stem and progenitor cells (HSPCs) are collected through leukapheresis or BM aspirates, enriched for $CD34^+$ cells and genetically modified by gene addition, using lentiviral vectors expressing β-globin or fetal Hb gene under the control of globin transcriptional regulatory elements, or gene editing approaches. Once corrected, HSPCs are subjected to quality control tests and then reinfused into patients directly after manipulations or after cryopreservation and thawing. Before transplantation, patients are treated with chemotherapy to deplete endogenous HSPCs and favour the engraftment of corrected cells (Ferrari *et al*, 2021) (Fig. 17).

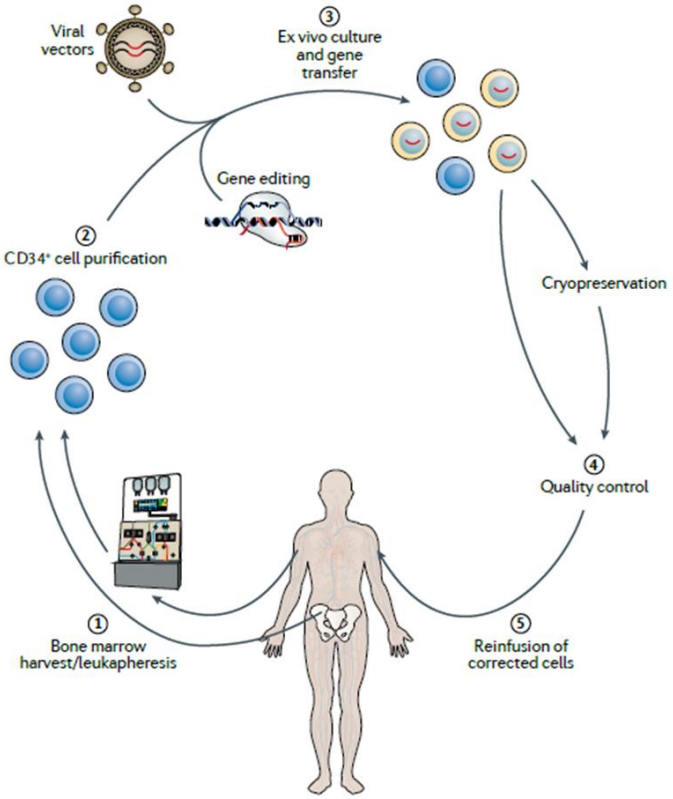

Figure 17. Gene therapy for BThal. *Stepwise procedure of gene therapy: 1) autologous HSPC collection, 2) CD34⁺ enrichment, 3) gene therapy by gene addition using viral vectors or gene editing, 4) quality control tests, 5) transplantation of corrected cells (Modified from Ferrari et al., 2021).*

In the first clinical trial for BThal, TDT patients were infused with autologous HSPCs transduced with BB305 lentiviral vector encoding for a β-globin transgene with anti-sickling properties (HbA^{T87Q}). 80% of non-$\beta^0\beta^0$ patients and 38% of $\beta^0\beta^0$ patients achieved transfusion independence and the remaining patients reduced the number of transfusions (Thompson *et al*, 2018).

Moreover, in TIGET-BTHAL clinical trial, nine TDT patients, three adults and six children, were treated with intrabone administration of autologous HSPCs transduced with the lentiviral vector GLOBE encoding for β-globin gene under the control of a minimal locus control region (LCR) (Marktel *et al*, 2019; Miccio *et al*, 2008). Adult patients displayed reduced transfusion requirements and three out of four evaluable children reached transfusion independence (Marktel *et al.*, 2019).

Gene editing directly corrects genetic mutations or destroys specific DNA sequences by using nucleases, such as zinc finger nucleases (ZFNs) and clustered regularly interspaced short palindromic repeat (CRISPR)-associated nuclease Cas9. Recently, gene

editing approaches for BThal have been developed to target BCL11A gene in order to restore the expression of fetal Hb, thus increasing Hb concentrations and ameliorating anemia (Antoniani *et al*, 2018; Locatelli F., 2022).

In both allogeneic and autologous transplantation setting, the transplanted HSPCs and the recipient BM microenvironment are central elements for a successful outcome. Thus, a deep understanding of the status of HSCs and BM niche and the factors that affect them is essential to improve the success of HSCT for BThal patients.

4 – BThal HSC and BM niche

In the allogeneic HSCT the host BThal niche could reduce the engraftment of the normal donor HSPCs, whereas in the autologous setting, both the donor HSPCs and the BM niche are altered and can compromise the clinical outcome. Although HSCs and the BM microenvironment play a central role in the therapeutic success of HSCT, they are still poorly investigated in BThal. Little is known about how chronic hemolysis and IE, and subsequent stress signals, such as iron, ROS and inflammatory cytokines, alter the BM niche and HSC pool.

Recent studies have shown BThal HSC dysfunction due to the prolonged persistence into an impaired BM niche in *th3* mice (Aprile *et al*, 2020). Alterations of BM cell populations, such as stromal cells (Crippa *et al.*, 2019), and accumulation of toxic molecules, including iron and ROS, can negatively affect BThal HSCs.

4.1 – HSCs

Recently, Aprile et al. reported for the first time an impaired BThal HSC function using *th3* mouse model recapitulating severe BThal intermedia (Aprile *et al.*, 2020). The authors analysed the most primitive HSCs defined with SLAM family markers as Lin^-, $cKit^+$, $Sca1^+$ $CD48^-$ $CD150^+$ (Oguro *et al.*, 2013) and they found a reduced absolute number of HSCs in *th3* mice as compared to wt. Moreover, *th3* HSCs have decreased quiescence and are more actively cycling, as shown by increased % of HSCs in S and G2/M phase at the expense of G0 phase, and significant lower frequency of label-retaining cells in *th3* mice. These data were further confirmed by RNAseq analyses performed on sorted *th3* HSCs, revealing a positive enrichment of "cell cycle G1/S phase

transition" category, and reduced expression of stemness genes, including *Cdkn1c*, *Runx1l1*, *Fgd5* and *Hes1*. In line with increased cell proliferation, *th3* HSCs accumulate DNA damages.

To evaluate HSC function, the authors performed *in vitro* serial replating assay and key transplant experiments. In particular, primary transplantation of an equal number of wt and *th3* HSCs into *th3* mice revealed a competitive disadvantage of *th3* HSCs as compared to the wt grafted counterpart, which was further worsen after secondary transplantation, thus indicating reduced repopulating ability and self-renewal. However, the *th3* HSC defects were restored upon transplantation into wt recipients.

Overall, these results suggest that BThal HSC dysfunction is not intrinsic but it's caused by an altered BM niche. Consistently, Gene Set Enrichment Analysis (GSEA) on RNAseq data revealed a significant enrichment of genes associated with cellular responses to stress in the *th3* HSC transcriptome profile, thus indicating that stress signals in the BThal BM niche alter HSC function.

Interestingly, the defects in HSC frequency and cell cycle are absent in newborn animals, whereas they appear around 4-weeks of age and get worse in adult mice, thus HSC dysfunction derives from the prolonged residence in impaired BM niche, which is progressively worsened by disease progression.

Of note, no differences in the frequency of *th3* MMPs and more committed progenitors were reported, which could imply a different behaviour between HSCs and progenitors in BThal niche that requires further investigations.

In line with the findings in the murine model, TDT patients have increased frequency of $CD34^{+}CD38^{-}$ primitive HSPCs in the S/G2/M phase of the cell cycle as compared to healthy donors. Moreover, TDT $CD34^{+}$ display higher response to stress stimuli, including oxidative stress and DNA damage, and reduced expression of key stemness genes (Aprile *et al.*, 2020; Lidonnici M.R., 2021), thus suggesting that also TDT HSPCs are exposed to a stressed BM niche.

Overall, these studies point out the active role of BM niche in regulating HSC fitness. Moreover, the reversibility of *th3* HSC dysfunction by interaction with a healthy BM niche prompt a deeper investigation of the cell populations and stress factors in BThal BM niche to ameliorate current HSCT protocols for BThal patients.

4.2 – Stromal cells

Bone abnormalities, such as enlargement of cranial and facial bones, spontaneous fractures and bone loss, are common features of BThal patients (Voskaridou & Terpos, 2004). Also *th3* mice exhibit reduced bone volume and number of trabeculae, and increased bone fragility (Vogiatzi *et al.*, 2010). The causes of bone disease are controversial and include endocrinopathies, BM expansion and IO. Recently, Aprile et al. showed that the low bone mass in *th3* mice is caused by decreased levels of circulating hormone PTH, which was already reported low in BThal patients (Angelopoulos *et al*, 2006; Aprile *et al.*, 2020). PTH is a key regulator of bone metabolism and HSC maintenance through Notch signaling (Calvi *et al.*, 2003). Moreover, it directly acts on MSCs by priming them towards OB lineage (Fan *et al*, 2017). Low PTH levels in *th3* mice reduce OB activity and inhibit their secretion of the Notch ligand JAG1 and OPN, both critical regulators of HSC function, thus causing *th3* HSC defects (Aprile *et al.*, 2020). *In vivo* administration of PTH to *th3* mice rescues bone defects, as shown by increased bone mineral density (BMD), enhances the expression of JAG1 and OPN by stromal cells, ultimately resulting in the rescue of *th3* HSC frequency and quiescence, and amelioration, but not complete normalization, of repopulating ability.

Also, *th3* MSCs have reduced frequency and JAG1 secretion due to decreased PTH levels (Aprile *et al.*, 2020). These data were corroborated also by findings in patients' samples (Crippa *et al.*, 2019).

Overall, these findings indicate that oBs and MSCs are impaired and defective crosstalk between HSCs and stromal cells alters HSC function in BThal. Correction of HSC-stromal niche crosstalk improves HSC function in *th3* mice, paving the way towards novel strategies aimed to correct BM niche to preserve HSC function. However, lack of a complete restoration to normal levels of *th3* HSC repopulating ability upon PTH treatment suggests that in the complex BThal BM niche other cellular and molecular factors might be involved in regulating HSCs.

4.3 – The role of IO in BThal BM niche

IO, caused by IE and therapeutic blood transfusions, is a hallmark of BThal pathophysiology. Clinical reports revealed that the iron burden before and after transplant

affects the outcome of HSCT, thus adequate management of IO is required to ameliorate BThal BM niche and improve HSC function (Pilo & Angelucci, 2019). Upon transplantation with HLA-matched related donor cells, higher mortality was reported in BThal pediatric patients with extensive hepatic siderosis as compared to patients with lower liver damage (Lucarelli *et al*, 1996), thus suggesting that transplant outcome is influenced by the quality of chelation that patients received before transplant. Serum ferritin normalizes after HSCT only in few patients with limited iron burden before transplant but the vast majority of patients still display IO and require ICT (Angelucci & Pilo, 2016). Therefore, a deep understanding of the role of iron in BThal BM niche and HSCs is pivotal for a successful therapeutic outcome.

IO damages the most primitive $CD146^+$ $CD271^+$ MSCs in BThal patients. Recently, Crippa et al. reported that BThal MSCs uptake and accumulate excess iron, as shown by direct evaluation of intracellular iron content by Perl's staining, and upregulation of iron transporters, including *TFR1*, and ferritin upon *in vitro* iron administration (Crippa *et al.*, 2019). IO generates oxidative stress, thus reducing the frequency and the proliferation of BThal MSCs and impairing their differentiation. Given the crucial role of MSCs in preserving HSC function and stemness, the authors investigated whether IO negatively affects the crosstalk between MSCs and HSCs, thus impairing HSCs. Interestingly, BThal MSCs exhibit reduced expression of key hematopoietic supportive factors, such as *SCF*, *CXCL12* and *ANGPT1*, and fail to expand HSCs in transwell migration assay and 2D co-culture experiments. To test BThal MSC function *in vivo*, they were co-transplanted together with healthy HSPCs into immunodeficient mice and the reduced engraftment suggests that BThal MSCs fail to sustain HSCs. Moreover, BThal MSCs are less efficient in generating a proper niche *in vivo*. Indeed, transplantation of a humanized ossicle, consisting in gelatin scaffold pre-seeded with BThal MSCs, healthy ECs and HSPCs, into immunodeficient mice showed reduced number of hematopoietic cells and a delay in the formation of bone and vessels as compared to ossicles containing healthy MSCs. Of note, treatment with iron chelation in presence of iron reduced the expression of iron transporters and restored the HSC-MSC niche crosstalk.

Overall, these data suggest that IO impairs BThal MSCs, thus negatively impacting on HSCs.

IO can indirectly affect HSCs by altering other BM niche populations, such as osteolineage cells but little is known about how iron damages these cells in BThal (Terpos & Voskaridou, 2010). Moreover, IO might induce vascular inflammation with increased expression of pro-inflammatory cytokines and enhanced adhesion of RBCs, leukocytes and platelets to the endothelium, thus causing BThal EC dysfunction and favouring thrombotic events (Voskou *et al.*, 2015; Gursel *et al*, 2018).

Finally, recent studies have shown that free iron in SCD anemia can induce Mφs switching towards M1 phenotype (Vinchi *et al*, 2016), which was reported to reduce HSC self-renewal, thus proposing a link between IO-Mφs-HSCs also in BThal.

However, we cannot exclude a direct impact of IO on HSCs. HSCs can uptake and store iron and intracellular IO impairs their repopulating ability and self-renewal through ROS production (Muto *et al.*, 2017). Increased ROS levels drive HSC differentiation, whereas excessive ROS destroy cell components culminating in cell death. Nevertheless, the direct effect of IO and the resulting ROS on BThal HSCs is still unexplored (Zhou *et al*, 2022).

Overall, these findings highlight multi-factorial alterations in BThal BM niche, in which hormonal factors, such as PTH, cytokines and stress signals, including iron, ROS and inflammatory molecules, secondary to the primary genetic defect, damage HSCs directly or indirectly through other BM cell populations. Identification of key cellular and molecular players will help to improve HSC transplantation and gene therapy approaches for BThal (Fig. 18).

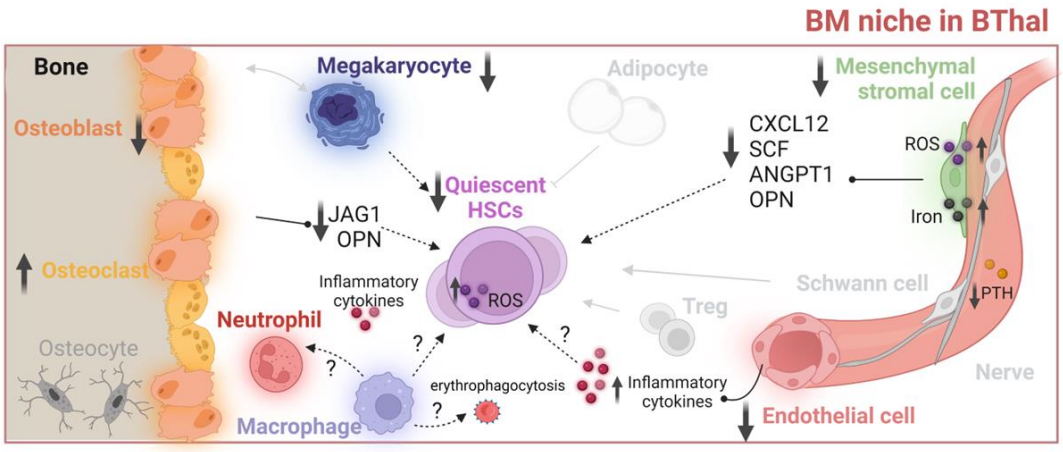

Figure 18. BThal BM niche. *BThal HSC function is impaired due to the chronic persistence into an altered BM niche. Several BM niche populations, such as oBs, MSCs, MKs and Mφs, are impaired and toxic molecules, including iron, ROS and inflammatory cytokines, accumulates in BThal BM niche, potentially causing HSC functional decline (Modified from Aprile et al., 2022).*

AIM OF THE WORK

Cellular metabolism is a key regulator of HSC maintenance and HSCs adapt their metabolic state to signals in the BM niche. The presence of ROS at physiological levels drives HSC proliferation and differentiation by enhancing glycolysis and OXPHOS, but when in excess ROS damage cellular components ultimately resulting in cell death. Iron is an important source of ROS within the cell and recent evidence highlighted its role in regulating HSC self-renewal and differentiation. However, the effects of iron on HSC metabolism are still unexplored.

Our previous studies revealed an impaired function and activated transcriptional responses to stress in HSCs from thalassemic *th3* mice, characterized by systemic and chronic IO. Moreover, we found a positive enrichment of genes involved in metabolic processes in *th3* HSC transcriptome profile. We also reported that IO impairs BM mesenchymal stromal cells in BThal patients. However, there is no evidence of the direct effect of IO on HSCs in BThal.

The proposal of this project is to gain new insight about the role of iron on HSC biology and to investigate which metabolic pathways are triggered by intracellular iron levels. Understanding the metabolic programs induced by iron might be crucial to identify novel therapeutic target for hematological disorders with impaired iron homeostasis.

To this aim, we investigated intracellular iron content and resulting ROS accumulation, mitochondrial activity and metabolism of HSCs in *th3* mice and, as proof-of-concept in normal mice treated with different regimens of iron. Finally, to explore the feasibility of correction strategies in BThal, we evaluated the restoration of *th3* HSC frequency and quiescence after the targeting of dysregulated mechanisms.

RESULTS

1 – HSCs display intracellular and mitochondrial iron overload in *th3* mice

Previous studies from our group showed impaired function of BThal HSCs due to prolonged exposure to stress signals in the BM niche (Aprile *et al.*, 2020). Among them, IO was reported to alter BM MSCs in BThal patients (Crippa *et al.*, 2019) but its impact on HSCs is still unknown. We hypothesized that accumulation of iron might directly affect HSC function.

To explore the effects of IO and iron regulation in BThal HSCs, we performed RNA-sequencing (RNAseq) analysis of HSCs from *th3* mice, that recapitulate the major features of severe BThal intermedia, including IO (Yang *et al,* 1995). Lineage negative cells (Lin^-), enriched in hematopoietic stem and progenitor cells, were immunoselected and HSCs were purified from Lin^- cells using FACS-based methods. HSCs were phenotypically defined as SLAM HSCs: Lin^-, $cKit^+$, $Sca1^+$ $CD150^+$ $CD48^-$ cells (Kiel *et al*, 2005; Oguro *et al.*, 2013) Fig. 1A). From pools of 3 mice each we obtained around 5000 SLAM HSCs. Analysis of differentially expressed genes (DEG) by DeSEQ Software revealed a statistically significant enrichment of genes involved in iron transport and homeostasis in *th3* SLAM HSCs (Fig. 1B). Among them, transferrin receptor 1 (*Tfrc*), ferritin (*Fth1, Ftl1*), *Steap3,* and ferroportin (*Slc40a1)* are upregulated (Fig. 1C), thus suggesting abnormal iron homeostasis. Moreover, the positive enrichment of genes encoding enzymes involved in heme synthesis, such as *Hmbs*, *Alad*, *Cpox* and *Fech* (Fig. 1B) could indicate increased heme production, a mechanism that might result from increased intracellular iron accumulation (Poli *et al*, 2021). Thus, we hypothesized that altered iron homeostasis might be involved in *th3* SLAM HSC dysfunction.

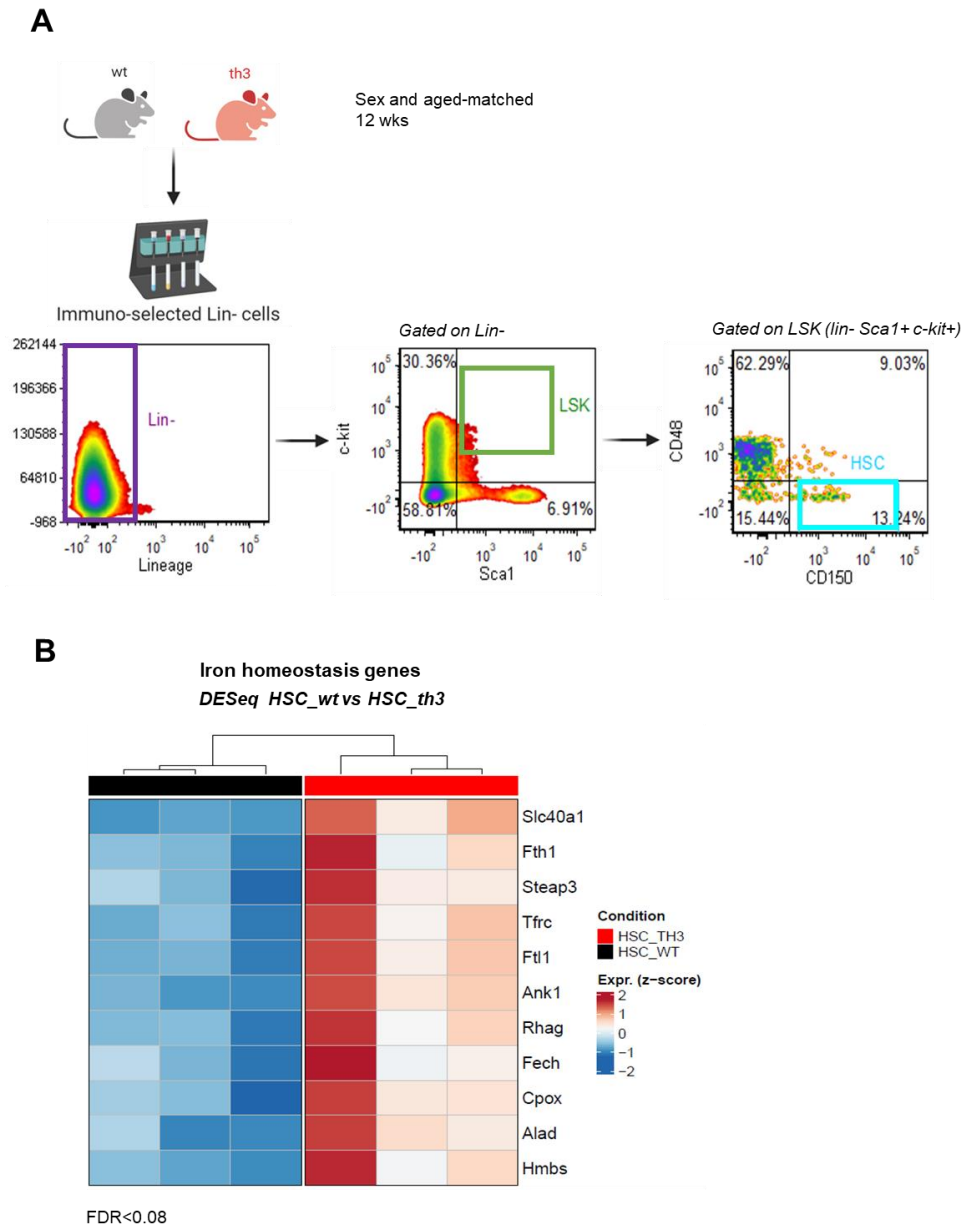

C

Gene symbol	Gene name	Function	FC HSC Th3 vs HSC wt	FDR
Tfrc	Transferrin receptor 1	Fe^{3+} importer	1.811	<0.05
Steap3	STEAP family member 3	Metalloreductase reducing Fe^{3+} to Fe^{2+}	1.815	<0.01
Fth1	Ferritin heavy chain 1	Iron storage	1.409	<0.05
Ftl1	Ferritin light chain 1	Iron storage	1.432	<0.05
Slc40a1	Ferroportin 1	Fe^{2+} exporter	2.395	<0.05

Figure 1. Upregulation of iron homeostasis genes in th3 HSCs. *(A) Gating strategy of HSCs based on SLAM expression in LSK fraction from adult th3 and age-matched wt mice. (B) Analysis of Differentially expressed genes (DEG) by DESeq software reveals the upregulation of iron transport and iron homeostasis genes in th3 SLAM HSCs compared to wt (wt, n=3 pools; th3,*

n=4 pools). (C) Fold change (FC) and FDR of iron transport and homeostasis genes among DEG between wt and th3 SLAM HSCs (wt, n=3 pools; th3, n=4 pools).

Iron enters the cell in the form of ferric ion (Fe^{3+}) bound to the transferrin receptor 1 by receptor-mediated endocytosis. Once in the endosome, Fe^{3+} is released from the complex and is reduced to ferrous iron (Fe^{2+}), which, in turn, enters the transient cytosolic labile iron pool (LIP), available for immediate cellular use. LIP is involved in cellular processes such as DNA synthesis and repair and cell cycling. In contrast, excess Fe^{2+} is exported by ferroportin or converted to Fe^{3+} and stored in ferritin (Gao *et al*, 2019). To directly measure the intracellular content of iron in HSCs, we stained Lin^- cells with the iron-sensitive fluorophore calcein acetoxymethyl ester (calcein-AM), the fluorescence of which is quenched on binding to free metabolically active Fe^{2+} in the cytoplasm (Kakhlon & Cabantchik, 2002). The median fluorescent intensity (MFI) of calcein-AM was significantly lower in *th3* SLAM HSCs as compared to wt controls, thus indicating an increased intracellular iron aboundance of almost 2-fold (Fig. 2A).

As control, we evaluated iron content in macrophages identified by the expression of F4/80 surface marker. $F4/80^+$ macrophages control and maintain iron homeostasis by mediating the erythrophagocytosis of damaged or senescent erythrocytes mainly in the spleen but also in the BM (Korolnek & Hamza, 2015). As expected, *th3* splenic $F4/80^+$ macrophages accumulated more iron than the wt counterparts, whereas no differences were found between *th3* and wt $F4/80^+$ macrophages derived from BM. When we compared in wt mice the intracellular iron content of SLAM HSCs to that of splenic and BM $F4/80^+$ macrophages isolated from the same mouse, we found a higher calcein-AM MFI, indicating a lower intracellular iron content in SLAM HSCs. However, *th3* SLAM HSCs displayed intracellular iron content similar to those of wt $F4/80^+$ macrophages that are normally involved in iron phagocytosis (Fig. 2B).

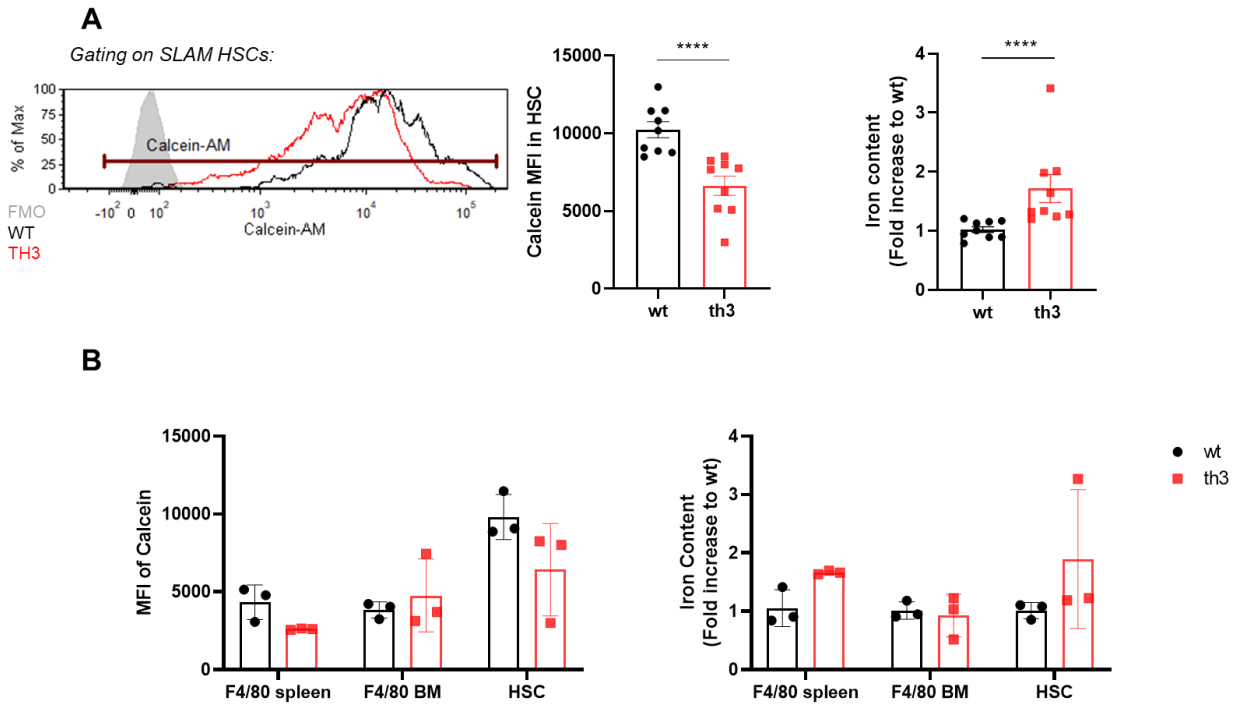

Figure 2. Intracellular iron accumulation in th3 HSCs and macrophages. *(A) Quantification of intracellular iron content in th3 and wt SLAM HSCs by flow cytometry. Representative flow cytometry histogram and Mean Fluorescence Intensity (MFI) of calcein-am is reported. On the right data are expressed as fold increase to wt (wt, n=9; th3, n=9). (B) Quantification of intracellular iron content in splenic F4/80⁺ macrophages, BM F4/80 ⁺ macrophages and SLAM HSCs from th3 and wt mice. MFI of calcein-am is reported, on the right data are expressed as fold increase to wt (wt, n=3; th3, n=3).*
*Mann-Whitney test: ****, p<0.0001.*

The increased iron phagocytosis by t*h3* splenic F4/80$^+$ macrophages confirmed the role of the spleen as the major organ involved in storage of iron in excess in *th3* mice. By contrast, the absence of differences in terms of intracellular iron content between *th3* and wt BM F4/80$^+$ macrophages could indicate lack of excess iron in *th3* BM. Nevertheless, the upregulation of *Tfrc* (Fig. 1B-C), the only identified iron importer, suggest that *th3* HSCs can uptake iron from the microenvironment. Thus, the data in F4/80$^+$ BM macrophages seem to be related to the ability of calcein-AM dye to detect minimal variations of intracellular iron content.

Thus, we wondered whether other molecular mechanisms could contribute to intracellular IO in *th3* HSCs. Heme, an iron-containing porphyrin, constitutes 95% of the total iron in humans and heme degradation mediated by heme oxygenase 1 (*Hmox1*) releases iron in the cellular cytoplasm (Donegan *et al*, 2019). *Hmox1*-mediated heme-iron

recycling has been reported to worsen *th3* phenotype and inhibition of *Hmox1* ameliorates anemia and reduces liver IO in *th3* mice (Garcia-Santos *et al*, 2018). However, the effects of heme-iron recycling in HSCs have not been investigated so far. Our RNAseq and Droplet digital PCR (ddPCR) analyses revealed an upregulation of *Hmox1* in *th3* SLAM HSCs (Fig. 3A-B), thus suggesting an involvement of *Hmox1*-mediated heme degradation in intracellular IO.

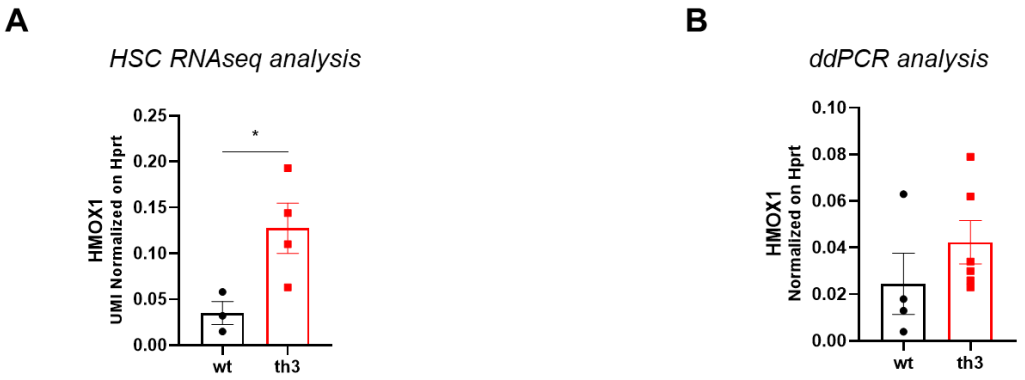

Figure 3. Upregulation of Hmox1 in th3 HSCs. *Expression levels of Hmox1 in wt and th3 SLAM HSCs. (A) RNAseq normalized expression on Hprt housekeeping gene (wt, n=3 pools; th3, n=4 pools). (B) ddPCR analysis using Hprt as housekeeping gene (wt, n=4 pools; th3, n=6 pools). Mann-Whitney test: *, p<0.05.*

Since mitochondria are major hubs for iron storage and utilization, we wondered whether mitochondria in *th3* HSCs accumulate iron. To test this, we stained Lin^- cells with mito-FerroGreen, a fluorescent probe that selectively detects mitochondrial free Fe^{2+}, constituting the mitochondrial iron pool (Hirayama *et al*, 2018). Mito-FerroGreen contains a mitochondria-targeted group that drives its entry into the organelle. Once in the mitochondria, it reacts with free Fe^{2+} and exhibits green fluorescence. Interestingly, we found a significant higher % of Mito-FerroGreen$^+$ SLAM HSCs and MFI of Mito-FerroGreen in *th3* mice, thus suggesting increased Fe^{2+} content in mitochondria (Fig. 4).

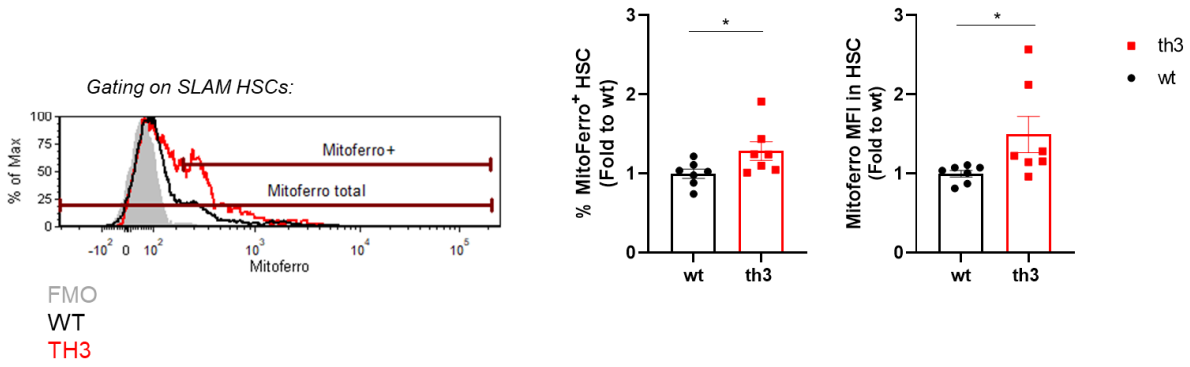

Figure 4. Iron accumulation in mitochondria in th3 HSCs. *Quantification of iron content in mitochondria in th3 and wt SLAM HSCs by flow cytometry. Representative flow cytometry histogram and MFI of Mito-FerroGreen dye is reported. Data are expressed relative to wt (wt, n=7; th3, n=7).*
*Mann-Whitney test: *, p<0.05.*

Collectively, these data indicate for the first time intracellular and mitochondrial IO in *th3* SLAM HSCs.

2 – HSCs have dysfunctional mitochondria in *th3* mice

Mitochondrial iron is mainly utilized in heme synthesis and iron-sulfur cluster biogenesis, and also some of the ETC complexes contain iron. Thus, iron level perturbations can negatively impact mitochondrial health and function (Dixon *et al.*, 2012; Moroishi *et al.*, 2011). However, the link between iron and mitochondria in HSCs is still missing. Given the increased mitochondrial iron content, we hypothesized an impairment in mitochondrial fitness in *th3* HSCs.

To address this possibility, we first examined the expression of genes involved in mitochondrial processes. Mitochondria are dynamic organelles and mitochondrial function is regulated by cycles of biogenesis, fission, fusion and degradation through mitophagy, which in concert constantly participate in the remodelling of the mitochondrial network (Chan, 2012). RNAseq normalized expression, as Unique Molecular Identifier (UMI) counts normalized to *Hprt* housekeeping gene, revealed the downregulation of mitochondria related genes in *th3* SLAM HSCs. UMI are short

sequences used to uniquely tag each transcript during library preparation before cDNA amplification, in order to filter out duplicate reads and PCR errors with a high level of accuracy and report unique reads (Sena *et al*, 2018). We found a reduced expression of *Tfam* and *Tfb1m*, the major regulators of mitochondrial biogenesis (Fig. 5A), along with the downregulation of key players of mitophagy (Fig. 5B), such as *Ulk1*, *Optn*, *Gabarapl1* and *Map1lc3b*. Collectively, these data suggest a reduced biogenesis of new mitochondria and the accumulation of damaged mitochondria in *th3* HSCs. Moreover, we reported a reduced expression of genes involved in mitochondrial fission, including the cytosolic initiator Dynamin-related protein 1 (*Drp1*) and fission mediators, such as *Mff*, *Fis1* and *Mief1*. (Fig. 5C). Of note, a reduced mitochondrial fission has already been linked to impaired mitochondria function in normal HSCs (Hinge *et al.*, 2020). Thus, altered mitochondrial dynamics might be responsible for impaired mitochondrial activity of *th3* HSCs.

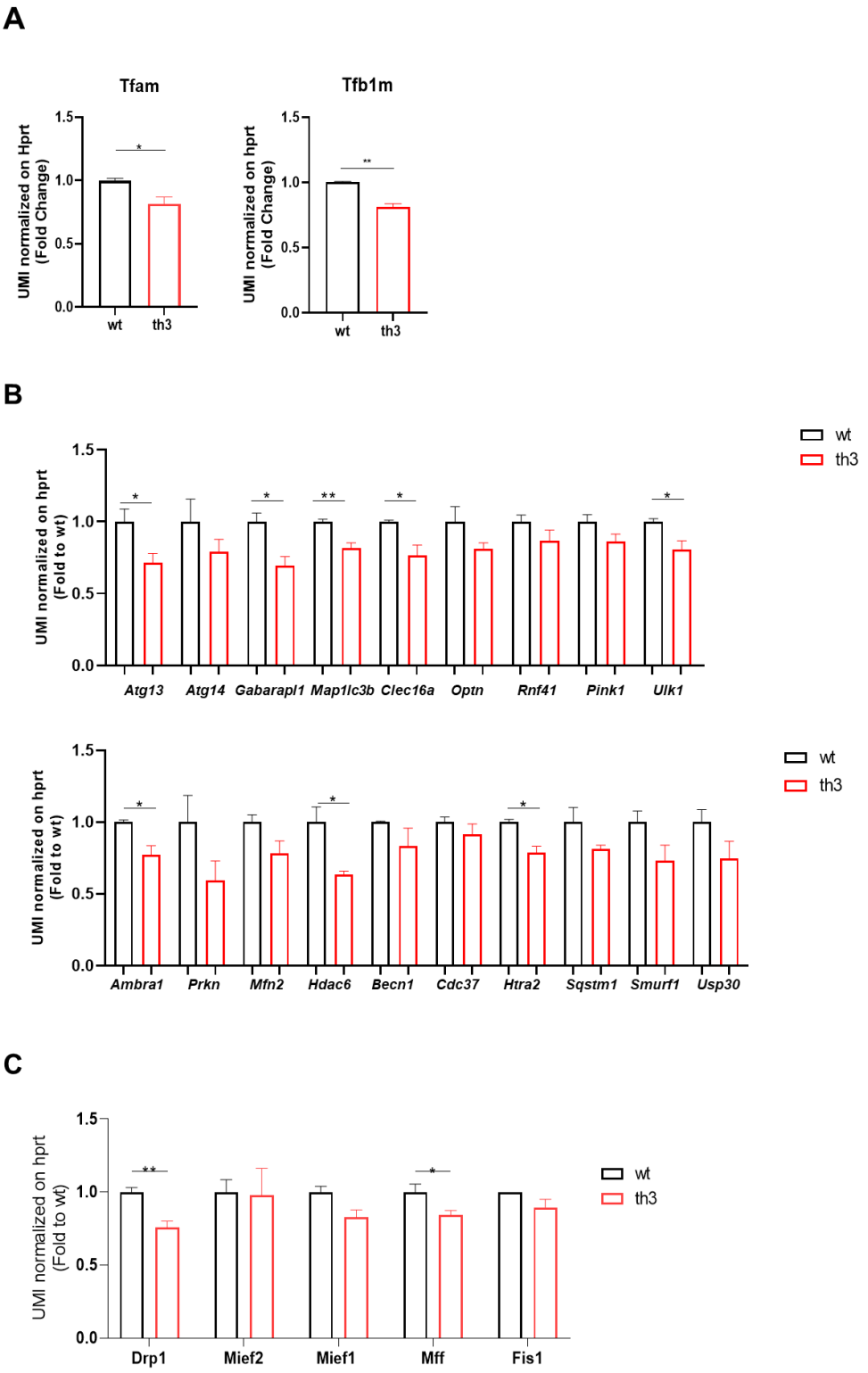

Figure 5. Downregulation of mitochondrial dynamic genes in th3 HSCs. *(A) RNAseq normalized expression to Hprt housekeeping gene of Tfam, Tfb1m in SLAM HSCs from wt and th3 mice (wt, n=3 pools; th3, n=4 pools). (B) RNAseq normalized expression to Hprt housekeeping gene of key mitophagy players in SLAM HSCs from wt and th3 mice (wt, n=3 pools; th3, n=4 pools). (C) RNAseq normalized expression to Hprt housekeeping gene of mitochondrial*

fission genes Drp1, Mief2, Mief1, Mff and Fis1 in SLAM HSCs from wt and th3 mice (wt, n=3 pools; th3, n=4 pools).
*Mann-Whitney test: **, p<0.01; *, p<0.05.*

To evaluate if these transcriptional alterations result in changes of the network of mitochondria in *th3* HSCs, we analysed mitochondrial mass by flow cytometry after staining Lin^- cells with Mitotracker-green (MTG) dye. MTG selectively accumulates in the mitochondrial matrix, regardless of mitochondrial activity (Presley *et al*, 2003). We reported a lower total MFI of MTG in *th3* SLAM HSCs due to reduced frequency and MFI in MTG^{high} HSCs, thus suggesting reduced mitochondrial mass (Fig. 6A).

Since the reduced mitochondrial mass could be due to reduced number of mitochondria and/or their size, we analysed mitochondria by transmission electron microscopy (TEM). TEM analysis usually requires millions of cells, making it challenging to be applied to rare cell populations, such as HSCs. For this reason, we used a specific approach for sample preparation for TEM studies (Kumar & Filippi, 2016). We processed pellet of sorted SLAM HSCs from 3 pool of age and sex-matched wt mice and 2 pool of age and sex-matched *th3* mice. Interestingly, we found an equal number per cell but a reduced size of mitochondria in *th3* SLAM HSCs (Fig. 6B).

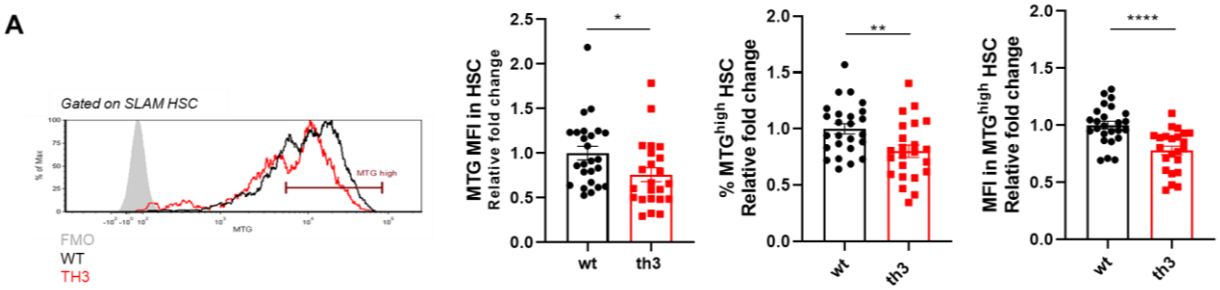

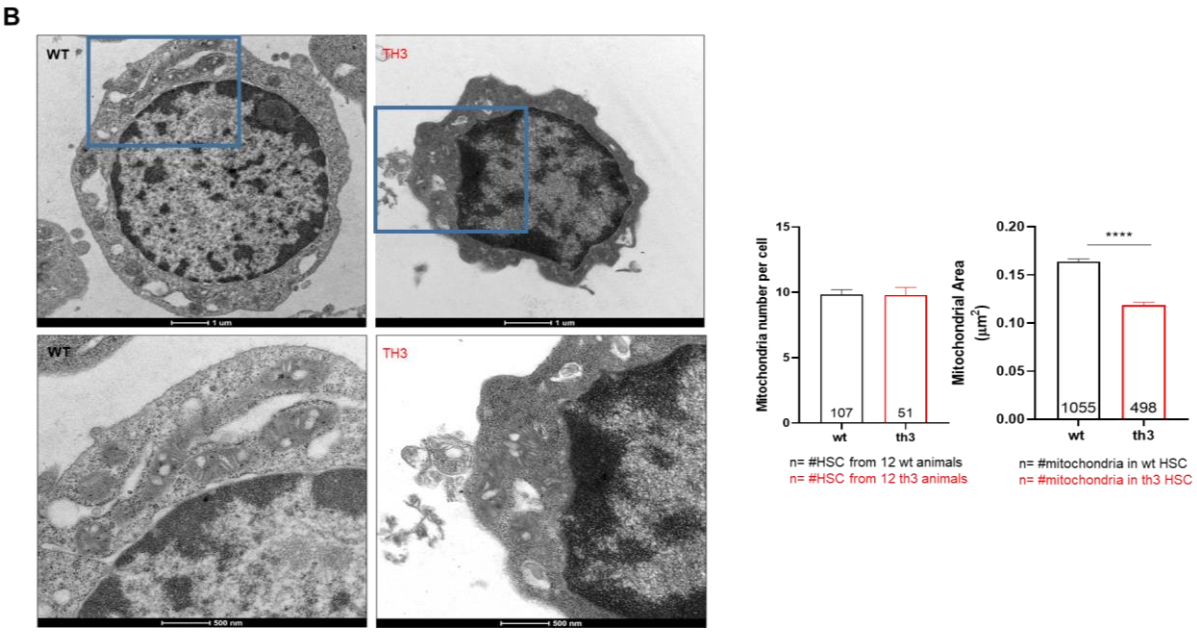

Figure 6. Reduced mitochondrial size in th3 HSCs. *(A) Quantification of mitochondrial mass in th3 and wt SLAM HSCs by flow cytometry. Representative flow cytometry histogram and total MFI of MTG, % MTG^{high} HSC and MFI in MTG^{high} HSC are reported (wt, n=25; th3, n=23). (B) Left: representative electron micrographs of wt and th3 SLAM HSCs, a magnified view of the cell area highlighted in blue is shown on the bottom. Scale bar, 500 nm.; Right: quantification of number and size of mitochondria in th3 and wt SLAM HSCs; n indicates cell numbers and mitochondria numbers, respectively.*
*Mann-Whitney test: ****, p<0.0001; **, p<0.01; *, p<0.05.*

Given the defect in size, we asked whether mitochondria in *th3* HSCs were functional. Mitochondrial activity in SLAM HSCs was measured using the cationic fluorescent probe tetramethylrhodamine ethyl ester (TMRE). TMRE accumulates in the mitochondrial matrix in proportion to the MMP, the electrical gradient between the negatively charged mitochondrial matrix and the positively charged intermembrane space, as the result of the ETC activity and ion concentration (Perry *et al.*, 2011). Thus, MMP is a widely recognised measure of mitochondrial function. We found reduced TMRE total MFI, one-half of that in wt, and lower % of TMRE^{+} *th3* SLAM HSCs, indicating that mitochondria were less active (Fig. 7A). To confirm TMRE responsiveness to MMP in our experimental setting, we treated in parallel Lin^{-} cells with FCCP, that disrupts MMP, after TMRE staining. FCCP depolarized mitochondria to the same extent in wt and *th3* HSCs thus indicating that differences in TMRE fluorescence reflected differences in MPP (Fig. 7B).

We categorised HSCs based on TMRE intensity as MMP^{high} and MMP^{low} by setting two markers at the side of the MFI, while allowing for a gap between high and low that spans at least 15% of each sample, as already published (Liang *et al.*, 2020; Mansell *et al.*, 2021). Based on this, most of SLAM HSCs in wt mice were classified as MMP^{high}. In contrast, only 10% of SLAM HSCs in *th3* mice were classified as MMP^{high}, thus suggesting a high fraction of HSCs with low mitochondrial activity (Fig. 7C). Notably, our data of TMRE distribution in wt HSCs are in line with previous works showing 55-75% of SLAM HSCs as MMP^{high} in wt mice (Liang *et al.*, 2020; Mansell *et al.*, 2021).

To check if the reduced mitochondrial activity was a bias of the reduced mitochondrial mass, we also normalized mitochondrial activity on mitochondrial mass. The TMRE/MTG ratio was reduced by 60% in *th3* SLAM HSCs as compared to wt (Fig. 7D), thus indicating that mitochondria have reduced function, regardless their reduced size.

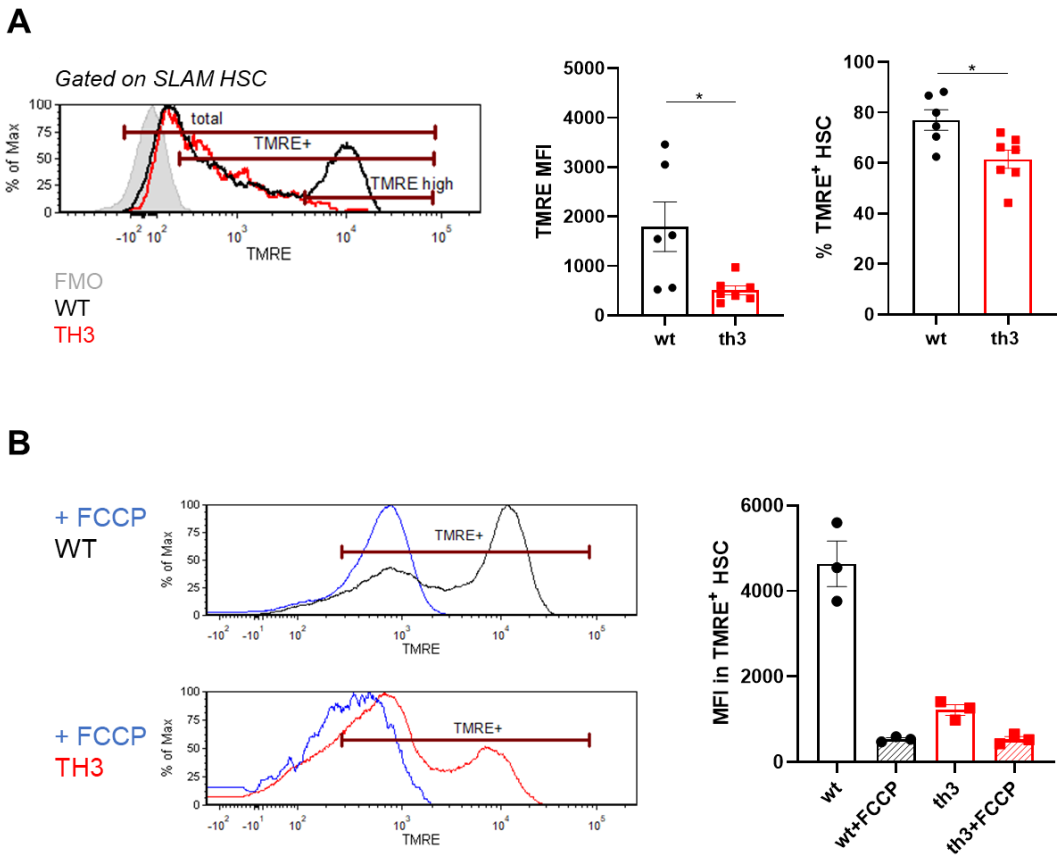

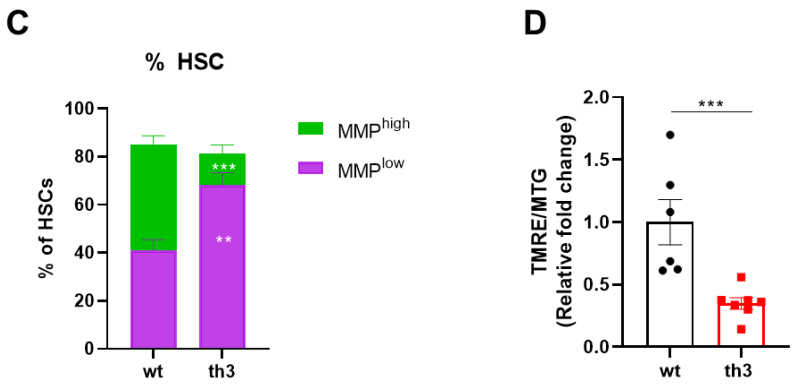

Figure 7. Reduced mitochondrial membrane potential in th3 HSCs. *(A) Quantification of mitochondrial activity in th3 and wt SLAM HSCs by flow cytometry. Representative flow cytometry histogram and TMRE MFI (left) and % TMRE$^+$ SLAM HSC (right) are reported (wt, n=6; th3, n=7). (B) Representative flow cytometry histogram (left) and MFI in TMRE$^+$ HSCs (right) at basal level and after FCCP treatment are reported (wt, n=3; th3, n=3). (C) Classification of wt and th3 SLAM HSCs based on TMRE MFI as MMP^{high} and MMP^{low} HSCs. % of cells is reported (wt, n=6; th3, n=7). (D) Normalization of mitochondrial activity on mitochondrial mass in th3 and wt SLAM HSCs by flow cytometry. TMRE/MTG ratio is reported, expressed as fold change to wt (wt, n=6; th3, n=7).*
*Mann-Whitney test: ***, p<0.001; **, p<0.01; *, p<0.05.*

Overall, these data show mitochondrial dysfunction in *th3* HSCs.

3 – BThal HSCs rely on glycolysis for energy production

Given the crucial role of mitochondria in cell metabolism (Spinelli & Haigis, 2018) and our results showing mitochondrial dysfunction, we next investigated *th3* HSC metabolism. Glycolysis and mitochondrial OXPHOS generate energy in the form of ATP. While glycolysis is not an efficient energy-producing process because it generates only two ATP molecules per molecule of glucose, OXPHOS produces 36 ATP molecules upon complete oxidation of one glucose molecule. Since OXPHOS occurs in the mitochondrial matrix and IMM, it is dependent on the integrity of mitochondrial structure and function (Seyfried *et al*, 2020b; Stanga *et al*, 2020). Therefore, our results of reduced mitochondrial mass and function led us to hypothesize an altered metabolic state of *th3* HSCs.

To verify this aspect, we first measured ATP levels on sorted SLAM HSCs by a luciferase-based luminescent assay. The luminescent signal released after the luciferin-

luciferase reaction is directly proportional to the amount of intracellular ATP. We generated a standard curve with samples with known ATP concentrations ranging from 1nM to 50nM and we firstly verified whether the assay was able to detect ATP in 500 wt HSCs. We used pools of wt progenitors, including primitive progenitors MPP and committed progenitors HPC-1 and HPC-2, as controls since they were reported to have higher ATP content as compared to HSCs (Takubo *et al*, 2013). The luminescence values corresponding to the ATP content in HSCs fall within the sensitive range of the assay, indicating that we were in the right experimental conditions to discriminate ATP variations between samples. Moreover, we confirmed higher ATP content in progenitors (Fig. 8A). We then analysed *th3* SLAM HSCs and we found a low ATP content, which is one-half of that in wt (Fig. 8B), that might indicate a low-energy metabolism.

To address the degree to which mitochondrial OXPHOS is involved in energy production, we analysed ATP levels on sorted SLAM HSCs after oligomycin administration. Oligomycin inhibits ATP synthase, the last complex of the ETC. Hence, the decrease in ATP content after oligomycin treatment reflects the ATP produced by mitochondrial OXPHOS (Fig. 8C). In line with mitochondrial dysfunction, inhibition of OXPHOS lowered the ATP content in wt cells but had a minor effect in *th3* HSCs, thus indicating a reduced OXPHOS-dependent metabolism (Fig. 8D). Of note, only 21% of ATP was produced by OXPHOS in *th3* HSCs versus 44% OXPHOS-derived ATP in wt HSCs (Fig. 8E), thus suggesting that *th3* HSCs rely only to a small extent on OXPHOS for their energy production. Interestingly, the reduced OXPHOS-derived ATP mirrored the reduced frequency of MMP^{high} HSCs in *th3* mice (Fig. 8E, 7C).

A

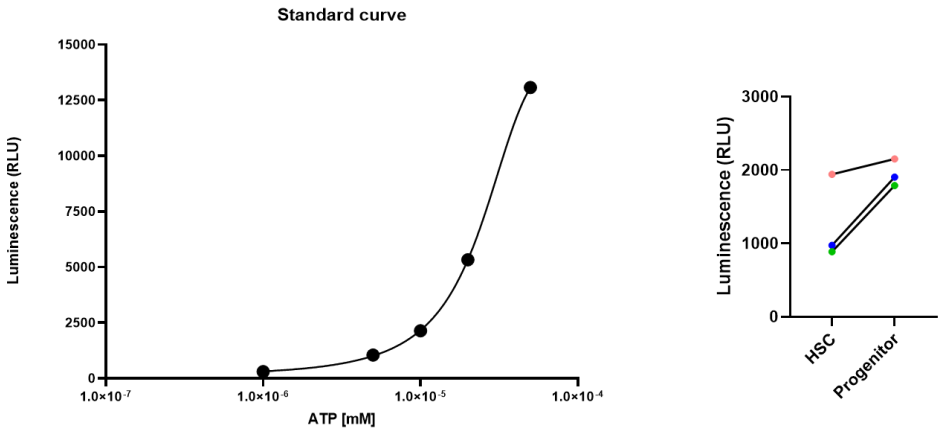

B

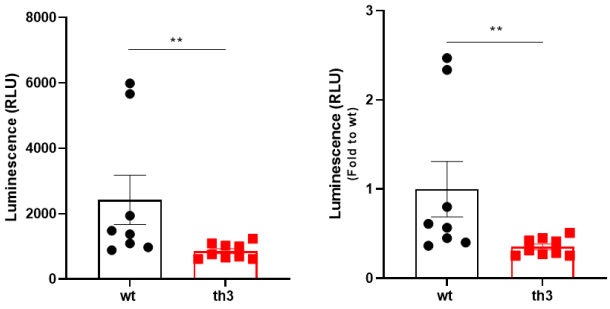

C

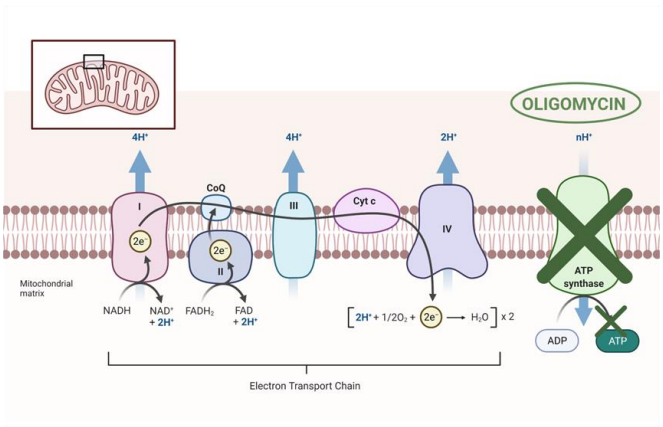

Statistical analyses:
Ctrl vs oligo: paired (Wilcoxon)
Wt vs th3: unpaired (Mann-Whitney)

D

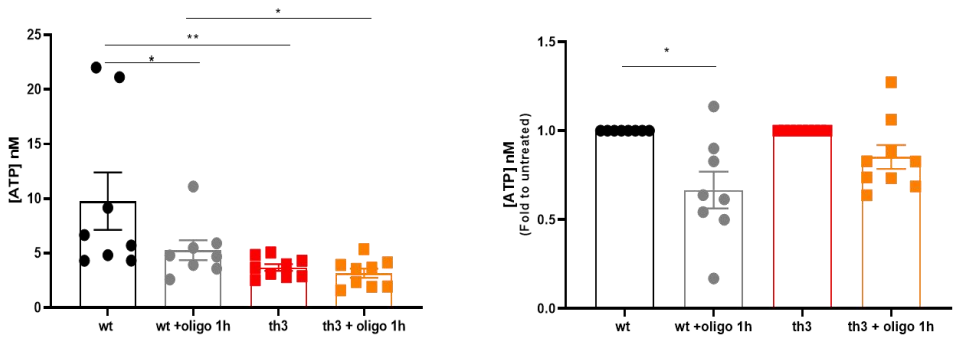

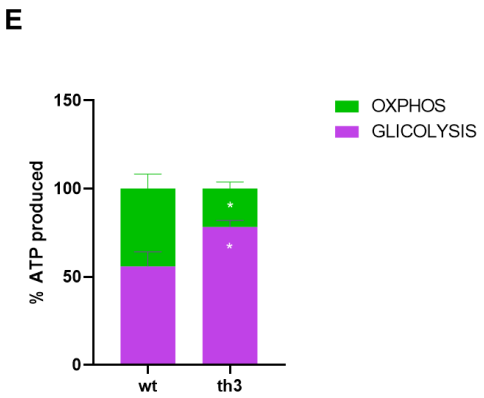

Figure 8. Reduced OXPHOS in th3 HSCs. *(A) Setting of ATP assay: on the left standard curve with known ATP concentrations in x and luminescence in y is reported, on the right luminescence output in 500 sorted wt SLAM HSC and 500 sorted progenitors from the same mice after incubation with CellTiter-Glo 2.0. (B) Luminescence output in 500 sorted th3 and wt SLAM HSCs after incubation with CellTiter-Glo 2.0. On the right data are expressed as fold change to wt (wt, n=8; th3, n=9). Mann-Whitney test: **, p<0.01. (C) Scheme showing the mechanism of action of oligomycin. Created with BioRender.com; (D) ATP content (nM) at basal level and after oligomycin treatment in 500 sorted th3 and wt SLAM HSCs. On the right data are expressed as fold change to untreated (wt, n=8; th3, n=9). Mann-Whitney test for wt vs th3: **, p<0.01; Wilcoxon test for untreated vs treated samples: *, p<0.05. (E) % of ATP produced by OXPHOS and glycolysis based on ATP assay after oligomycin. Mann-Whitney test: *, p<0.05.*

Since OXPHOS and glycolysis are the two main metabolic pathways involved in cellular ATP generation, we next analysed glycolytic metabolism. Interestingly, our RNAseq data showed a positive enrichment of glycolytic genes, including the ones encoding glycolytic enzymes, such as triosephosphate isomerase (*Tpi1)*, glyceraldehyde-3-phosphate dehydrogenase (*Gapdh)* and pyruvate kinase (*Pklr)*, in *th3* SLAM HSCs (Fig. 9A). Notably, pyruvate kinase is a key rate-limiting enzyme of glycolysis, and its upregulation together with that of other glycolytic genes might suggest glycolysis-dependent energy production.

According to the "classical" model of HSC bioenergetics, quiescent HSCs have low mitochondrial activity because of preferential use of glycolysis over OXPHOS. On the contrary, differentiation requires high mitochondrial activity and OXPHOS for the generation of high ATP levels (Chandel *et al*, 2016). Given our previous published data showing a more active cycling profile of *th3* HSCs (Aprile *et al.*, 2020), these intriguing findings raised the possibility that glycolysis may more readily support active HSCs with mitochondrial dysfunction. This hypothesis would be in line with the latest studies by

Liang et al. showing that active HSCs display both high mitochondrial activity and high glycolysis (Liang *et al.*, 2020). However, when there is a reduced mitochondrial function, as in *th3* HSCs, glucose could be preferentially broken down during glycolysis to generate ATP.

To test this hypothesis, we measured the glucose uptake by SLAM HSCs, using the fluorescent glucose analogue 2NBDG (2-[N-(7-nitrobenz-2-oxa-1,3-diazol-4-yl)amino]-2-deoxy-D-glucose) (Zou *et al*, 2005) under defined metabolic conditions (pyruvate, glucose and glutamine free medium). *Th3* mice displayed the same frequency of $2NBDG^{+}$ HSCs but their HSCs uptake 1.4-fold more glucose as compared to wt, thus suggesting increased glycolytic flux (Fig. 9B).

We then analyzed the intracellular lactate content, the end-product of glycolysis, in sorted SLAM HSCs by fluorometric assay. The fluorescent output released after the probe-enzyme reaction is directly proportional to the amount of intracellular lactate. We found reduced intracellular levels of lactate in *th3* SLAM HSCs (Fig. 9C). Once produced, lactate is rapidly exported by MCT family transporter (Halestrap & Price, 1999), thus our finding could indicate increased lactate extrusion in the extracellular space consequent to high glycolysis.

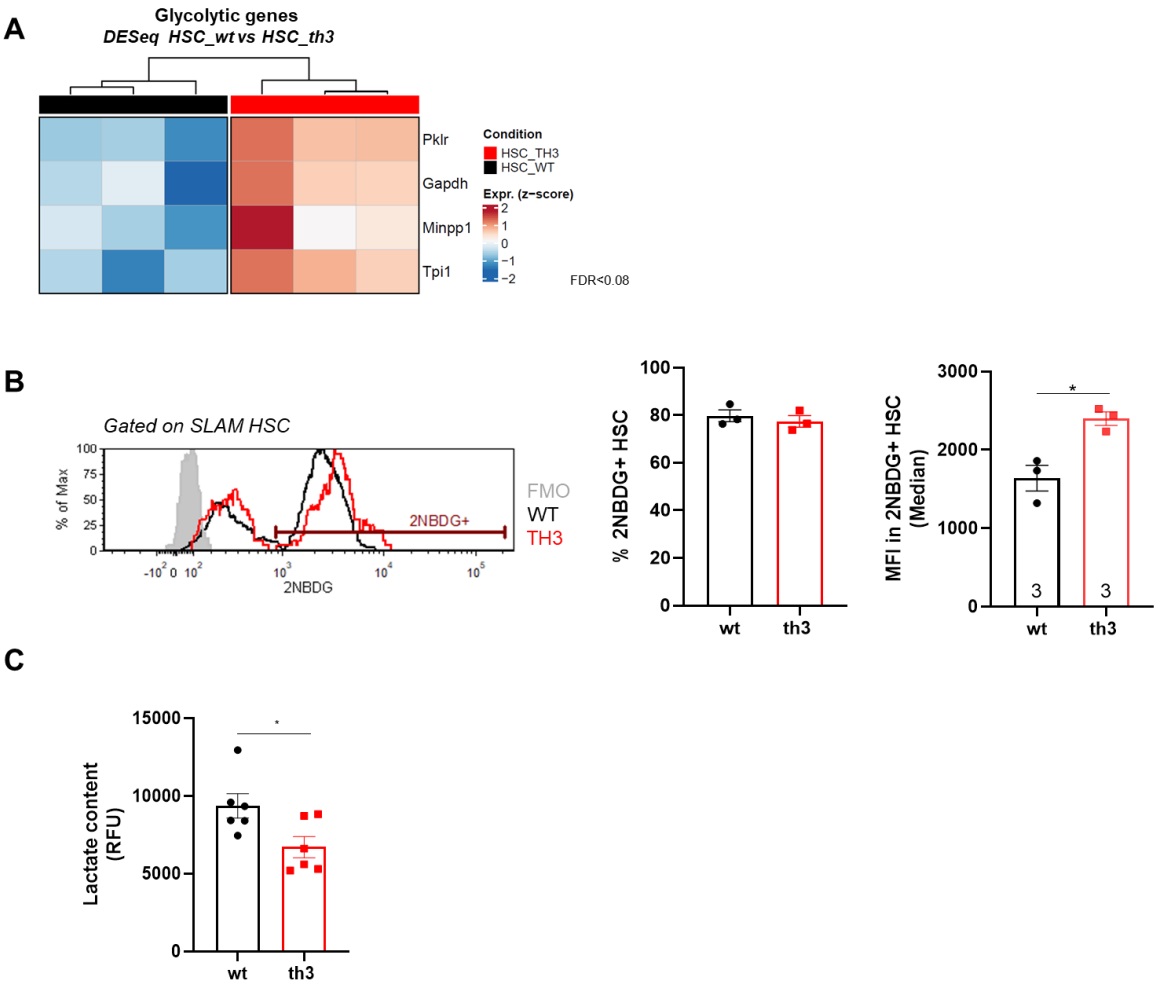

Figure 9. Glycolysis dependence of th3 HSCs. *(A) Analysis of DEG by DESeq software reveals the upregulation of glycolytic genes in th3 SLAM HSCs compared to wt (wt, n=3 pools; th3, n=4 pools). (B) Quantification of the fluorescent glucose analog 2NBDG uptake by SLAM HSCs from th3 and wt mice. Representative flow cytometry histogram and % 2NBDG⁺ HSC and MFI in 2NBDG⁺ HSC are reported (wt, n=3; th3, n=3). (C) Quantification of intracellular lactate content using a commercial assay in 500 sorted th3 SLAM HSCs compared to wt (wt, n=6; th3, n=6).*
*Mann-Whitney test: *, p<0.05.*

Collectively, these data suggest that *th3* HSCs preferentially rely on glycolysis rather than OXPHOS for their energy demands, because of the mitochondrial defect and despite the higher cycling rate. This process could be similar to the Warburg effect reported in proliferating cancer cells, which switch to aerobic glycolysis (Vander Heiden *et al*, 2009). Under Warburg effect the conversion of glucose to lactate is faster than the complete oxidation of glucose in the mitochondria through OXPHOS so that cancer cells do not have lower ATP. However, the reduced ATP levels in *th3* HSCs could indicate less efficient glycolysis as compared to wt HSCs (Fig. 8B).

4 – Oxidative stress impairs *th3* HSC function by causing mitochondrial dysfunction

ROS are representative of a heterogeneous chemical class that includes hydroxyl radicals (OH^-) and superoxide anions (O_2^-), as well as non-radical species such as hydrogen peroxide (H_2O_2) (Bigarella *et al.*, 2014). When ROS are tightly regulated by antioxidant system under physiological conditions, they act as second messengers in several cellular functions, including cell growth, differentiation and survival. However, when ROS levels exceed the antioxidant enzyme system, an excessive accumulation of ROS occurs, leading to intracellular oxidative stress with protein, lipid and nucleotide damage.

Since iron gives rise to ROS via the Fenton and Haber–Weiss reactions, we hypothesized that its toxicity on mitochondria is mediated by oxidative stress. To verify this hypothesis, we performed Gene Set Enrichment Analysis (GSEA) on our RNAseq data from sorted wt and *th3* SLAM HSCs and we analysed antioxidant genes. We found a positive enrichment of antioxidant genes in the *th3* HSC transcriptome profile, as shown by the GSEA enrichment plot (Fig. 10A). Catalase (Cat), peroxiredoxins (Prdx), thioredoxins (Txn), glutathione peroxidase (Gpx) and glutathione reductase (Gsr) represent the first line of defence against excess ROS and were all upregulated in *th3* SLAM HSCs. Moreover, the increased expression of *Sod2*, a mitochondria-restricted enzyme that is specifically induced when levels of ROS in the mitochondria fail to be neutralized (Pani *et al*, 2009), suggested accumulation of mitochondrial ROS (mtROS) in *th3* HSCs (Fig. 10B).

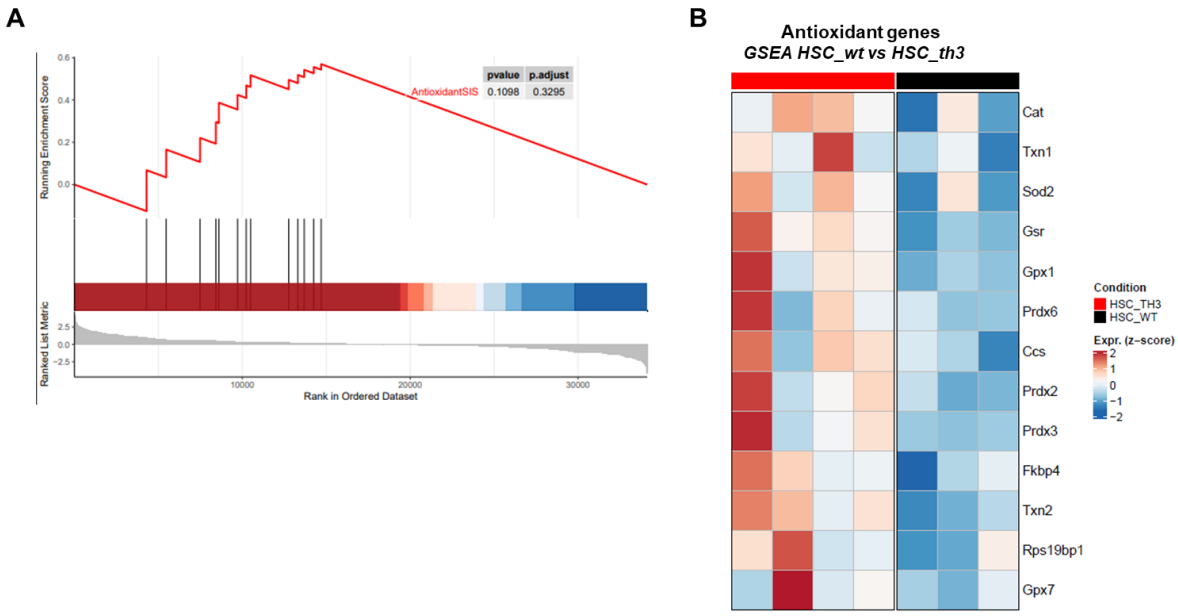

Figure 10. Activation of antioxidant defence system in th3 HSCs. *(A) GSEA enrichment plot of the antioxidant genes in cellular responses to stress category from the Reactome Pathway database, showing the profile of the running enrichment score and the positions of gene set members on the rank-ordered list. Enrichment in th3 HSCs vs wt HSCs is reported. (B) Heatmap for antioxidant genes in cellular responses to stress category in A. p-value=0.1.*

To further confirm these data, we stained Lin- cells with mitosox dye. MitoSOX™ has a mitochondria targeted group and, once in the mitochondria, it is oxidized by superoxide and exhibits fluorescence (Dikalov & Harrison, 2014). Despite the upregulation of antioxidant system, *th3* SLAM HSCs had higher mtROS content than wt ones, as shown by the increased frequency of MitoSOX$^+$ HSCs and the 2-fold higher MitoSOX MFI, thus resulting in an oxidative stress status (Fig. 11).

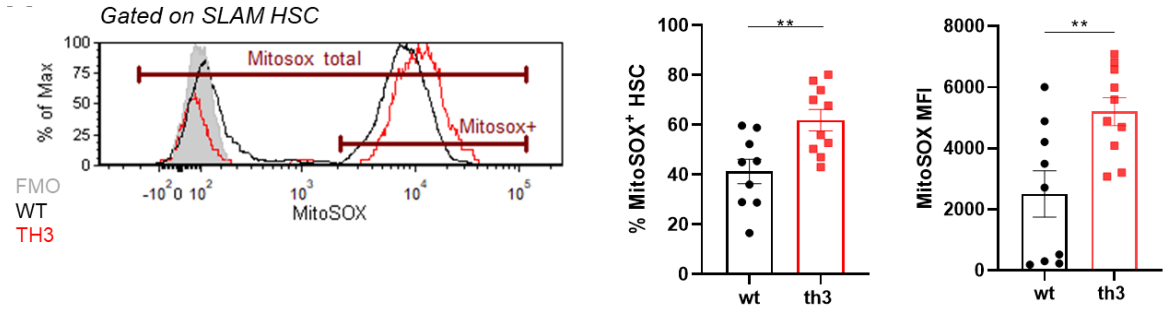

Figure 11. Oxidative stress in th3 HSCs. *Quantification of mitochondrial ROS (mtROS) in th3 and wt SLAM HSCs by flow cytometry. Representative flow cytometry histogram and % MitoSOX$^+$ HSC and MFI of MitoSOX are reported (wt, n=9; th3, n=10).*
*Mann-Whitney test: **, p<0.01.*

To functionally prove that IO-derived ROS cause mitochondrial dysfunction and to verify whether mitochondrial damage is reversible, we decreased mitochondrial ROS *in vivo* by the administration of the mitochondria-specific antioxidant MitoQ (Murphy & Smith, 2007). We treated *th3* mice by intraperitoneal injection of 2mg/kg MitoQ for 5 days (Fig. 12A). MitoQ treatment efficiently reduced mtROS to wt levels and enhanced MMP in *th3* SLAM HSCs (Fig. 12B-C), thus indicating that oxidative stress is the cause of mitochondrial dysfunction. Importantly, these results demonstrated that the mitochondrial damage in HSCs is reversible. Given the positive results on mitochondrial activity, we wondered whether MitoQ treatment could also restore *th3* HSC metabolism. Interestingly, SLAM HSCs from MitoQ-treated *th3* mice showed one-half of glucose uptake than untreated HSCs (Fig. 12D), thus suggesting that in presence of functional mitochondria HSCs are able to oxidize the glycolysis-derived pyruvate during OXPHOS, without the need to enhance glucose uptake as in HSCs from untreated *th3* mice. Collectively, we reported that MitoQ short-term treatment is sufficient to switch HSC metabolism from glycolysis to the more energetic OXPHOS, providing a new tool to modulate HSC metabolism.

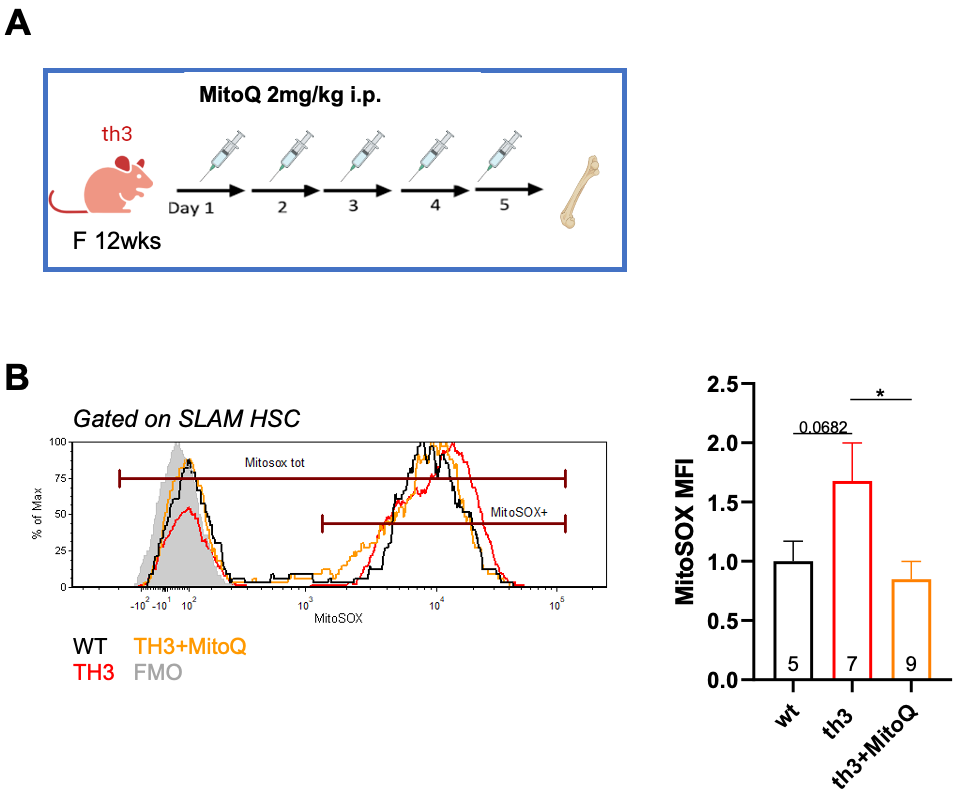

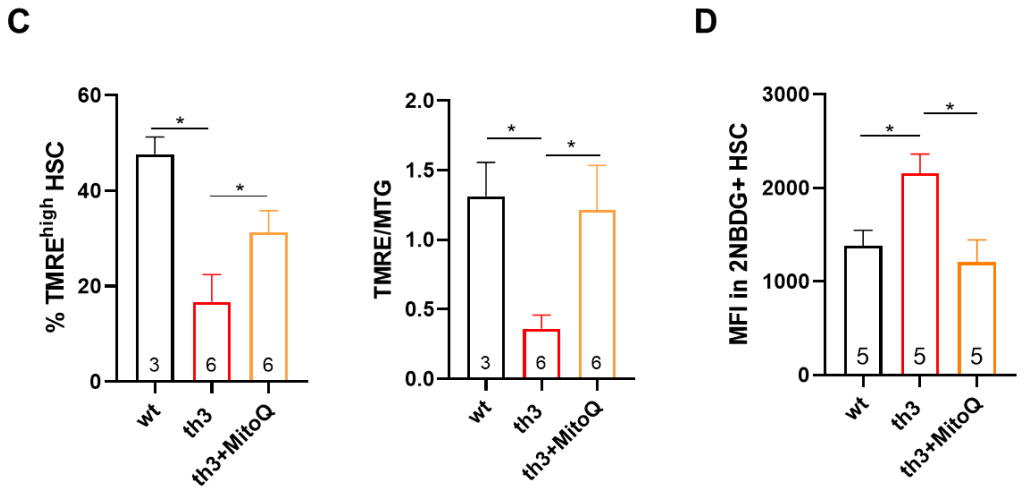

Figure 12. MitoQ treatment restores mitochondrial activity in th3 HSCs. *(A) Strategy of in vivo reduction of mtROS in th3 mice using MitoQ. (B) Quantification of mtROS in SLAM HSCs from MitoQ-treated th3, th3 and wt mice. Representative flow cytometry histogram and MFI of MitoSOX are reported (wt, n=5; th3, n=7; th3+MitoQ=9). (C) Quantification of mitochondrial activity in SLAM HSCs from MitoQ-treated th3, th3 and wt by flow cytometry. Percentage of TMRE^{high} SLAM HSC (left) and TMRE/MTG ratio (right) are reported (wt, n=3; th3, n=6; th3+MitoQ=6). (D) Quantification of the fluorescent glucose analog 2NBDG uptake by SLAM HSCs from MitoQ-treated th3, th3 and wt mice. MFI in 2NBDG^{+} HSC is reported (wt, n=5; th3, n=5; th3+MitoQ=5).*
*Kruskal-Wallis test: *, p<0.05.*

Mitochondrial activity and metabolism significantly control HSC function and fate. Alterations in mitochondrial fitness impact on HSC function, causing loss of repopulating ability in HSCs (Hinge *et al.*, 2020). We previously reported a reduced frequency, loss of quiescence, impaired self-renewal and repopulating ability of *th3* HSCs (Aprile *et al.*, 2020). We hypothesized that IO and the resulting oxidative stress could alter *th3* HSC function by impairing mitochondrial fitness. To address this possibility, we firstly investigated the HSC frequency after MitoQ administration. The proportion of *th3* SLAM HSCs on Lin- cells was higher after MitoQ treatment, although did not reach wt levels (Fig. 13A). Moreover, MitoQ treatment slightly increased the proportion of SLAM HSCs in G0/G1 phase (Fig. 13B). However, further analyses after prolonged MitoQ administration are required to check for a complete restoration of *th3* HSC frequency and quiescence to normal levels. In addition, transplantation experiment of sorted HSCs from MitoQ *th3* mice will be pivotal to understand whether the rescue of mitochondrial activity could restore HSC repopulating ability and self-renewal.

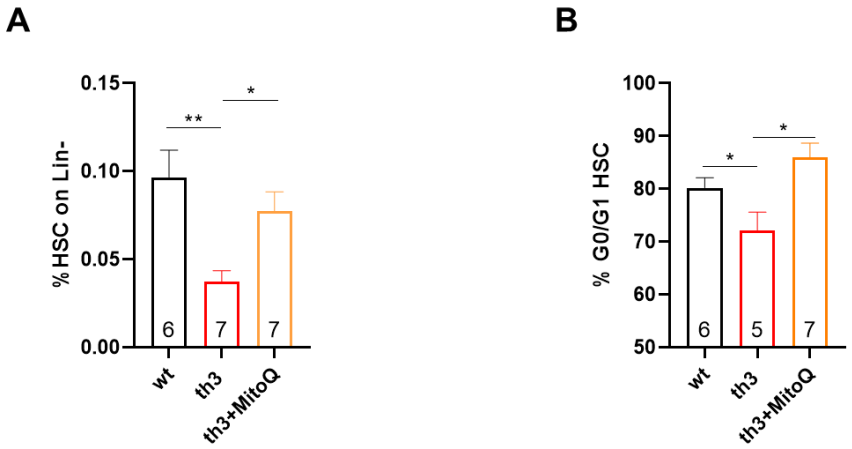

Figure 13. MitoQ treatment improves th3 HSC frequency and cell cycle defects. *(A) Frequency of MitoQ-treated th3, th3 and wt HSCs on BM Lin- cells (wt, n=6; th3, n=7; th3+MitoQ=7). (B) Percentage of quiescent HSCs (in G0/G1 phase) in MitoQ-treated th3, th3 and wt mice. 7-AAD/Ki-67 staining was performed to discriminate between G0 and G1 phases (wt, n=6; th3, n=5; th3+MitoQ=7).*
*Kruskal-Wallis test: *, p<0.05; **, p<0.01.*

Interestingly, MitoQ treatment ameliorated RBC parameters and anemia by increasing RBC count, Hb and hematocrit (HCT) (Fig. 14). These results are consistent with the high intracellular ROS content of RBCs due to IO and hemoglobin defect (Fibach & Dana, 2019).

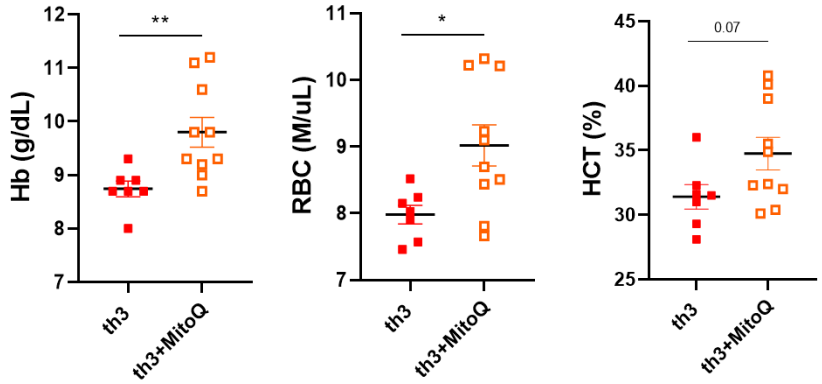

Figure 14. MitoQ treatment ameliorates anemia in th3 mice. *Whole blood analysis of erythroid parameters (Hb, RBC count and HCT) of MitoQ-treated th3 and th3 mice (th3, n=7; th3+MitoQ=10).*
*Mann-Whitney test: **, p<0.01; *, p<0.05.*

Overall, these findings indicate that oxidative stress impairs HSC function by damaging mitochondria, as well as the erythroid compartment, in *th3* mice. *In vivo* short-term treatment with MitoQ is able to restore mitochondrial function in HSCs and ameliorate hematological parameters, thus MitoQ treatment could be a promising strategy for improving current BThal therapeutic approaches by acting both on long-term HSC potential and anemia.

5 – Progenitor cells have different responses to IO in *th3* mice

HSCs sustain the blood system throughout lifetime. This is reached by their ability to self-renew but also to generate progenitors, which no longer possess the capacity for self-renewal but can differentiate into committed lineages of the entire hematopoietic system. Multipotent progenitors (MPPs) can give rise to all major hematopoietic lineages in transplantation assays in lethally irradiated recipients but fail to engraft long-term (Kiel *et al.*, 2005). MPPs and HSCs can be distinguished based on the expression of the SLAM family marker CD150. Indeed, MPPs are phenotypically defined as Lin^- $ckit^+$ $Sca1^+$ $CD48^-$ $CD150^-$, whereas HSCs are Lin^- $ckit^+$ $Sca1^+$ $CD48^-$ $CD150^+$. Both MPPs and HSCs $CD48^-$ are contained in the LSK (Lin^- $ckit^+$ $Sca1^+$) cell population along with more committed progenitors $CD48^+$ HPC-1 and HPC-2. LSKs are normally referred as Hematopoietic Stem and Progenitor Cells (HSPCs), including the most primitive progenitors (Oguro *et al.*, 2013).

We found that IO-derived ROS in *th3* HSCs cause mitochondrial dysfunction, impaired cell metabolism and function. Since HSCs give rise to LSKs and MPPs, we wondered whether these defects are transferred to the progeny during cell division.
Our flow cytometry strategy allows to identify HSCs, MPPs and LSKs in the same sample and to analyse iron content, ROS levels and mitochondrial activity also in MPPs and LSKs from the same animals that were evaluated for HSCs.

Surprisingly, at steady state wt HSCs, MPPs and LSKs had the same iron content but in the stressed *th3* BM niche, MPPs and LSKs derived from iron overloaded HSCs did not accumulate intracellular IO, as shown by calcein-AM MFI (Fig. 15A). Since cells evolved sophisticated systems to maintain iron homeostasis, the lack of iron accumulation in *th3* progenitors might result from efficient iron detoxification.

Moreover, no differences in the frequency of MitoSOX^{+} cells and MitoSOX MFI were found in *th3* MPPs and LSKs as compared to wt, thus suggesting the absence of oxidative stress in *th3* primitive progenitors (Fig. 15B). As expected on the basis of a more active cell cycle and oxidative metabolism, progenitors accumulate more mtROS than HSCs in wt mice. Of note, *th3* HSCs showed similar ROS levels to MPPs and LSKs (Fig. 15B), which is consistent with their already published more cycling profile (Aprile *et al.*, 2020). To counteract excessive ROS, cells upregulate various antioxidant enzymes (Bigarella *et al.*, 2014) and our finding that progenitors can tolerate higher ROS than HSCs could suggest that the antioxidant system might be more active to promptly counteract excess ROS. Therefore, we speculated that *th3* progenitors more efficiently neutralize free iron and ROS by enhancing iron-utilizing pathways and potentiating the antioxidant system respectively.

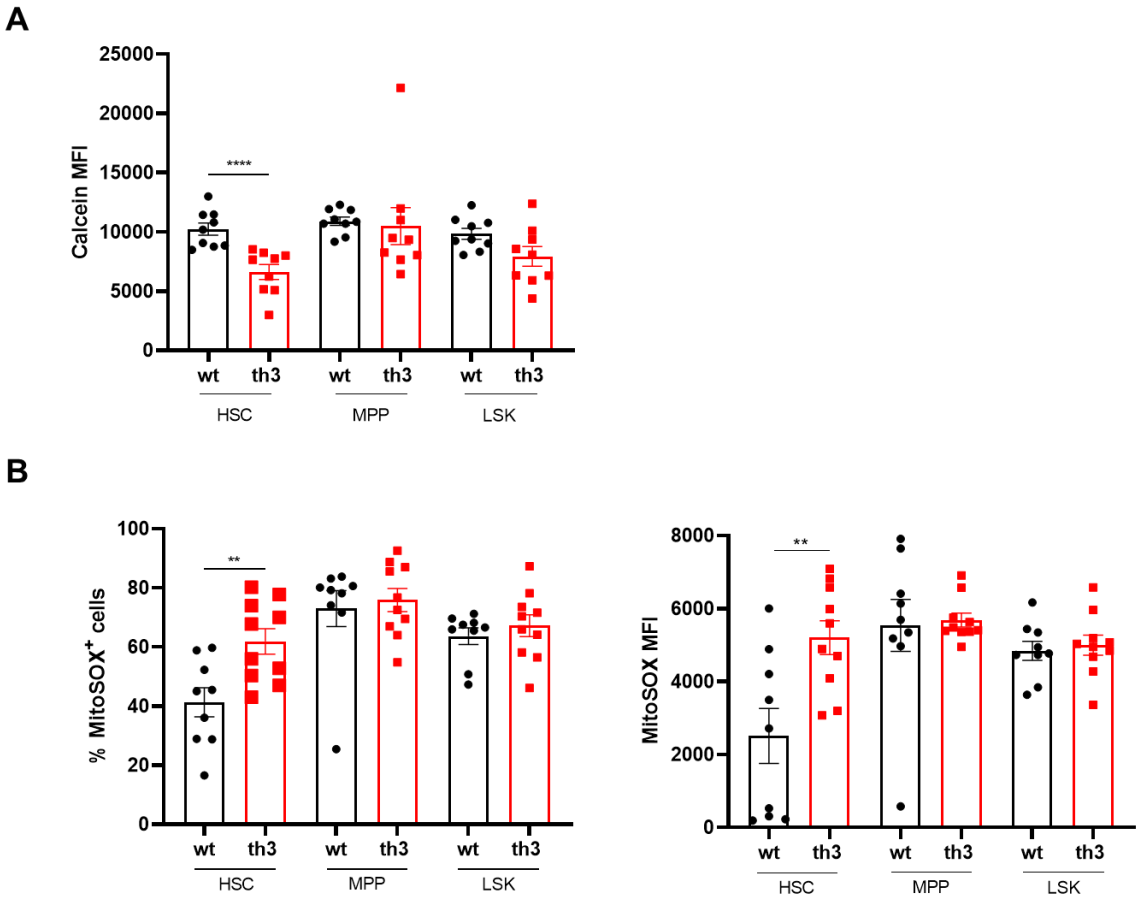

Figure 15. Th3 progenitors do not accumulate iron and mtROS. *(A) Quantification of intracellular iron content in th3 and wt HSCs and progenitors by flow cytometry. MFI of calcein-am is reported (wt, n=9; th3, n=9). (B) Quantification of mtROS in th3 and wt HSCs and*

progenitors by flow cytometry. % MitoSOX^{+} cells and MFI of MitoSOX are reported (wt, n=9; th3, n=10).
*Mann-Whitney test: ****, p<0.0001; **, p<0.01.*

Since IO-derived ROS cause mitochondrial dysfunction and functional defects in HSCs, we could assume normal mitochondrial function in *th3* progenitors. However, if HSCs transfer damaged mitochondria to the progeny during asymmetric cell division, we might expect dysfunctional mitochondria also in progenitors, despite their ability to detoxify iron and ROS. To test this, we checked whether mitochondrial damage was still present in *th3* progenitors. Firstly, we analysed mitochondrial mass by MTG dye. Both the % of MTG^{high} cells and MTG MFI in MPPs and LSKs were unchanged between wt and *th3* mice (Fig. 16A). Then, we investigated MMP, as a measure of mitochondrial activity. Surprisingly TMRE MFI and also TMRE MFI normalized on MTG MFI were lower in *th3* MPPs as compared to wt but no differences were found in the LSK compartment (Fig. 16B-C), confirming mitochondrial dysfunction in *th3* MPPs but not in LSKs.

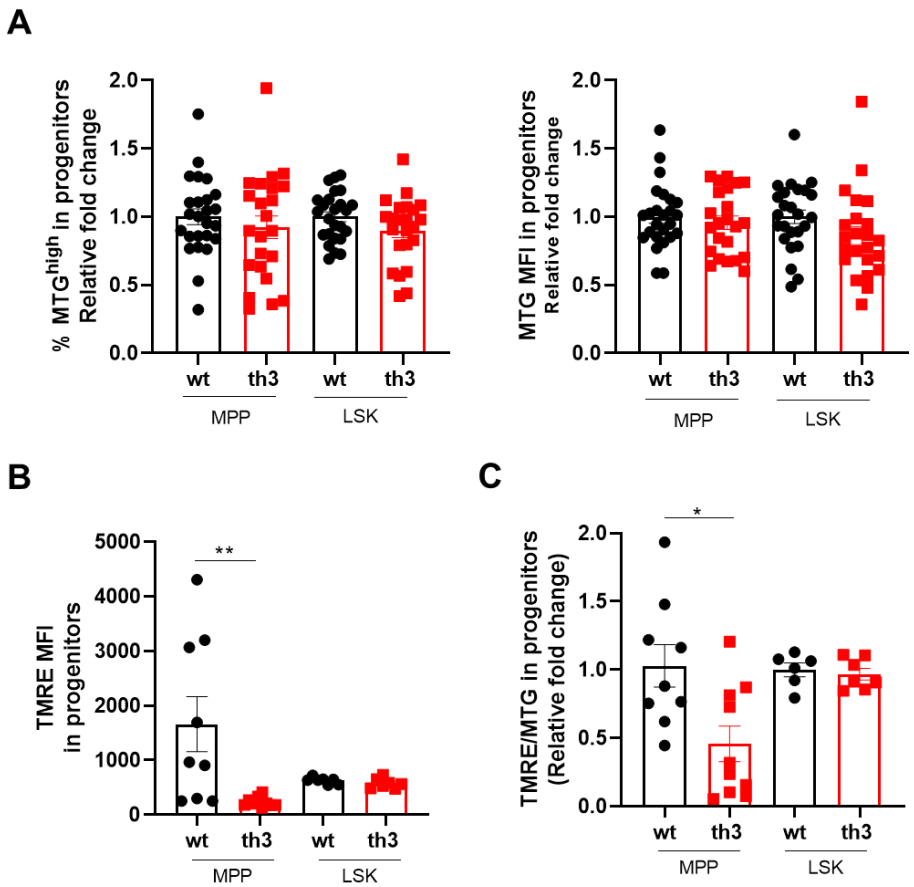

Figure 16. Mitochondrial damage is progressively lost in th3 progenitors. *(A) Quantification of mitochondrial mass in th3 and wt progenitors by flow cytometry. % MTG^{high} cells and MFI in MTG^{high} cells are reported (wt, n=25; th3, n=23). (B) Quantification of mitochondrial activity in th3 and wt progenitors by flow cytometry. TMRE MFI is reported ((MPP: wt, n=9; th3, n=10, LSK: wt, n=6; th3, n=7). (C) Normalization of mitochondrial activity on mitochondrial mass in th3 and wt progenitors by flow cytometry. TMRE/MTG ratio is reported, expressed as fold change to wt (MPP: wt, n=9; th3, n=10, LSK: wt, n=6; th3, n=7).*
*Mann-Whitney test: **, p<0.01; *, p<0.05*.

Collectively, our findings indicate that only HSCs have intracellular IO and the resulting mitochondrial oxidative stress whereas progenitors that reside in the same iron-overloaded BM niche do not, thus suggesting more efficient iron and ROS detoxification. HSCs and MPPs have impaired mitochondrial function but the downstream early progenitors LSKs do not, indicating that the rescue of mitochondrial activity occurs in the MPP-LSK transition. We speculate that *th3* HSCs transfer their dysfunctional mitochondria to MPPs during cell division but MPPs fail to repair the inherited mitochondria, despite their ability to promptly neutralize excess iron and ROS. On the contrary, LSKs efficiently remove dysfunctional mitochondria.

6 – IO alone is sufficient to impair mitochondrial fitness in HSCs

In the stressed BThal BM microenvironment, different niche components and soluble factors may have a role in altering *th3* HSC function, hypothesizing a multifactorial mechanism (Aprile *et al.*, 2022). To dissect the specific role of IO on HSC metabolism and function we induced IO in wt mice. In this way, we avoided confounding elements within the complexity of the diseased BM microenvironment, that could hamper the study of the effects of IO on HSCs.

We established both an acute and chronic IO mouse models by treating wt mice with a single subcutaneous injection of 25mg/ml iron dextran (WT_IO_AC) (Zhang *et al.*, 2022) and by intraperitoneal injection with 25mg/ml iron dextran every three days for 4 weeks (WT_IO_CH) (Chai *et al.*, 2015), to reproduce a persistent damage, as in *th3* mice (Fig. 17A). Mice were euthanized 24h following the single or last dose.

We confirmed the establishment of IO mouse models by the analysis of serum iron levels, macroscopic examination of spleen and liver and histological analyses of iron deposits in spleen, liver and BM of treated animals.

As previously reported (Gardenghi *et al*, 2007), *th3* mice displayed equal serum iron levels to that of wt since the spleen is able to sequester excess iron derived from IE and RBC hemolysis (Fig. 17B). Moreover, excess iron is used by proliferating erythroid precursors. Conversely, both acute and chronic IO models showed significantly higher serum iron levels in a dose-dependent manner as compared to untreated mice.

In line with the fact that spleen and liver are the major sites of extramedullary hematopoiesis and iron storage in BThal, these organs were enlarged in *th3* mice as compared to wt (Fig. 17C). Macroscopically, the spleen of chronic IO mice showed increased size as compared to untreated wt controls. Moreover, the liver of chronic IO mice was enlarged and more pigmented as compared to both wt controls and *th3* mice, likely indicating liver toxicity consequent to excess iron deposition (Fig. 17C).

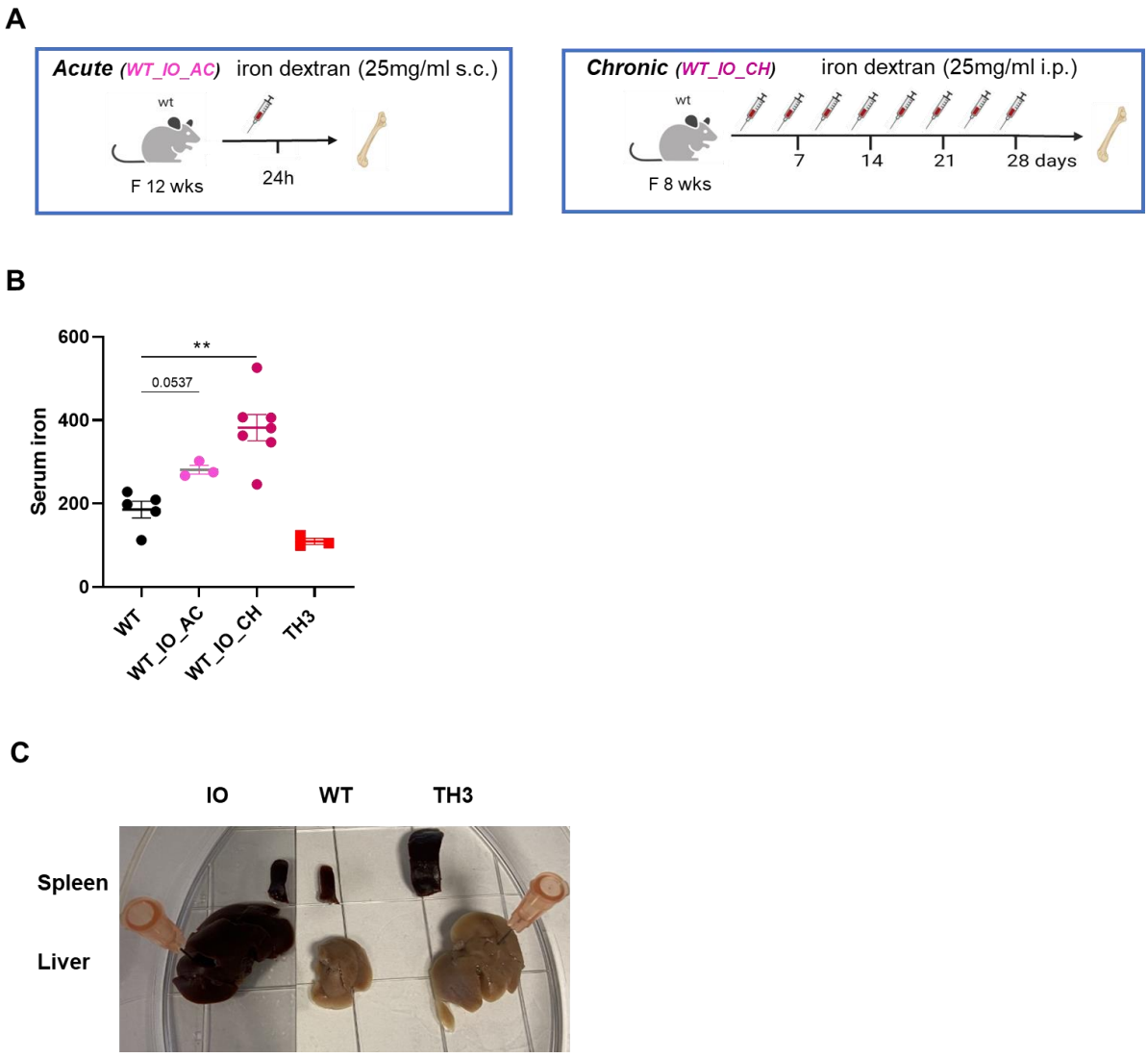

Figure 17. Establishment of systemic WT_IO mouse model. *(A) In vivo administration regimen of iron dextran to wt mice to generate acute and chronic IO model. (B) Quantification of serum iron levels (μg/dL) (wt, n=5; WT_IO_AC, n=3; WT_IO_CH, n=7; th3, n=3). (C) Macroscopic appearance of spleen (top) and liver (bottom) of WT_IO_CH, wt and th3 mice.*
*Kruskal-Wallis test: *, p<0.05; **, p<0.01.*

We then performed Perl's iron staining on spleen and liver sections from IO mice to detect Fe^{3+} accumulation. Fe^{3+} deposits in tissues appear blue as the result of the reaction with the soluble ferrocyanide to form the insoluble Prussian blue pigment (Iezzoni, 2018). As expected, *th3* spleen displayed more iron deposits that the wt counterpart. Surprisingly, chronic IO mice showed increased iron accumulation in the spleen as compared to both wt and *th3* mice, raising the possibility that chronic administration of iron dextran could generate a more severe condition of IO (Fig. 18). This hypothesis was further confirmed by histological analyses of the liver sections stained with Perl's. While iron deposits were barely detectable in *th3* liver by Perl's staining, chronic IO mice displayed several enlarged iron deposits (Fig. 19A). To check whether our treatment regimen caused liver iron toxicity, we measured serum alanine aminotransferase (ALT) and aspartate aminotransferase (AST), commonly used biomarkers for liver damage. Although ALT is mainly found in the liver, AST is also present in other organs, such as heart, muscle, kidney, brain, pancreas and lung (Sookoian & Pirola, 2015). Serum ALT and AST were both higher in *th3* mice as compared to wt, whereas only ALT was increased in chronic IO mice. Therefore, chronic administration of iron dextran for 4 weeks resulted in excess iron accumulation in the liver, which in turn caused organ damage. Acute IO mice showed increased iron deposition in the spleen and in the liver as compared to both wt and *th3* mice, but they did not exhibit liver injury (Fig. 18-19).

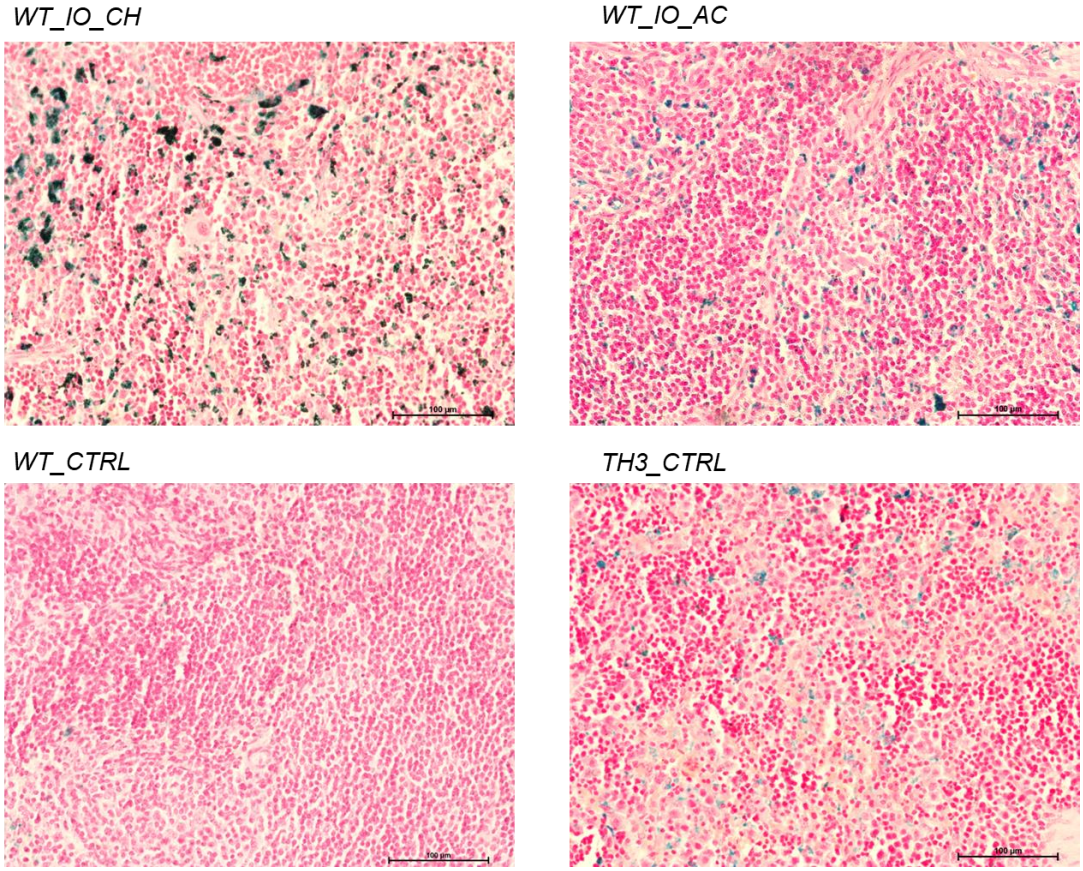

Figure 18. Iron deposition in the spleen of WT_IO mice. *Histological analyses of spleen subjected to Perl's iron staining. Representative images of wt, WT_IO_AC, WT_IO_CH and th3 spleen sections are shown. Magnification 20X. Scale bar, 100µM.*

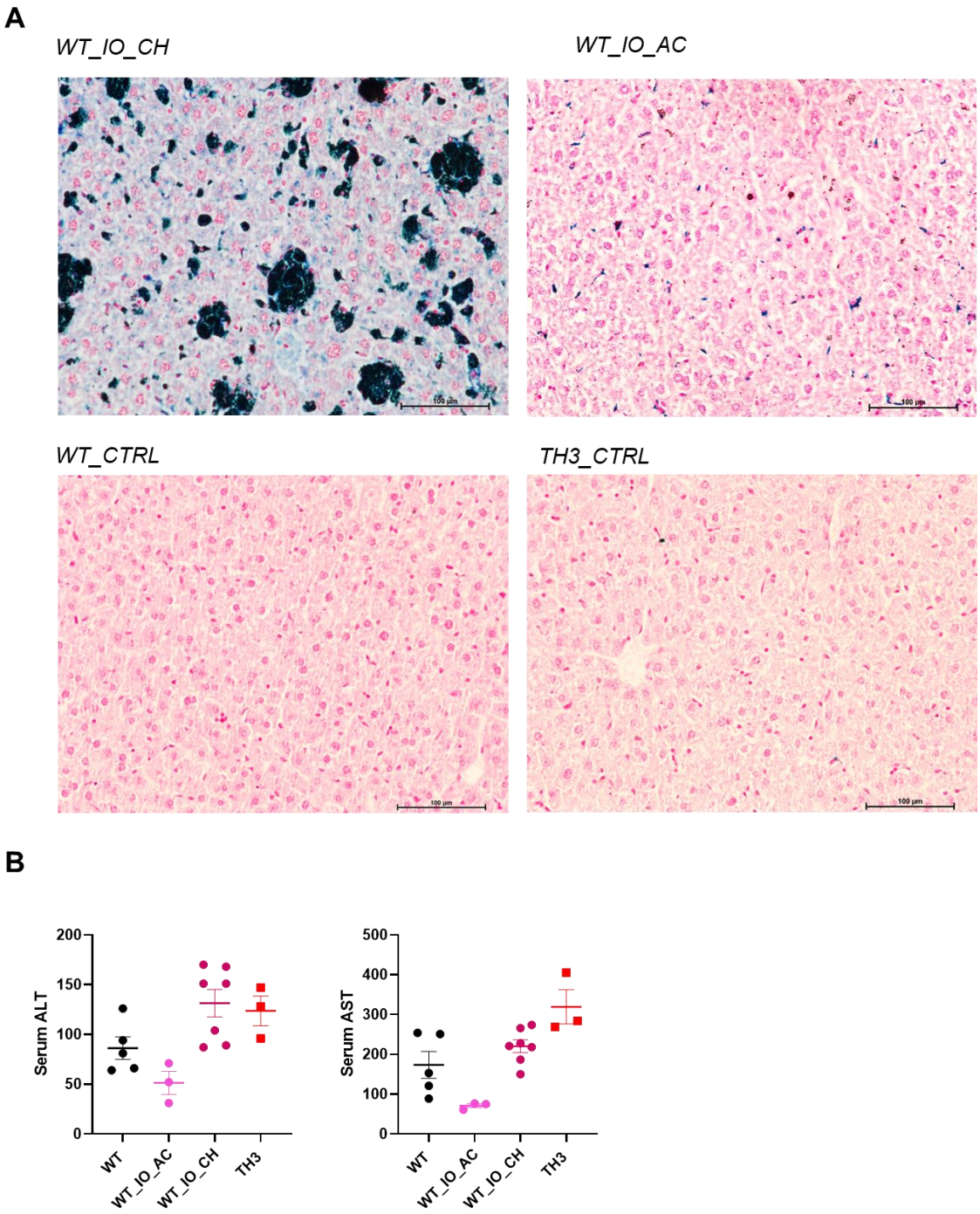

Figure 19. Iron accumulation in the liver of WT_IO mice. *(A) Histological analyses of liver subjected to Perl's iron staining. Representative images of wt, WT_IO_AC, WT_IO_CH and th3 liver sections are shown. Magnification 20X. Scale bar, 100μM. (B) Quantification of serum ALT and AST levels (U/L) (wt, n=5; WT_IO_AC, n=3; WT_IO_CH, n=7; th3, n=3). Kruskal-Wallis test: *, p<0.05.*

To verify whether our acute and chronic IO mouse models could be exploited to study IO in the BM microenvironment and its effects on HSC metabolism and function, we

investigated iron accumulation histologically on BM cells and we analysed intracellular iron content. Briefly, BM cells from chronic IO, acute IO and control mice were spotted into a slide, fixed and then stained with Perl's staining. Fe^{3+} deposits were not detected in *th3* and acute IO BM (Fig. 20A). Consistently, analysis of intracellular iron levels by calcein-AM staining of BM cells from *th3* and acute IO mice revealed absence of intracellular iron accumulation. Also, BM F4/80^{+} macrophages, specialized in iron uptake and storage, did not exhibit increased intracellular iron content in *th3* and acute IO mice, as shown by calcein-AM staining (Fig. 20B). Notably, while Perl's staining allows the detection of Fe^{3+} once it is released from ferritin, calcein-AM allows the detection of intracellular free reactive Fe^{2+}. These findings suggest that *th3* and acute IO mice mainly accumulated iron in the spleen, rather than in the liver and BM. On the contrary, chronic IO BM displayed higher iron deposition, as shown by Perl's staining (Fig. 20A). In addition, calcein-AM staining showed a trend of increased iron content in BM F4/80^{+} macrophages of chronic IO mice, as reflected by higher calcein-AM quenching in the presence of iron (Fig. 20B).

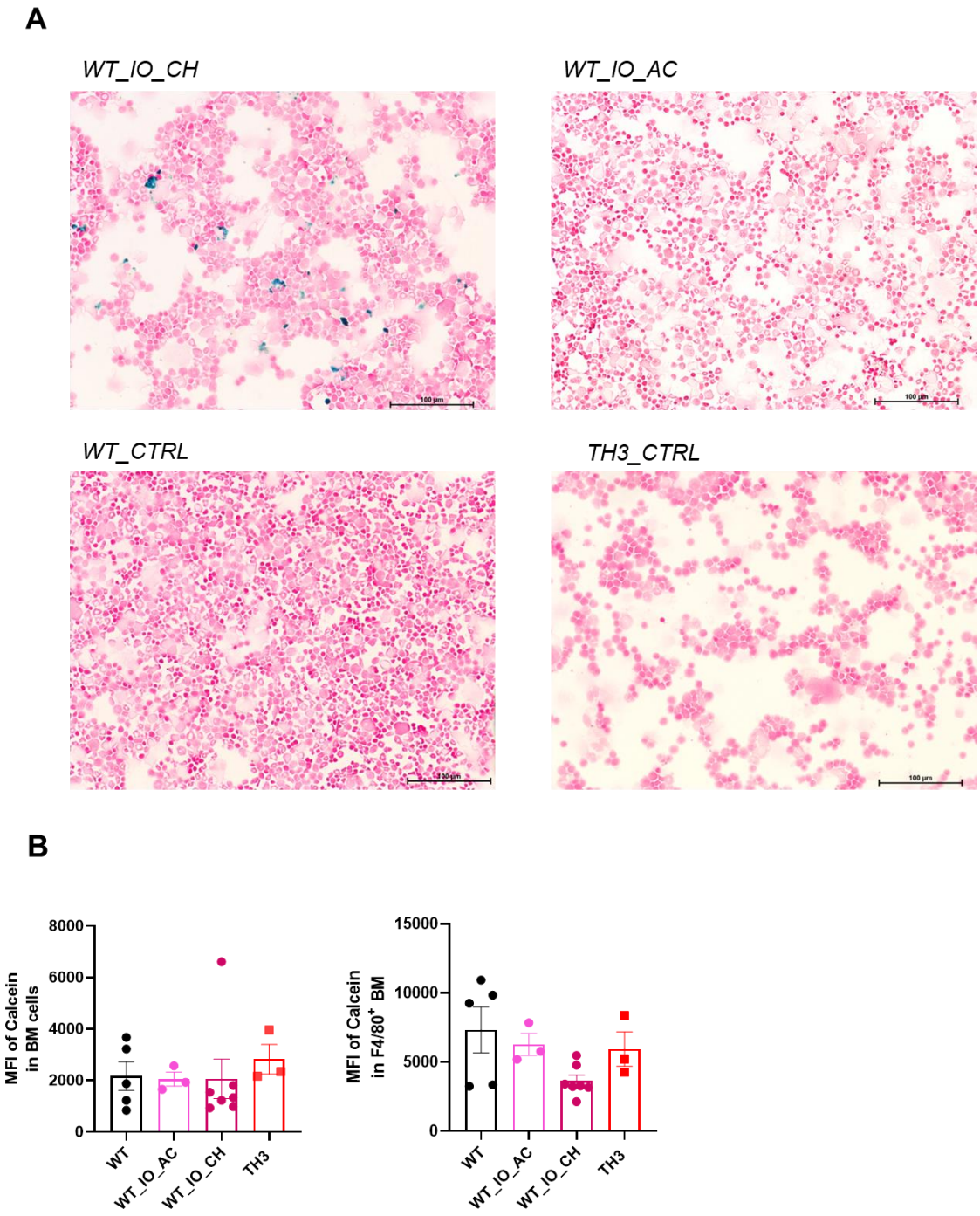

Figure 20. Iron accumulation in the BM of WT_IO mice. *(A) Histological analyses of cytospin of BM cells subjected to Perl's iron staining. Representative images of wt, WT_IO_AC, WT_IO_CH and th3 BM cells are shown. Magnification 20X. Scale bar, 100μM. (B) Quantification of intracellular iron content in wt, WT_IO_AC, WT_IO_CH and th3 BM cells and F4/80⁺ macrophages by flow cytometry. MFI of calcein-am is reported. (wt, n=5; WT_IO_AC, n=3; WT_IO_CH, n=7; th3, n=3).*
*Kruskal-Wallis test: *, p<0.05.*

We then evaluated intracellular iron levels in SLAM HSCs after calcein-AM staining of Lin$^-$ cells. We confirmed higher intracellular iron content in *th3* HSCs than wt, as already reported (Fig. 21, 2A). Moreover, HSCs from both acute and chronic IO mice had intracellular iron levels comparable to that of *th3* HSCs. Unexpectedly, a single injection of iron dextran is sufficient to achieve intracellular IO in HSCs.

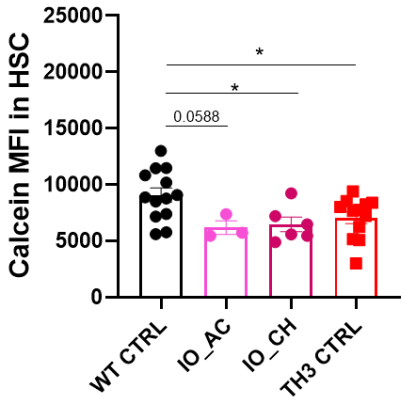

Figure 21. Intracellular iron overload in HSCs from WT_IO mice. *Quantification of intracellular iron content in wt, WT_IO_AC, WT_IO_CH and th3 SLAM HSCs by flow cytometry. MFI of calcein-am is reported. (wt, n=13; WT_IO_AC, n=3; WT_IO_CH, n=6; th3, n=12). Kruskal-Wallis test: *, p<0.05.*

Collectively, these data demonstrate that both acute and chronic administration of 25mg/ml of iron dextran to wt mice are able to generate systemic IO mouse models with high serum iron levels. Under acute treatment, iron preferentially accumulates in the spleen, as in *th3* mice. On the contrary, the chronic treatment induces a more severe IO phenotype, characterized by high iron deposition in spleen and BM and excessive liver iron content leading to organ damage. For these reasons, chronic IO could be exploited to study the effects of iron on BM niche as exacerbated model of IO. Moreover, both the established IO mouse models show intracellular IO in HSCs, confirming that HSCs can uptake and store iron. Whether HSCs are a preferential site for iron accumulation in the BM in IO conditions remains to be explored.

To demonstrate whether IO alone is sufficient to damage mitochondrial fitness through ROS production, flow cytometric analyses of mtROS and mitochondrial activity were performed.

The frequency of MitoSOX$^+$ SLAM HSCs increased in a dose-dependent manner after iron dextran administration (Fig. 22).

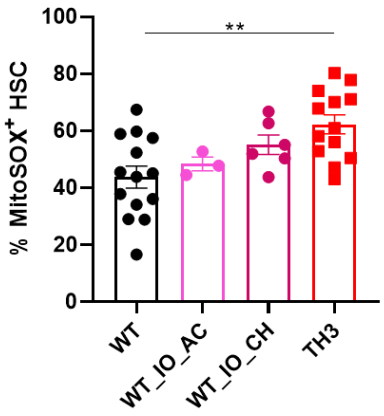

Figure 22. Increased mtROS content in HSCs from WT_IO mice. *Quantification of mtROS in wt, WT_IO_AC, WT_IO_CH and th3 SLAM HSCs by flow cytometry. % MitoSOX$^+$ HSC is reported (wt, n=14; WT_IO_AC, n=3; WT_IO_CH, n=6; th3, n=13).*
*Kruskal-Wallis test: **, p<0.01.*

Importantly, we found a statistically significant reduction in the % and MFI of TMRE$^+$ SLAM HSCs and TMRE total MFI in IO mice, as compared to wt controls, indicating that IO causes mitochondrial dysfunction in HSCs. Notably, chronic IO and *th3* HSCs showed comparable levels of TMRE MFI (Fig 23).

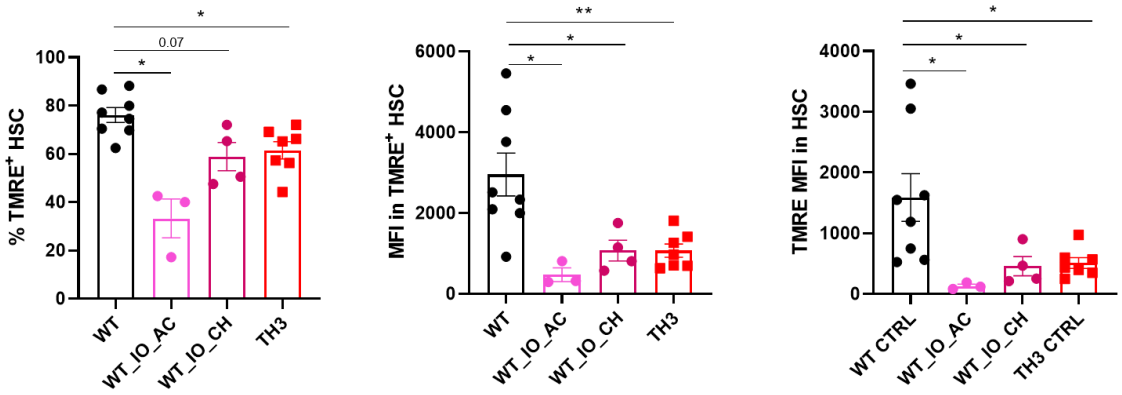

Figure 23. Iron overload reduces mitochondrial activity in HSCs from WT_IO mice. *Quantification of mitochondrial activity in SLAM HSCs from wt, WT_IO_AC, WT_IO_CH and th3 mice by flow cytometry. Percentage of TMRE⁺ SLAM HSC (left), MFI in TMRE ⁺ SLAM HSC (center) and TMRE MFI (right) are reported. (wt, n=8; WT_IO_AC, n=3; WT_IO_CH, n=4; th3, n=7).*
*Kruskal-Wallis test: **, p<0.01; *, p<0.05.*

Overall, HSCs from both acute and chronic IO mouse model recapitulate what we reported in *th3* mice: intracellular IO, high mtROS resulting in oxidative stress and consequent mitochondrial dysfunction. Therefore, IO alone is sufficient to reduce mitochondrial activity in HSCs from wt mice. Interestingly, the mitochondrial dysfunction induced with a single dose of iron dextran could suggest a direct effect of IO on HSCs rather than an indirect effect mediated by other BM cell populations.

We previously reported absence of iron accumulation and mitochondrial oxidative stress in *th3* MPPs and LSKs progenitors (Fig. 15-16). We wondered whether the different behaviour of HSCs and progenitors is peculiar to BThal, as a results of a plethora of stress signals in the BM niche, or intrinsically determined. To address this, we analysed intracellular iron content and mtROS in progenitors in the IO mouse models.

No differences were found between IO and controls MPPs/LSKs in terms of intracellular iron levels and mtROS, thus suggesting that HSCs and progenitors display a different sensibility to iron also in a normal wt BM niche (Fig. 24A-B).

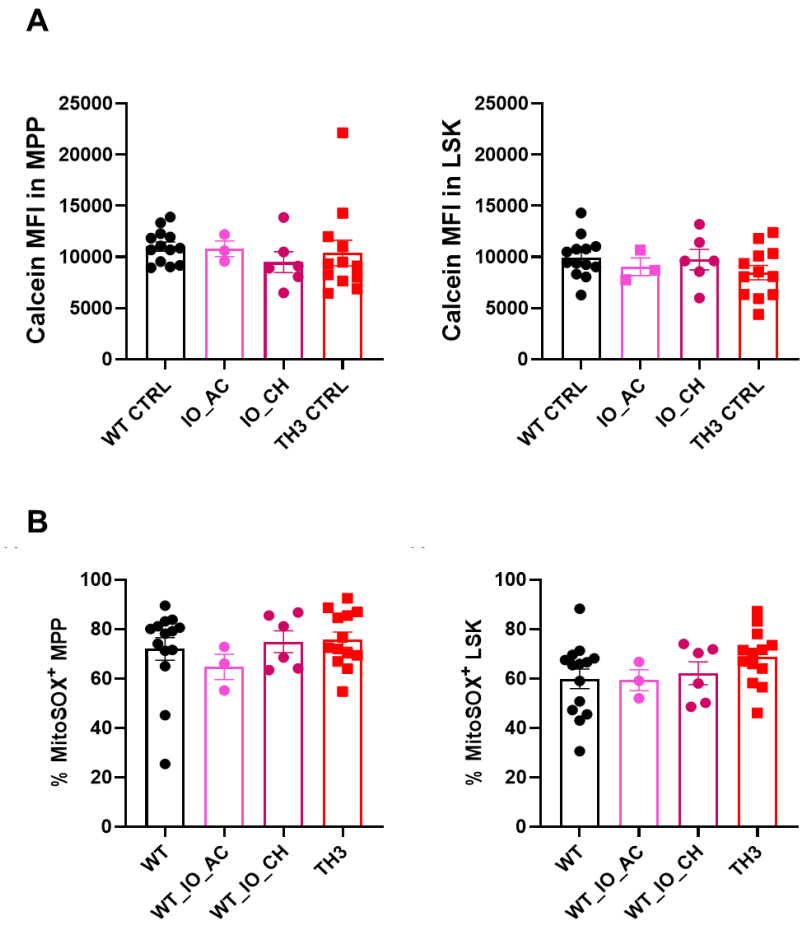

Figure 24. Iron deposits and the resulting oxidative stress are absent in progenitors from WT_IO mice. *(A) Quantification of intracellular iron content in wt, WT_IO_AC, WT_IO_CH and th3 progenitors by flow cytometry. MFI of calcein-am is reported (wt, n=13; WT_IO_AC, n=3; WT_IO_CH, n=6; th3, n=12). (B) Quantification of mtROS in wt, WT_IO_AC, WT_IO_CH and th3 progenitors by flow cytometry. % MitoSOX⁺ cells is reported (wt, n=14; WT_IO_AC, n=3; WT_IO_CH, n=6; th3, n=13).*
*Kruskal-Wallis test: *, $p<0.05$.*

In *th3* mice IE results in anemia and IO. IO could further worsen IE and complicate the clinical picture. Indeed, IO induces oxidative stress in RBCs, resulting in increased cell death and reduced Hb levels (Taher *et al.*, 2018). Therefore, we checked whether *in vivo* administration of iron dextran to wt mice could damage RBCs and hemoglobin synthesis. The number of RBCs and the Hb levels did not show significant difference between IO and wt control mice (Fig. 25). These data suggest that iron alone, at least at the dosage and time used, is not sufficient to induce in wt mice IE and anemia to levels comparable to that of *th3* mice.

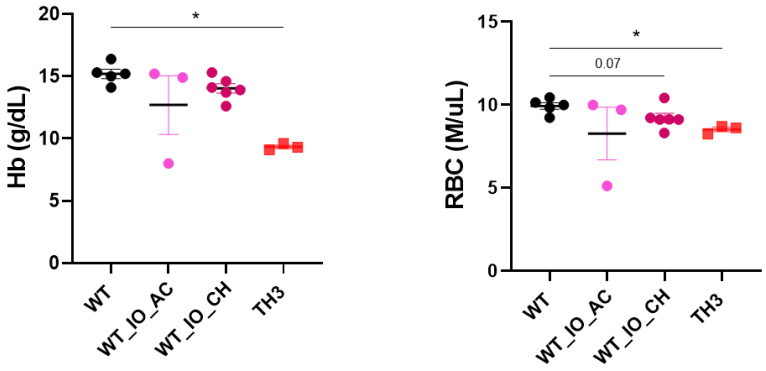

Figure 25. Normal hematological parameters in WT_IO mice. *Hemoglobin levels (Hb, g/dL) and red blood cell count (RBC, 10^6/µl), respectively, in peripheral blood of wt, WT_IO_AC, WT_IO_CH and th3 mice (wt, n=5; WT_IO_AC, n=3; WT_IO_CH, n=6; th3, n=3). Kruskal-Wallis test: *, p<0.05.*

Overall, we generated acute and chronic IO mouse models that show high serum iron levels, iron deposition in the major iron storage organs and more importantly intracellular IO in HSCs. These models display mitochondrial oxidative stress and reduced mitochondrial function in HSCs, thus demonstrating that intracellular IO alone damages mitochondria through ROS generation. We also reported for the first time a different response to iron in HSCs and progenitors.

DISCUSSION

HSC function is regulated by complex interactions with the local BM microenvironment, defined as “niche”. In physiological conditions, cytokines and growth factors secreted by different BM cell populations, biochemical factors and physical stimuli within the niche control the balance between self-renewal and differentiation, thus maintaining HSC homeostasis. However, studies in aged BM niche or hematologic malignancies have shown that several stress signals can alter the crosstalk between HSCs and other BM niche components or can directly affect HSCs (Batsivari *et al.*, 2020). Among the stress signals, the effects of iron on HSC maintenance have recently gained increasing attention.

Iron exerts fundamental roles by taking part in oxygen transport, cell metabolism and signaling as a component of the prosthetic group of many proteins. However, free iron can participate in harmful chemical reactions that produce toxic ROS, therefore HSCs, similarly to other cells, finely regulate intracellular iron levels maintaining low free iron content and a bias towards iron storage in ferritin to limit ROS production (Kao Y-R, 2021). On the contrary, intracellular IO in HSCs promotes oxidative stress, leading to their dysfunction and exhaustion (Chai *et al.*, 2015; Muto *et al.*, 2017). Similarly, intracellular iron deficiency reduces HSC self-renewal and repopulating ability *in vivo* (Wang *et al.*, 2020; Zhang *et al.*, 2022). Both excessively high and low concentrations of iron in culture decrease HSC number (Zhang *et al.*, 2022). Overall, these findings suggest that both intracellular IO and iron deficiency negatively impact on HSC behavior and limiting iron accumulation is essential to preserve stem cell function.

HSCs adapt their metabolic state to their function: quiescent HSCs have low energy requirements and depend on anaerobic glycolysis, whereas active HSCs require high energy for proliferation and differentiation thus enhance OXPHOS, glycolysis and FAO. Since iron has emerged as a key regulator of HSC self-renewal and differentiation, we wondered whether it exerts its regulatory role on HSCs by modulating their metabolism. Recently, low intracellular iron content has been reported to sustain HSC expansion through upregulation of mitochondrial FAO (Kao Y-R, 2021) but a deep characterization of the role of iron as extrinsic regulator of HSC metabolism is lacking.

Both IO and iron deficiency were reported to impair mitochondria in cells other than HSCs, thus affecting cell metabolism. However, the effects of iron fluctuations on mitochondrial fitness in HSCs are still unexplored.

To gain new insight about the role of iron on HSC biology and to understand which metabolic pathways are triggered by intracellular iron levels, we studied HSC metabolism in BThal, as a model of systemic IO. Previous studies from our group revealed a reduced quiescence, impaired function and activated transcriptional responses to stress in HSCs from *th3* murine model, recapitulating the major features of BThal intermedia, including IO. *Th3* functional defects are rescued upon transplantation into a wt BM niche, thus indicating that stress signals in the BM microenvironment impair HSC function (Aprile *et al.*, 2020). We also reported that IO reduces the hematopoietic supportive capacity of BM MSCs in BThal patients, thus impairing HSC expansion and repopulating ability *in vivo* (Crippa *et al.*, 2019). However, there is no evidence of the direct effect of IO on HSCs in BThal. We hypothesized that IO and the resulting oxidative stress might directly impairs HSCs. Moreover, the positive enrichment of genes encoding metabolic enzymes and antioxidants in *th3* HSC transcriptome profile prompted a deeper investigation of HSC metabolism in response to chronic IO, making *th3* mice an ideal model to study the link between iron, ROS and metabolic regulation of HSCs.

In the present study, we uncovered that intracellular iron levels affect the metabolic programs underlying HSC function in BThal. BThal HSCs directly sense iron and intracellular IO negatively impacts on HSC metabolism and function by impairing mitochondrial fitness through ROS generation. These findings added novel insight about the role of iron regulation and metabolism in HSC biology and might also provide clues for improving therapeutic solutions for BThal and other clinical conditions associated to IO.

1 – Abnormal iron homeostasis in *th3* HSCs

We directly measured free reactive iron, commonly known as LIP, in HSCs from *th3* mice, showing higher iron content as compared to wt, thus indicating intracellular IO. This finding was unexpected since iron mainly accumulates in the liver, heart and spleen of BThal patients and within the BM it is mostly utilized by erythroid cells for hemoglobin

synthesis. The intracellular IO in *th3* HSCs could indicate a novel role of HSCs in taking part in iron homeostasis.

The increased LIP size accompanied by positive enrichment of *Tfr1* suggests that intracellular IO is the result of enhanced iron uptake from the microenvironment by HSCs. However, the molecular mechanism leading to intracellular IO is still unknown. To maintain iron homeostasis, *Tfr1* is downregulated in IO conditions due to inactivation of IRP1/2 system (Hentze *et al.*, 2010). We can speculate that the dysregulation of the iron-sensing machinery due to a prolonged exposure to IO in the niche causes excessive free iron accumulation in *th3* HSCs, a mechanism similar to that reported for BThal MSCs that upregulate the expression of *Tfr1* after treatment with iron *in vitro* (Crippa *et al.*, 2019).

The upregulation of *HO-1* expression could contribute to increase the LIP in *th3* HSCs. HO-1 is involved in iron recycling by degrading free heme to release iron and the antioxidant biliverdin and bilirubin. Heme homeostasis has been mainly studied in RBCs, where high amount of heme is required for their differentiation, and little is known about heme regulation and its effects on HSC function. Heme is the most potent inducer of HO-1 (Chiabrando *et al.*, 2014) and interestingly our RNAseq data showed an upregulation of genes encoding enzymes involved in heme synthesis, such as *Hmbs*, *Alad*, *Cpox* and *Fech,* suggesting increased heme production. Therefore, we hypothesize that the increased *Tfr1*-mediated iron uptake from the BM niche causes intracellular IO and triggers a vicious circle with enhanced heme synthesis, that in turn induces heme degradation through *HO-1*, thus further increasing iron accumulation in *th3* HSCs. Consistently, HO-1 activity was reported to mediate IO in the liver of *th3* mice and inhibition of HO-1 decreases liver iron and improves anemia (Garcia-Santos *et al.*, 2018). Furthermore, upregulation of HO-1 in HSPCs was found to decrease their engraftment (Adamiak *et al*, 2016), which correlates with our results of reduced repopulating ability of *th3* HSCs (Aprile *et al.*, 2020).

Th3 HSCs exhibit also increased expression of the iron storage protein ferritin (*Fth1*, *Ftl1*) and the iron exporter *Fpn*, which under normal conditions limit excess intracellular free iron. However, intracellular IO, despite the upregulation of ferritin and *Fpn*, suggests an impairment of iron storage and export. FPN is regulated post-transcriptionally by the hepatic hormone hepcidin, which sustains systemic iron homeostasis and in BThal

hepcidin expression is reduced due to increased production of ERFE by proliferating RBCs. Moreover, FPN and ferritin translation are controlled by IRPs, which maintain intracellular iron homeostasis by binding to IREs in mRNA encoding for proteins involved in iron metabolism. In particular, IRPs bind to *Ft* and *Fpn* thus repressing their translation in iron deficiency condition, whereas IRPs are inactivated in IO conditions to increase iron mobilization from the stores and iron export (Hentze *et al.*, 2010). However, ferritin and *Fpn* upregulation seems to be insufficient to counteract the accumulation of excess reactive iron in *th3* HSCs.

Given the central role of mitochondria in iron metabolism, we wondered whether mitochondria show abnormal accumulation of iron in *th3* HSCs. Interestingly enhanced accumulation of the iron-sensitive dye Mitoferro-green in the mitochondrial matrix revealed increased free Fe^{2+}, thus suggesting potentially harmful effects on mitochondrial fitness.

2 – IO causes mitochondrial dysfunction in HSCs

We reported that *th3* HSCs have reduced mitochondrial mass, as shown by reduced accumulation of the specific mitochondrial dye MTG by flow cytometry. We further confirmed this finding by TEM analysis, which enabled us to directly measure the area of single mitochondria, showing reduced mitochondrial size.

MMP is the electric gradient between the two sides of IMM resulting from the ETC activity, thus it is a widely recognised measure of mitochondrial function (Perry *et al.*, 2011). *Th3* HSCs stained with TMRE dye, that accumulates in the mitochondrial matrix in proportion to MMP, showed reduced mitochondrial activity, regardless of their decreased mass, as shown by lower TMRE/MTG ratio. Moreover, we categorized HSCs in MMP^{low} and MMP^{high} based on TMRE intensity as previously reported (Liang *et al.*, 2020; Mansell *et al.*, 2021; Qiu *et al.*, 2021) and we further confirmed these data, showing a reduced fraction of MMP^{high} HSCs in BThal.

In the past, staining with mitochondrial dyes, such as MTG and TMRE, led to erroneous conclusions. In particular, Snoeck group reported that HSCs display low MTG fluorescence due to dye efflux rather than reduced mitochondrial mass. Indeed, blocking efflux pumps with verapamil results in higher MTG fluorescence (de Almeida *et al.*,

2017). The effect of verapamil in modulating TMRE fluorescence is still controversial in the field (Liang *et al.*, 2020; Mansell *et al.*, 2021). Although we detected reduced mitochondrial mass by TEM and we functionally proved reduced mitochondrial activity by ATP analyses in *th3* HSCs, we will perform MTG and TMRE staining in the presence of verapamil to further confirm our data.

Mitochondrial function is dynamically controlled by cycles of biogenesis, fusion, fission and degradation through mitophagy, which continuously shape the mitochondrial network. Strikingly, our RNAseq data revealed an overall downregulation of mitochondrial dynamics in *th3* HSCs, that could contribute to mitochondrial dysfunction. We found reduced expression of *Tfam* and *Tfb1m*, the major regulators of mitochondrial biogenesis (Gleyzer *et al*, 2005), thus suggesting a reduced generation of new mitochondria. Mitophagy specifically degrades dysfunctional mitochondria and the balance between mitochondrial biogenesis and mitophagy regulates mitochondrial number within the cell. Interestingly, we found decreased expression of key mitophagy players, such as *Ulk1*, *Optn*, *Gabarapl1*, *Map1lc3b* and *parkin* in *th3* HSCs (Bingol & Sheng, 2016), thus suggesting accumulation of damaged mitochondria. Since the reduced generation of new mitochondria is balanced by an impaired degradation, the mitochondrial number is maintained constant, as confirmed by TEM analysis showing the same number of mitochondria per cell in *th3* and wt HSCs. Recently, it has been reported that loss of *Parkin* leads to the accumulation of damaged mitochondria, with low mass and activity in HSCs (Ho *et al.*, 2017), and reduces their self-renewal and repopulating ability (Ito *et al.*, 2016), a condition that might be similar to the one observed in BThal.

We also found reduced mitochondrial fission in *th3* HSCs, as indicated by decreased expression of the fission initiator *Drp1* and fission mediators, such as *Fis1*, *Mff* and *Mief1/2*. These data are in line with reduced mitophagy since mitochondrial fragmentation through fission usually precedes mitophagy (Youle & van der Bliek, 2012). Moreover, pharmacological inhibition and genetic deletion of *Drp1* has been shown to reduce mitochondrial activity and impair repopulating ability of HSCs (Hinge *et al.*, 2020). Therefore, we speculate that altered mitochondrial dynamics, in particular reduced mitophagy and fission, might be responsible for impaired mitochondrial activity and *th3* HSC functional defects. Since our RNAseq data showed subtle differences of gene

expression between *th3* and wt samples, we need to demonstrate whether they result in differences of biological functions. Thus, immunofluorescence analyses of specific mitochondrial proteins, such as Tomm20, or Drp1 will be exploited to examine the distribution of mitochondrial network within HSCs and evaluate the number and area of mitochondrial fragments, as a measure of mitochondrial fission. Moreover, immunofluorescence analyses of the mitophagy player *Map1lc3b* will be pivotal to confirm reduced mitophagy in *th3* HSCs.

Given the complexity of BThal BM niche, in which different stress signals can affect mitochondrial fitness and HSC metabolism, making it difficult to dissect various stimuli/effects, we decided to study the effects of IO specifically on mitochondria in wt context. To this aim, we generated acute and chronic IO mouse models by *in vivo* administration of iron dextran to wt mice, as previously reported (Chai *et al.*, 2015; Zhang *et al.*, 2022). Interestingly, we described in these models for the first time the link between iron and mitochondria in HSCs, unveiling that IO alone is sufficient to induce mitochondrial dysfunction. Both acute and chronic IO mice displayed systemic IO, as shown by higher serum iron and iron accumulation in the spleen and liver. Of note, chronic IO mice had increased iron deposition in the BM, thus suggesting a more severe phenotype than acute IO and *th3* mice. Systemic IO resulted in intracellular IO in HSCs to comparable levels of those of *th3* mice, thus confirming that HSCs can uptake iron from the microenvironment, and caused reduced mitochondrial function, as shown by decreased MMP. Interestingly, acute IO mice were treated with a single dose of iron dextran and in just 24h they developed mitochondrial dysfunction, thus suggesting a direct effect of IO on mitochondria in HSCs. To specifically identify which molecular pathways are activated by IO and directly affect mitochondria and HSC function, we will set up *in vitro* culture of sorted HSCs from IO and *th3* mice and we will evaluate the expression of specific mitochondrial genes (e.g. *Drp1* and *parkin*) after treatment with iron chelators.

In chronic IO conditions, such as *th3* and chronic IO wt mice, we cannot exclude also an indirect effect of IO on HSCs by affecting other BM niche populations. Among the hematopoietic cells, Mφs play an essential role in iron homeostasis by recycling iron from senescent erythrocytes. Under normal conditions, splenic Mφs are the major cell populations involved in erythrophagocytosis but also $F4/80^{+}VCAM1^{+}CD169^{+}$ER-

$HR3^{+}Ly6G^{+}$ Mφs in the erythroblastic islands participate in iron recycling and delivery primarily to RBCs (Jacobsen *et al*, 2014). Recently, GR-$1^{-/low}$ $CD115^{int}$ $F4/80^{+}$ $SSC^{int/low}$ $CD169^{+}$ Mφs were reported to increase erythrophagocytosis and provide iron to HSCs under regenerative stress. Conversely, depletion of this population of BM Mφs reduced iron in the BM and in HSCs and impaired HSC differentiation (Zhang *et al.*, 2022). Our unpublished data showed increased frequency of erythroblastic island Mφs in *th3* mice, suggesting increased iron accumulation in the BM. To check whether Mφs contribute to intracellular IO in BThal HSCs, we performed a broad evaluation of intracellular iron content in BM and splenic $F4/80^{+}$ Mφs. As expected, we found a trend to increased iron accumulation in splenic $F4/80^{+}$ Mφs, suggesting an increased erythrophagocytosis. On the contrary, there were no differences in intracellular iron content between wt and *th3* $F4/80^{+}$ BM Mφs, suggesting that they are not involved in iron recycling. However, deeper analyses of different populations of BM Mφs, including GR-$1^{-/low}$ $CD115^{int}$ $F4/80^{+}$ $SSC^{int/low}$ $CD169^{+}$ Mφs (Chow *et al.*, 2011), are required to assess their role in regulating iron availability and delivery to BThal HSCs.

Furthermore, iron reduces the secretion of regulatory cytokines by stromal cells, thus impairing HSPCs in chronic IO mice (Okabe *et al.*, 2014). Accordingly, we have reported that intracellular IO reduces the supportive capacity of human BThal MSCs, resulting in impaired HSC expansion *in vitro* and engraftment *in vivo* (Crippa *et al.*, 2019). Also bone defects have been associated with IO in BThal patients. Iron deposits were found along the mineralization front in the bones and were correlated with impaired bone mineralization and focal osteomalacia in BThal patients with suboptimal ICT (Mahachoklertwattana *et al*, 2003). Interestingly, we reported reduced OB activity due to low levels of PTH, and consequent impaired HSC function in *th3* mice (Aprile *et al.*, 2020). Moreover, IO in the circulation causes vascular inflammation by increasing the expression of pro-inflammatory cytokines and adhesion molecules in ECs, thus resulting in vascular stiffness and EC dysfunction (Cheung *et al*, 2002; Voskou *et al.*, 2015). However, the exact molecular mechanism by which iron damages these cell populations and consequently alters the crosstalk between HSCs and stromal cells is still unknown. Direct measurement of intracellular iron content and evaluation of supportive factor secretion will be pivotal in understanding the contribution by stromal cells to mitochondrial dysfunction and functional defects of *th3* HSCs.

3 – IO impairs HSC metabolism and function through ROS generation

Free iron is a well-known prooxidant molecule since it can participate in Fenton and Haber-Weiss reactions, thus generating ROS. Moreover, degradation of heme, the predominant form of iron in the cell, releases iron, further increasing ROS levels (Chiabrando *et al.*, 2014).

To verify whether iron toxicity on mitochondria is mediated by oxidative stress, we measured mtROS levels. Strikingly, we found increased mtROS content in *th3* HSCs, consistent with intracellular IO. Moreover, *th3* HSCs showed upregulation of many genes encoding antioxidants, which are mainly located in the cytosol and mitochondria, close to the sources of ROS to limit oxidative stress. Intracellular IO was already reported to induce the transcription of antioxidant genes in HSCs, albeit inefficient in neutralizing the excess of ROS (Muto *et al.*, 2017). The increased expression of *Sod2*, which is induced by high mtROS, suggests mitochondrial oxidative stress (Pani *et al.*, 2009). Therefore, we hypothesized that mtROS accumulation activate antioxidants, which however fail to counteract mtROS increase, thus generating oxidative stress.

To demonstrate that IO leads to oxidative stress in HSCs, we treated wt mice with iron dextran for one month and then we checked mtROS levels. IO chronic mice showed mitochondrial oxidative stress and reduced mitochondrial activity in HSCs, indicating that iron regulate HSC mitochondrial function.

We then reduced mtROS in *th3* mice by *in vivo* administration of the mitochondria-targeted antioxidant MitoQ to prove that ROS cause mitochondrial dysfunction and to verify whether mitochondrial damage is reversible. MitoQ treatment completely rescued mitochondrial activity, as shown by increased MMP in MitoQ *th3* mice. Moreover, the lower glucose uptake might suggest that HSCs maximize the production of ATP from pyruvate through OXPHOS. Importantly, ROS reduction increased HSC frequency and quiescence, thus indicating beneficial effects on *th3* HSCs. Ongoing transplantation experiments of sorted HSCs from MitoQ *th3* mice will show whether the rescue of mitochondrial function restores also BThal HSC repopulating ability and self-renewal.

The evaluation of mitochondrial activity and metabolism, as well as HSC quiescence and function, after iron chelation strategies is pivotal to prove that intracellular IO is one of the upstream causes of mitochondrial alterations and HSC dysfunction in BThal.

Given the complexity of the disease context, we expect that other sources of ROS, in addition to intracellular IO, could contribute to oxidative stress in BThal and the complete rescue of mitochondrial function after MitoQ could result from its ability to efficiently eliminate mtROS, regardless of their origin.

Recent advances have highlighted the critical role of inflammation as source of oxidative stress, affecting HSC fate. HSCs proliferate, rapidly differentiate and lose self-renewal capacity in response to many inflammatory signals, such as IFNs, TNFs, IL-1, G-CSF and DAMPs, and the activation of the inflammatory cascade results in ROS production (King & Goodell, 2011). Since, hemolysis and IE leads to the release of DAMPs into the circulation, we hypothesize a status of chronic sterile inflammation in BThal (Mendonca *et al*, 2016). Heme is one of the major DAMPs and it can activate TLR signaling and cause inflammasome formation in immune cells, including macrophages and neutrophils, thus resulting in the release of pro-inflammatory cytokines and ROS (Bozza & Jeney, 2020; Vinchi *et al*, 2021).

Moreover, variations of oxygen levels are associated with higher ROS in HSCs. BM is widely recognized hypoxic tissue and hypoxia preserves HSC quiescence and function by limiting OXPHOS and consequent ROS production (Kobayashi *et al.*, 2019; Mantel *et al.*, 2015). Also increased hypoxia (around 1,5%) causes ROS accumulation (Chandel *et al*, 1998; Waypa & Schumacker, 2002). HSCs mainly localize in areas with an intravascular pO_2 of about 3% and an extravascular pO_2 around 2% in the BM. However, deep hypoxic regions, with extravascular pO_2 around 1%, were detected but HSCs were not found in these areas, thus suggesting that localization to the regions of deepest hypoxia impairs HSC maintenance (Christodoulou *et al.*, 2020). In BThal, anemia is expected to generate tissue hypoxia, although direct measurement in the BM has not been performed so far, and deepest hypoxia could potentially impair HSC function by enhancing ROS.

4 – Active HSCs rely on a low-energy metabolism

To verify whether reduced MMP resulted in impaired *th3* HSC metabolism, we analysed ATP content both at basal level and after oligomycin treatment. Oligomycin inhibits ATP synthase thus abrogating ATP generation by OXPHOS. Since the two major

metabolic pathways involved in ATP production are OXPHOS and glycolysis, the remaining ATP amount after oligomycin administration is assumed to derive from glycolysis. We adopted this strategy because of the limited number of HSCs, making it difficult to perform accurate metabolic analyses through seahorse assay and metabolomic analysis.

Although intracellular ATP content is a balance between ATP generated by metabolic pathways and ATP utilized by cellular processes, commonly ATP detection is based on *ex vivo* luminescent assays, that do not consider ATP fluctuations in time but *bona fine* reflect cellular energetic metabolism. Therefore, high ATP levels indicate high energetic metabolism, whereas low ATP levels are usually found in cells with low basal metabolism.

While OXPHOS generates 36 ATPs, glycolysis produces only 2 ATPs per each glucose molecule. The minimal reduction in ATP content after oligomycin suggested glycolytic metabolism of *th3* HSCs. These findings were further confirmed by RNAseq analyses, showing positive enrichment of glycolytic enzymes, including *Tpi1*, *Gapdh* and *Pklr*. Moreover, glucose uptake assay revealed that *th3* HSCs uptake glucose more efficiently than the wt counterparts. Consistently, reduced intracellular lactate content indicated more rapid lactate extrusion in the extracellular space. Overall, our data revealed increased glycolytic dependency to compensate for reduced OXPHOS due to mitochondrial dysfunction in *th3* HSCs. However, since the remaining intracellular ATP after oligomycin reflecting glycolysis is reduced as compared to wt, we speculate that also glycolysis is less efficient in *th3* HSCs.

According to the general consensus in HSC biology, quiescent HSCs, that display low energy requirements, depend on glycolysis, whereas active HSCs enhances both glycolysis and OXPHOS to meet their increased energy demands (Filippi, 2021). Recently, the most primitive HSC compartment was classified based on mitochondrial activity into MMP^{low} and MMP^{high} HSCs and the vast majority of HSCs are MMP^{high}, actively cycling and primed towards differentiation with high mitochondrial activity and glycolysis, whereas only 25% of HSCs are quiescent MMP^{low} (Liang *et al.*, 2020; Mansell *et al.*, 2021). Our data are in line with these recent works and showed higher MMP^{high} HSCs in wt mice.

The increased proportion of MMP^{low} HSCs in *th3* mice is apparently in contrast with literature data linking HSC cell cycle, stemness and mitochondrial activity. MMP^{low} HSCs were reported to be mostly quiescent, label-retaining and with higher self-renewal (Liang *et al.*, 2020). On the contrary, *th3* HSCs are mostly cycling and show reduced stemness signature and self-renewal as compared to wt (Aprile *et al.*, 2020). Since mitochondria are defective, *th3* HSCs are unable to produce ATP through OXPHOS and rely on glycolysis, despite active cycling activity.

Therefore, we proposed that loss of HSC stemness in *th3* mice results from mitochondrial dysfunction and limited OXPHOS, thus suggesting an essential role of OXPHOS in preserving HSC function. In our model IO-derived ROS act on HSC function by affecting mitochondrial fitness and bioenergetic (Fig 1).

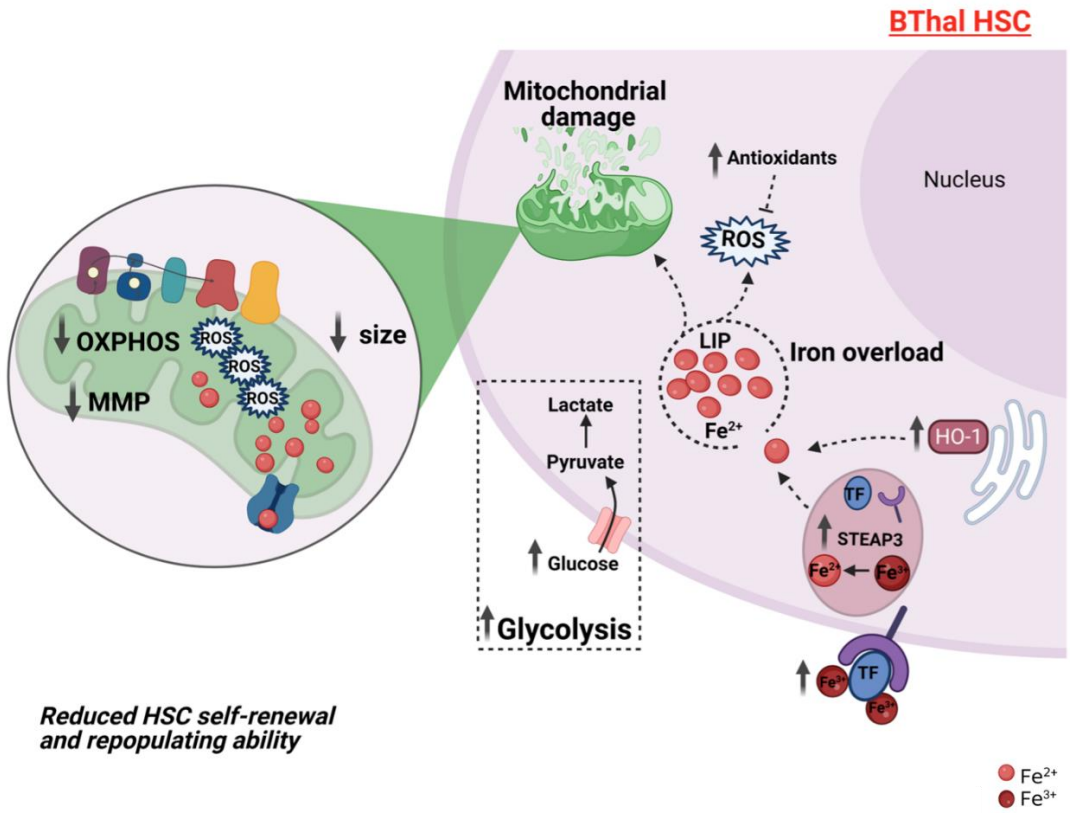

Figure 1. Working model of regulation of HSC metabolism and function by IO-derived ROS in BThal. *The upregulation of Tfr1 and Ho-1 leads to high intracellular free iron in the cytoplasm, which constitutes the LIP (labile iron pool), and in mitochondria, thus promoting ROS generation in HSCs. The activation of the antioxidant system fails to counteract excessive ROS thus leading to mitochondrial oxidative stress. As a result, mitochondria are impaired with low mass and activity, thus BThal HSCs cannot use OXPHOS and they enhance glycolytic metabolism to produce the energy required for their active cycling activity. Impaired mitochondrial activity ultimately results in reduced HSC frequency and quiescence (created with BioRender.com).*

Overall, we showed that chronic exposure to IO-derived ROS damaged mitochondria and rewired energy metabolism. Restoration of mitochondrial function by *in vivo* administration of MitoQ reduced glycolytic flux, and rescued HSC frequency and quiescence in *th3* mice. These findings are in line with Ansò et al. showing that complex II-deficient HSCs display reduced OXPHOS, enhanced glycolysis and decreased quiescence and repopulating-ability (Anso *et al.*, 2017). Moreover, the rescue of *th3* HSC quiescence after amelioration of mitochondrial function indicates that in our model metabolism determines HSC cell cycle status. We cannot exclude that ROS, besides affecting mitochondria, act directly on HSC cell cycle and function. Indeed, ROS can directly react with kinases and transcription factors (Ito *et al.*, 2006; Juntilla *et al.*, 2010) and they can alter the epigenetic landscape (Huang *et al*, 2022).

Why reduced ATP levels allow HSC proliferation remains an open question. We speculated that *th3* HSC condition could be similar to that of proliferating cancer cells that rely on anaerobic glycolysis. Most tumor cells depend on anaerobic glycolysis, even in the presence of sufficient oxygen for OXPHOS, and this phenomenon is called "Warburg effect" (Oliveira *et al*, 2021). Notably, metabolic rewiring reminiscent of Warburg effect was reported in aged $CD34^+$ cells (Hennrich *et al*, 2018). As a possible explanation for Warburg effect, it was reported that proliferating cells primarily need glycolytic intermediates to generate biomass, thus a large amount of nucleotides, lipids and amino acids, beyond ATP (Vander Heiden *et al.*, 2009). These evidence might explain why *th3* HSCs proliferate despite glycolysis dependency.

5 – Mitochondrial damage is progressively rescued during HSC differentiation in BThal

We demonstrated that chronic IO results in intracellular IO in the cytoplasm and in mitochondria in *th3* HSCs. IO promoted oxidative stress, which in turn induced mitochondrial dysfunction and impaired mitochondrial metabolism, thus contributing to reduced frequency and quiescence of *th3* HSCs.

In the differentiation landscape, HSCs at the top of the hierarchy can undergo asymmetric cell divisions to maintain stem cell homeostasis and give rise to MMPs that differentiate into distinct lineages of the entire hematopoietic system throughout lifetime.

Given the stressed status of BM niche, mitochondrial damage and HSC functional defects in BThal, we wondered whether these alterations are transferred to the progeny during cell division. For these reasons, we took advantage of our flow cytometry strategy that allows the concurrent identification of HSCs, MMPs and LSKs including predominantly more committed progenitors, and we evaluated intracellular iron accumulation, mtROS levels and mitochondrial activity in progenitors.

Interestingly, wt HSCs, MPPs and LSKs showed the same iron content thus suggesting that in normal conditions also progenitors maintain low intracellular iron content. While BThal HSCs accumulated intracellular IO, no signs of intracellular IO and the consequent mitochondrial oxidative stress were found in progenitors, as shown by equal intracellular iron content and mtROS levels in *th3* MMPs and LSKs as compared to wt. Of note, we corroborated these findings in acute and chronic IO wt mice, showing that also in those models only HSCs displayed intracellular IO and mitochondrial oxidative stress but not MPPs and LSKs.

It is reasonable to assume that also progenitors are exposed to chronic IO. Recently, live-animal imaging showed that HSCs and MPPs occupy the same area in the BM in physiological conditions (Christodoulou *et al.*, 2020). Therefore, the lack of iron and ROS accumulation in progenitors led us to hypothesize that IO and ROS-induced toxicity is progressively solved during HSC differentiation. Cells uptake iron from the bloodstream and, once in the cytoplasm, free labile iron is immediately ready for cellular use. Given its high toxicity, cells developed sophisticated systems for maintaining a balanced cellular iron homeostasis. IRP1/2 system post-transcriptionally regulates iron uptake, storage in ferritin and export (Hentze *et al.*, 2010). Limiting iron uptake by *TFR1*, increasing iron storage in ferritin or enhancing iron export through *FPN* could reduce free iron content. Also the mitochondrial processes utilizing iron, such as heme synthesis and the assembly of Fe-S cluster contribute to minimize iron toxicity (Muhlenhoff *et al.*, 2015). Moreover, the regulation of iron toxicity can also occur at the level of its byproduct ROS. Since progenitors physiologically display higher ROS than HSCs, their antioxidant system could be more efficient in neutralizing excess ROS. To confirm these hypotheses, gene expression analyses of genes involved in iron homeostasis and ROS scavenging, and evaluation of intracellular heme content in progenitors will be pivotal.

But why *th3* HSCs have increased vulnerability to IO and ROS as compared to progenitors is still an open question. Genetic deletion of the iron homeostasis genes Fbxl5 in the hematopoietic system only affected HSCs but not differentiated cells (Muto *et al.*, 2017). Recently, Sankaran group showed that erastin, a potent ferroptosis inducer, causes oxidative stress, lipid peroxidation and ferroptosis in primitive human HSCs but not in progenitors (Zhao *et al.*, 2022). The high sensitivity of HSCs to iron perturbations could be a mechanism to limit the expansion of the stem cell pool, avoiding leukemia onset. However, progenitors, that adapt lineage expansion and differentiation to hematopoietic demands, could have evolved protective mechanisms in response to excess iron and ROS.

Strikingly, we found reduced mitochondrial activity in *th3* MPPs, recapitulating what we observed in *th3* HSCs, whereas LSKs had normal mitochondrial activity, thus suggesting that mitochondrial rescue occurs in the transition from MPPs to more committed LSKs. We speculated that *th3* HSCs, unable to repair or remove dysfunctional mitochondria, transfer to MPPs mitochondrial abnormalities during cell division. Moreover, the presence of mitochondrial damage in *th3* MPPs, even in absence of intracellular IO and mitochondrial oxidative stress, might suggest that MPPs promptly limit intracellular IO and mtROS levels with their efficient detoxification systems but fail to repair mitochondrial damage. One potential strategy to remove dysfunctional mitochondria is mitophagy and we already found reduced mitophagy as well as mitochondrial biogenesis and fission in *th3* HSCs, thus we can speculate that defects in mitochondrial dynamics are maintained also in MPPs. On the contrary, absence of mitochondrial dysfunction in LSKs could suggest that they efficiently remove dysfunctional mitochondria through mitophagy and produce new healthy mitochondria.

Since mitochondrial OXPHOS supports MPP differentiation, reduced mitochondrial activity could suggest impaired function and lineage output. Recently, high mitochondrial activity was reported to prime HSCs towards MK lineage at steady-state, thus suggesting that mitochondria control lineage output (Nakamura-Ishizu *et al.*, 2018). Therefore, it could be interesting to study how the inheritance of dysfunctional mitochondria could affect the function of MPPs and eventually prime them towards specific lineages in BThal. Moreover, whether iron and the resulting ROS prime HSCs towards specific lineages is still unexplored and we could study these aspects by using *th3* mice, as a model of stressed BM niche, and more simplified model of IO wt mice.

6 – Targeting the BM niche in BThal

The identification and targeting of the key mechanisms influencing HSC function offer new avenues to improve HSCT for BThal patients. Recently our group highlighted multi-factorial alterations in BThal BM niche, in which secondary complications, such as bone defects and endocrinopathies, affect HSC maintenance. *In vivo* correction of the osteoblastic niche was able to ameliorate, but not completely rescue *th3* HSC activity (Aprile *et al.*, 2020), suggesting that additional molecular and cellular players are involved in HSC defects in BThal.

IO is the major source of ROS in BThal patients and many iron chelators are available to reduce iron accumulation in BThal patients. However, cases of absence of benefit have been reported and HSCT success depends on iron burden (Pilo & Angelucci, 2019). Our finding that BThal HSCs directly accumulate intracellular IO, suggests a crucial role of iron on HSC regulation, highlighting the importance of adequate and effective iron chelation therapies for a successful therapeutic outcome. In this view, it would be interesting to dissect how BThal HSCs sense iron and the molecular mechanisms leading to intracellular IO as well as the molecular pathways that link IO and mitochondrial damage.

Furthermore, we showed that IO-derived ROS directly reduce HSC frequency and quiescence, which are important for the amount and quality of HSCs harvested from patients for gene therapy and for their engraftment and repopulating ability once transplanted. Oxidative stress alters HSC function by impairing mitochondrial fitness and the reversibility of mitochondrial damage suggests a novel therapeutic target for improving HSCT, especially in the autologous setting of gene therapy. Although the proof that MitoQ restores HSC self-renewal and repopulating ability is still lacking, the significant positive and rapid effect of MitoQ on normalizing HSC mitochondrial activity and quiescence holds the promise that MitoQ administration could help restore damaged HSCs both before and after HSCT. Since oxidative stress, derived from IO or other stress signals in the BM niche, was reported to affect stromal cell populations, including MSCs and ECs (Crippa *et al.*, 2019; Voskou *et al.*, 2015), we speculate that treatment with MitoQ will favour HSC harvest and preserve their function both directly and indirectly, through amelioration of the BM niche. Moreover, we reported that MitoQ treatment increased Hb levels, RBC count and HCT, thus suggesting a positive effect on anemia.

Of note, several clinical trials have already showed MitoQ safety and efficacy for the treatment of vascular dysfunction, Parkinson disease and liver damage (Gane *et al*, 2010; Rossman *et al*, 2018; Snow *et al*, 2010).

Since mtROS are not the upstream cause of mitochondrial dysfunction and impaired HSC function, we expect that MitoQ treatment discontinuation might lead to increased mtROS levels, which in turn worsen BThal phenotype. Therefore, we should consider subjecting patients to prolonged treatment with MitoQ after HSCT in order to continuously neutralize the upcoming ROS.

A critical point will be to determine to what extent intracellular IO and mitochondrial damage are present and are responsible for HSC functional defects in BThal patients. To this aim, we will collect patients' samples and we will measure iron content, mtROS and mitochondrial activity in $CD34^{+}CD38^{-}$ primitive HSPCs.

Although *th3* mice recapitulate well the human pathology, they show some differences with BThal patients. *Th3* mice display primary IO with reduced hepcidin levels due to IE and hemolysis. However, they are transfusion independent, thus lacking secondary IO. Spleen of *th3* mice sequesters excess iron and the increased proliferation of erythroid precursors, even though ineffective, might consume iron, thus resulting in equal or low serum iron levels as compared to wt mice (Gardenghi *et al.*, 2007). On the contrary, patients with BThal intermedia and major have higher serum iron and ferritin levels (Taher & Saliba, 2017). Therefore, the prolonged residence of HSCs into patients' BM niche with high IO and oxidative stress might not be accurately reflected by weeks/months of exposure to damaged BM niche in mice.

Overall, our findings bring new insights in BThal pathophysiology and pave the way towards potential combined therapies to correct the genetic defect together with amelioration of the BM niche and HSC function.

7 – Future perspectives

Molecular mechanism leading to intracellular IO

Although we unravelled that BThal HSCs accumulate high levels of free reactive iron, it remains to be determined whether intracellular IO results from increased iron uptake from the BM niche or increased heme catabolism or both. To demonstrate whether

intracellular IO derives from the microenvironment, we will first validate our RNAseq data by the quantification of the iron importer Tfr1 at protein level, then we will analyse its role in mediating iron uptake in *th3* HSCs. If Tfr1 activity alone causes iron accumulation in *th3* HSCs, we might expect that loss of Tfr1 normalize intracellular iron levels. Of note, a recent work showed that Tfr1 haploinsufficiency results in reduced intracellular iron in erythroid precursors, thus improving IE and anemia in *th3* mice (Li *et al,* 2017) but no analyses on the stem cell compartment of *Tfr1*$^{+/-}$ *th3* mice were performed. We will take advantage of *Tfr1*$^{+/-}$ *th3* mouse model to analyse iron content and mitochondrial activity in HSCs. If intracellular IO derives from the niche, we might expect that *th3* HSCs accumulate further iron upon transplantation into *th3* recipients, whereas they are able to eliminate excess iron when not subjected to IO into wt recipients. Therefore, transplantation of HSCs from *Tfr1*$^{+/-}$ *th3* mice into *th3* recipients will unravel whether loss of Tfr1 is sufficient to normalize intracellular iron levels and restore *th3* HSC function. To avoid potential rebound effects of Tfr1 haploinsufficiency on iron regulation at systemic level and to dissect the effects of Tfr1-mediated iron uptake in HSCs we will treat sorted *Tfr1*$^{+/-}$ *th3* HSCs with iron *in vitro* and we will evaluate their function upon transplantation *in vivo*.

The upregulation of *HO-1* could suggest an additional mechanism leading to intracellular IO in *th3* HSCs. Direct measurement of intracellular heme content and analyses of protein levels of heme biosynthetic enzymes and HO-1 will be essential to demonstrate increased heme-iron recycling. To investigate the effects of heme catabolism on *th3* HSC metabolism and function, we will evaluate mitochondrial fitness and bioenergetic and HSC function upon inhibition of HO-1 by metalloporphyrins.

Given our RNAseq data, we reason that upregulation of iron uptake and heme degradation might act together to induce intracellular IO in HSCs. To test this, we will analyse *th3* HSC metabolism and function after administration of iron chelators non affecting free heme, such as DFX (Kontoghiorghes and Kontoghiorghe, cells 2020), and administration of metalloporphyrins *in vitro.*

Glycolysis dependency

A deep characterization of the glycolytic capacity and composition of metabolites in HSCs is required to understand how iron and ROS affect the global metabolic activity of these cells.

The Seahorse assay has been extensively used to analyse the oxygen consumption rate (OCR), as a measure of mitochondrial respiration, and extracellular acidification rate (ECAR), as a measure of glycolysis, in presence of metabolic inhibitors. This method requires a large amount of purified cells to obtain reliable results. Since HSCs are a rare population in the BM (0.0001% of total murine BM) and cannot be expanded without changing the metabolic profile and since they are quiescent with low metabolic activity as compared to many other cell types, it is extremely difficult to measure the OCR and ECAR of HSCs. To overcome these limitations, many groups analysed the metabolic profile of HSPCs as a surrogate for HSCs (Ansò *et al*, 2017; Nakamura-Ishizu *et al*, 2018; Liang *et al*, 2020) and recently the seahorse assay was optimized for LSKs (Scapin *et al*, 2019). However, the differences we have highlighted between BThal HSCs and progenitors, especially in terms of MMP, prevent us from using LSKs as a surrogate for HSCs.

A novel method to functionally profile energy metabolism has recently emerged. SCENITH (single-cell energetic metabolism by profiling translation inhibition) analyses metabolic dependencies with single-cell resolution by monitoring the changes in protein synthesis levels in response to metabolic inhibitors (Argüello *et al*, 2020). Protein synthesis consumes the majority of ATP produced by mitochondrial respiration and glycolysis, thus it can be used as readout of global metabolic activity. This method efficiently evaluated protein synthesis by flow cytometry in T cells and myeloid cell subsets. Since protein synthesis has already been extensively measured in HSCs (Mansell *et al*, 2022; Zhao *et al*, 2022) and SCENITH is based on flow cytometry, we reason that it could efficiently be used to study HSC metabolism. Of note, flow cytometry analysis is rapid and allow the metabolic profiling of multiple cell populations in parallel, including rare cell subsets, without the need for cell sorting, which can change the metabolic activity of the cells. Therefore, we will optimize the protocol for HSCs and we will apply it to HSCs from *th3* and IO wt mice. Moreover, we will use SCENITH to compare the metabolic profiles of HSCs and progenitors in the same sample.

To highlight which metabolites are affected by intracellular IO and oxidative stress, metabolome analyses are pivotal. We will perform targeted liquid chromatography-tandem mass spectrometry (LC-MS/MS) approaches as previously published (Schönberger *et al*, 2022) to identify TCA cycle metabolites, amino acids, lipids and retinoids in HSCs from *th3* and IO wt mice. Since MitoQ treatment normalized glucose uptake of *th3* HSCs, we will also evaluate the composition of metabolites after our rescue strategy to understand which metabolic pathways are involved in BThal HSC dysfunction. Finally, we will take advantage of metabolomic analyses to gain new insight about the different behaviour of HSCs and progenitors in BThal.

MATERIALS AND METHODS

BThal mouse model

Male and female C57BL/6 and C57BL/6-CD45.1 (B/6.SJLCD45a-Pep3b) wild-type (wt) mice were purchased from Charles River. C57BL6/Hbb$^{th3/+}$ mice lack both the b1 and b2 adult globin genes (Yang *et al.*, 1995), resulting in perinatal death in homozygosity but showing characteristics of severe BThal intermedia in heterozygosity. C57BL6/Hbb$^{th3/+}$ mice were purchased from The Jackson Laboratory and bred to maintain the colony in heterozygosity. In particular, heterozygous animals display dramatically reduced RBC counts, Hb concentration, hematocrit, and increased reticulocyte counts. Tissue and organ damage typical of BThal are also present in heterozygous C57BL6/Hbb$^{th3/+}$ mice, including splenomegaly, bone defects and iron deposition in spleen, liver and kidney. All animal experiments were performed in accordance with approved protocols of the Institutional Animal Care and Use Committees of San Raffaele Institute. All the analyses were performed on adult 12-14 weeks old mice.

IO mouse model

To generate acute IO mouse model (WT_IO_AC), female wt mice were treated with a single subcutaneous injection of 25 mg/ml iron dextran (Sigma, Cat #D8517) in saline and euthanized 24h later (Zhang *et al.*, 2022). To generate chronic IO mouse model (WT_IO_CH), female wt mice were injected intraperitoneally with 25 mg/ml iron dextran in saline every three days for 4 weeks and euthanized 24h after the last dose (Chai *et al.*, 2015). Control mice were injected with saline.

Cell isolation

Murine total BM cells were extracted from femurs and tibiae. Briefly, after cutting the epiphyses, the BM was flushed out by using a 1 ml syringe filled with ice cold MACS buffer supplemented with BSA and EDTA (Milteny Biotech, Cat #130.091.221). This step was repeated until all bone materials turned white as a marker that most of BM cells

were collected. Then, the cell suspension was filtered through a 70 μm cell strainer to obtain BM cells.

To analyse primitive progenitors and stem cell populations, Lin^- cells were isolated from total BM samples as a negative selection by depletion of cells expressing a panel of lineage markers. Total BM cells were labelled with a cocktail containing the following biotin-conjugated monoclonal antibodies: GR1 (granulocytes), CD11b (monocytes/macrophages), CD45R/B220 (B cells), CD5 (T cells), TER-119 (erythroid cells) at 4°C for 10 min. Then, cells were incubated with anti-biotin monoclonal antibodies conjugated to MicroBeads at 4°C for 15 min. Finally, cells passed through the MACS® Column in the magnetic field of a MACS Separator. While the labelled Lin^+ cells were retained on the column, the unlabelled Lin^- cells were collected. All staining was performed with commercially prepared antibodies in MACS Buffer (Milteny Biotech, Cat #130.091.221).

To isolate total spleen cells, spleen was collected and smashed repeatedly with a 5 ml plunger through a 40 μm cell strainer pre-wet with MACS buffer.

Flow cytometry and cell sorting

Flow cytometry analysis and FACS sorting of HSPC were performed with freshly isolated BM cells as previously described. For SLAM HSC, MPP and LSK analyses, Lin^- cells, enriched in stem and progenitors, were stained with Lin-Alexa700 (BioLegend, Cat #133313), CD117-APC (BD Pharmingen, Cat #553356), Sca1-PE-Cy7 (BD Pharmingen, Cat #558162) or Sca1-FITC (Cat #553335), CD48-PB (BioLegend, Cat #103418) or CD48-PE-Cy7 (BD Pharmingen, Cat #560731), CD150-PE (BD Pharmingen, Cat #562651) or CD150-BV421 (BD Horizon, Cat #562811), Fc Block (BD Pharmingen, Cat #553142). For FACS analyses of BM and spleen macrophages, BM cells and splenocytes were freshly isolated as previously described and labelled with F4/80-APC (eBioscence, Cat #17-480-182) and Fc Block. All the surface staining were performed with commercially prepared antibodies in MACS Buffer at 4°C for 30 min. All antibodies were titrated and validated using appropriate positive and negative control samples. Unstained cells, single stained compensation beads (BD Biosciences, Cat #552845) and

fluorescence minus one (FMO) were used for compensation and as a control to set appropriate gates.

FACS sorting was performed on FACSAria Fusion (BD Biosciences), whereas flow cytometry analyses were performed on FACS Canto II (BD Biosciences) and analyzed with FCS Express Software (De Novo Software).

Cell cycle analysis of SLAM HSCs

Lin^- cells were stained for surface markers, washed in MACS buffer, fixed and permeabilized to allow the antibody anti-Ki67 to enter the nucleus. Ki67 is a widely recognised marker of cell proliferation because it is not expressed in G0 quiescent cells, but its expression increases from G1 to M phase. Briefly, cells were fixed in Cytofix/Cytoperm buffer (BD Pharmingen, Cat #51-2090KE) for 30 min on ice, washed in PermWash buffer (BD Pharmingen, Cat #51-2091-KE), permeabilized with CytoPerm Plus buffer (BD Pharmingen, Cat #51-2356KC) for 10 min on ice, re-fixed in Cytofix/Cytoperm buffer for 5 min on ice, washed in PermWash buffer and incubated with anti-Ki67 (B56, BD Pharmingen, Cat #556026) for 30 min at room temperature (RT). Then, 7-AAD (BD Pharmingen, Cat #51-2359KC) was added right before sample acquisition. 7-AAD is a fluorescent DNA intercalator, allowing the categorization of cells within the major phases of cell cycle based on the differences in DNA content. Indeed, cells is G0/G1 phase have lower DNA content as compared to replicating cells in S phase with an intermediate DNA content and post-replicative cells in G2/M phase with high DNA content.

Evaluation of intracellular iron content

Lin^- cells were stained with 0.125 μM calcein-acetoxymethyl ester (Calcein-AM, Invitrogen, Cat #C3099) in DPBS for 5 min at 37°C. Then cells were washed with DPBS and stained for surface markers. Finally, calcein-AM fluorescence was analysed by flow cytometry. The acetoxymethoxy group (AM) renders the probe membrane permeable and, once in the cytoplasm, it remains trapped due to its hydrophilic nature. The intracellular Calcein-AM undergoes fluorescence quenching upon binding to free Fe^{2+} and this is directly proportional to the concentration of the LIP (Ma *et al,* 2015).

Therefore, high MFI of calcein-AM reflects low cytosolic free Fe^{2+}, conversely low MFI of calcein-AM indicates high cytosolic free Fe^{2+}.

Evaluation of mitochondrial iron content

Lin^- cells were stained with 5 μM Mito-FerroGreen (Dojindo, Cat #M489-10) in HBSS for 30 min at 37°C, after surface marker staining. Then cells were washed twice with HBSS and analysed by flow cytometry. Mito-FerroGreen contains a cationic and lipophilic triphenylphosphonium (TPP) group, which enters mitochondria. Fe^{2+} mediates the deoxygenation of the N-oxide group of the probe, leading to an enhanced fluorescence. Thus, Mito-FerroGreen fluorescence output is directly proportional to the amount of mitochondrial free Fe^{2+}, which constitutes the mitochondrial iron pool (Cilibrizzi *et al*, 2022; Hirayama *et al.*, 2018).

Analysis of mitochondrial mass

Lin^- cells were stained with surface antibody and then were labelled with 20 nM MitoTracker Green (MTG, Molecular Probes, Cat #M7514) in DPBS for 30 min at 37°C, as previously reported (Rimmele *et al*, 2015). Finally, cells were washed in DPBS and analysed by flow cytometry. MTG is a cell permeant dye that readily accumulates in the mitochondrial matrix independently of mitochondrial activity. Once in the organelle, it binds covalently to mitochondrial proteins by reacting with free thiol groups of cysteine residues. Thus, MTG fluorescence reflects the mitochondrial mass of the cell (Presley *et al.*, 2003).

Analysis of MMP

To investigate mitochondrial activity, we measured MMP, the electrical gradient between the mitochondrial matrix (negatively charged) and the intermembrane space (positively charged). More specifically, the electron transfer through the ETC complexes in the IMM provides the energy to drive protons (H^+) across the IMM into the intermembrane space. Here, protons are used by the ATP synthase to generate ATP. As a result, an electrical gradient, typically accounting for -180mV, between the two sides of the IMM is established. Thus, MMP is a widely recognised measure of mitochondrial function (Perry *et al.*, 2011). To measure MMP, Lin^- cells were stained for surface

markers and then labelled in DPBS for 15 min at 37°C with 50 nM tetramethylrhodamine ethyl ester (TMRE, abcam, Cat #113852), which accumulates in the mitochondrial matrix in proportion to the MMP. To avoid the decay of the dye signal, cells were not washed after TMRE staining and were analyzed by flow cytometry within 30 min. Probe responsiveness to MMP was tested using as negative control carbonyl cyaninde 4-(trifluoromethoxy) phenylhydrazone (FCCP, abcam, Cat #113852), which decreased TMRE fluorescence. Briefly, Lin^- cells were incubated with 2 μM FCCP for 10 min RT after TMRE staining and immediately analysed by flow cytometry.

Analysis of mtROS content

Lin^- cells were incubated with 1 μM MitoSOX™ Red Mitochondrial Superoxide Indicator (Molecular Probes, Cat #M36008) for 30 min at 37°C post surface staining, as previously described (Hinge *et al.,* 2020). MitoSOX™ is a highly selective probe for superoxide (O2•−), the predominant ROS in the mitochondria (Batandier *et al*, 2002). It contains the cationic and lipophilic TPP group, which drives it into mitochondria, where it reacts with superoxide, thus resulting in increased fluorescence (Kauffman *et al*, 2016).

Metabolic analyses

Glucose uptake assay

Freshly isolated Lin^- cells ($4x10^5$ cells/48-well) were cultured in 400 μl of XF RPMI medium pH 7.4 (Agilent, Cat #103576-100) without glucose, L-glutamine and pyruvate containing 100 μM of the fluorescent glucose analogue 2-(n-(7-nitrobenz-2-oxa-1,3-diazol-4-ylamino)-2-deoxyglucose (2-NBD-Glucose, 2NBDG, Invitrogen, Cat #N13195) for 1 h at 37°C (Zou *et al.*, 2005). Then, cells were washed twice in DPBS, stained for SLAM HSCs and analysed by flow cytometry for 2NBDG fluorescence in the FITC channel.

Intracellular ATP content

ATP levels were quantified in freshly FACS-purified SLAM HSCs by luminescent assay using CellTiter Glo 2.0 (Promega, Cat #G9241) in accordance with the manufacturer's recommendations, as previously described (Nakamura-Ishizu *et al.*,

2018). CellTiter Glo 2.0 is a two-in-one reagent that induces cell lysis and generation of a luminescent signal directly proportional to the amount of intracellular ATP. The luminescent output is the result of mono-oxygenation of luciferin catalysed by luciferase enzyme in the presence of ATP, oxygen and Mg^{2+}.

In brief, 500 SLAM HSCs were FACS-sorted into 1.5 ml microcentrifuge tube containing 300 µl SFEM medium (StemCell Technologies, Cat #09650) supplemented with 2 mM L-Glutamine. During sorting of the samples, the already collected ones were maintained at 37°C to avoid altering MMP. To recover after the mechanical stress of FACS-sorting procedure, cells were cultured into single 96-well of a white plate with clear bottom (Costar, Cat #3903) containing SFEM at 37°C for 1 h after sorting. Then, CellTiter Glo 2.0 reagent was added in 1:1 ratio to samples, followed by 2 min mixing on orbital shaker to induce cell lysis and 10 min incubation RT to stabilize the luminescent signal. Finally, luminescence (relative luminescent unit, RLU) was recorded using the Victor3 Multilabel Plate Reader (PerkinElmer). Every step was performed protected from light to avoid the decay of the luminescent signal. In parallel to sample preparation, samples with known ATP concentrations (varying from 1 µM to 1 nM) were generated and assayed in the same plate on which samples were analysed, in order to create a standard curve. ATP (Promega, Cat #P1132) was diluted in the same SFEM medium used for sample preparation. The intracellular ATP content was obtained from the interpolation of RLU of our samples with the RLU of the standard curve.

In some experiments, 500 SLAM HSCs were incubated with 1 µM oligomycin (Sigma, Cat #1404-19-9) in SFEM for 1h at 37°C before adding CellTiter Glo 2.0. Oligomycin inhibits ATP synthase, the last complex of the ETC, thus completely abrogating the amount of ATP generated by OXPHOS. As a result, the difference in intracellular ATP levels between oligomycin-treated to non-treated samples reflects the fraction of ATP produced by OXPHOS.

Intracellular lactate content

Since lactate is the end-product of glycolysis, lactate quantification is widely used for analysing glycolytic flux. Intracellular lactate levels were measured in freshly FACS-purified SLAM HSCs by fluorometric assay using Lactate Fluorometric Assay Kit (BioVision, Cat #K607-100) in accordance with the manufacturer's recommendations, as

previously reported (Takubo *et al.*, 2013). Lactate quantification is based on the reaction between lactate in the sample and enzyme in the kit, resulting in fluorescence emission (Ex/Em = 535/587 nm), which is directly proportional to the amount of intracellular lactate.

Briefly, 500 SLAM HSCs were FACS-sorted into 1.5 ml microcentrifuge tubes containing 300 µl DPBS. Cells were immediately pelleted, resuspended in 50 µl lactate assay buffer (BioVision, Cat #K607-100-1) and sonicated on ice with 100 amplitudes for 1 cycle of 25 s to punch the plasma membrane. Following sonication, samples were plated into single 96-well of a white plate with clear bottom (Costar) and incubated in 1:1 ratio for 30 min RT with the reaction mix, containing lactate enzyme (BioVision, Cat #K607-4) and lactate probe (BioVision, Cat #K607-2A) in lactate assay buffer. Lactate specifically reacted with an enzyme to generate a product, which interacted with lactate probe to produce fluorescence (relative fluorescent unit, RFU), that was recorded using the Victor3 Multilabel Plate Reader (PerkinElmer). Every step was performed protected from light to avoid the decay of the fluorescent signal. As ATP assay, a standard curve with known concentrations of lactate (BioVision, Cat #K607-5) was generated and assayed in the same plate on which samples were analysed. The intracellular lactate content was obtained from the interpolation of RFU of our samples with the RFU of the standard curve.

In vivo mtROS reduction

To decrease mtROS *in vivo, th3* female mice were treated with Mitoquinol (MitoQ), a mitochondrial-targeted coenzyme-Q10 (Murphy & Smith, 2007). MitoQ contains the TPP group that drives its entry into mitochondria, where it is reduced to the active ubiquinol antioxidant form by complex II of the ETC. MitoQ ubiquinol is oxidized by mtROS to the ubiquinone form, which is then rapidly reduced by complex II, restoring its antioxidant efficacy. 2 mg/kg MitoQ (Cayman, Cat# 89950) in DPBS were administered through intra-peritoneal (i.p.) injection for 5 days. Control mice were injected with DPBS. Mice were euthanized 24 h after the last dose and BM cells were isolated to analyse mtROS, MMP, glucose uptake, frequency and cell cycle of SLAM

HSCs. Furthermore, peripheral blood (PB) was collected to evaluate hematological parameters.

Perl's staining

To detect iron deposits, we performed Perl's staining of BM cells and Formalin-Fixed Paraffin-Embedded (FFPE) sections of spleen and liver. For BM sample preparation, $1x10^6$ total BM cells resuspended in 200 µl of MACS buffer were transferred in the cytofunnel placed on a slide and centrifuged for 5 min at 800 rpm low acceleration using Thermo Shandon Cytospin centrifuge. The slide containing BM cells was first left to dry for 20 min under the hood, then it was gently fixed in 4% paraformaldehyde (PFA) (ChemCruz, Cat #sc-281692) for 10 min at RT. Following fixation, the slide was washed three times in DPBS and stored at 4°C.

To obtain spleen and liver sections, organs were washed in DPBS after harvesting and fixed in 10% formalin (Bio-Optica, Cat #05-01005Q) for 24 h. After fixation, spleen and liver were washed three times in DPBS, processed with increasing concentration of ethanol and embedded in paraffin by Leica TP1020 Tissue Processor (Leica Biosystem). Then, 4 µm sections were cut from FFPE, mounted to a slide, dried, de-waxed and rehydrated through a decreasing scale of ethanol. Finally, slides were washed in distilled water and stored at RT.

Perl's staining was performed using the Iron stain kit (Abcam, Cat #ab150674) for the detection of Fe^{3+}, according to the manufacturer's instructions. Fe^{3+} deposits in tissues appear blue as the result of the reaction with the soluble ferrocyanide to form the insoluble Prussian blue pigment. Briefly, slides of BM cells, spleen and liver sections were incubated with working iron stain solution, containing potassium ferrocyanide solution and hydrochloric acid solution in 1:1 ratio, for 3 min at RT. Then slides were rinsed in distilled water and counterstained with nuclear fast red solution for 5 min at RT, resulting in red-coloured nuclei. After staining, slides were washed multiple times with distilled water and dehydrated in 95% ethanol followed by absolute ethanol. Once dried, slides were mounted using the DPX Mountant for histology (Sigma, Cat #06522) and analysed under Nikon Eclipse Ni-U optical microscope. Microphotographs (5 per case, 20x

magnification) were collected through the Nikon digital sight DS-U3 using the Nikon imaging software.

Transmission Electron Microscopy (TEM)

We used a specific approach for sample preparation with low cell number (Kumar & Filippi, 2016). Around 10,000 SLAM HSCs were FACS-sorted in a 1.5 ml microcentrifuge tube with DPBS and pelleted at 1,000 x g for 10 min. Then cells were fixed RT for 1 h in a fresh fixative solution of 0.1 M cacodylate buffer (Sigma-Aldrich, Cat #20840), containing 2.5% glutaraldehyde and 3% paraformaldehyde (PFA). After fixation, the tiny cell pellet was incubated with 2 mg/ml solution of Toluidine Blue (Electron Microscopy Sciences, Cat #22050) in cacodylate buffer for 20 min at RT, in order to make it visible in blue and facilitate the next steps of sample preparation. After staining, cells were washed three times with 0.1 M cacodylate buffer, transferred to a 0.5 ml microcentrifuge tube and embedded into agarose. The embedding into agarose before dehydration and resin embedding is a crucial step for clustering the limited number of cells together. Firstly, 4% low melting agarose (Sigma-Aldrich, Cat #A4718) dissolved in 0.1 M cacodylate buffer was added to the cell suspension, then cells were immediately spun down at the bottom of the tube by centrifugation at 1,000 x g for 10 min. Finally, the microcentrifuge tube containing cells was transferred to 4°C to allow agarose solidification. The solidified agarose was trimmed into one piece of about 1-2 mm containing the cell pellet, transferred to a new 1.5 ml microcentrifuge tube and washed multiple times with 0.1 M cacodylate buffer. At this point, the cell pellet was incubated for 1h at 4°C with 1% osmium tetroxide (OsO_4) (Electron Microscopy sciences, Cat #9190), which reacts with lipids, resulting in intense black staining. Thus, the osmification step is essential to add density and contrast to biological samples. After osmification, the cell-pellet agarose piece was washed with 0.1 M cacodylate buffer, ready for dehydration, infiltration and embedding into resin. Firstly, the sample was dehydrated by incubation in a series of solutions with increasing concentrations of alcohol (from 25% to 100% ethanol), gently removing water to avoid artefact generation. Each dehydration step took 15 min at RT. Following dehydration, the solvent was gradually replaced with ascending concentrations of liquid resin (Epon 812, Sigma-Aldrich) at RT

and then the sample was placed in a pyramid tip shaped mold at 60°C for 72 h for resin polymerization. Finally, ultra-thin sections (70-100 nm) of the pyramid block were cut using a diamond knife, mounted on grids and analysed with an electron microscope. Images were collected on Talos L120C TEM (ThermoFischer Scientific, Brno) available at San Raffaele Advanced Light and Electron Microscopy BioImaging Center (ALEMBIC).

Mitochondria were manually segmented on Fiji (ImageJ) software (Schindelin *et al*, 2012). The mean number of mitochondria per SLAM HSC in wt and *th3* mice and the area of each mitochondrion in wt and th3 SLAM HSCs were reported on excel spread sheet. At least 30 SLAM HSCs from each wt sample (n=3) and 15 SLAM HSCs from each *th3* sample (n=2) were collected.

Hematological and biochemical analyses

PB was collected from the retro-orbital vein into EDTA-coated microvette tubes (Sarstedt, Cat #20.1341) and placed on a rocking shaker to prevent coagulation. Whole blood count analysis, including hemoglobin and red blood cell counts were performed using an automated hematology analyzer (Hemocytometer IDEXX PROCYTE). Iron concentration and liver parameters were measured with a standard clinical autoanalyzer (ILab Aries) on serum obtained after PB centrifugation at 200 x g for 20 min.

RNA extraction

Sorted SLAM HSCs were pelleted and stored at -80°C. The day of RNA extraction, pellets were thawed and total RNA was extracted using AllPrep DNA/RNA MicroKit (Qiagen, Cat #80284) following manufacturer's instructions, as schematized in Fig. 1.
Briefly, pellets of at least 1,000 HSCs were lysed by adding a highly denaturating guanidineisothiocyanate–containing RLT buffer, which immediately inactivates DNases and RNases, and homogenized by vortexing for 1 min. The lysate was then passed through an AllPrep DNA spin column, which selectively bound genomic DNA, whereas the flow-through containing RNA and proteins was used for RNA purification. 70% ethanol was added to the flow-through from the AllPrep DNA spin column to provide

appropriate binding conditions for RNA, and the sample was transferred to a RNeasy MinElute spin column placed on a 2 ml collection tube. Then, the column was centrifuged for 15 s at 11,000 rpm, the flow-through was discarded and two step of washing and centrifugation were performed with RW1 and RPE buffer, respectively. 80% ethanol was added to the column, followed by centrifugation at 11,000 rpm for 2 min. Finally, the column was dried by centrifugation at full speed (14,800 rpm) for 5 min and RNA was eluted in 14 µl water.

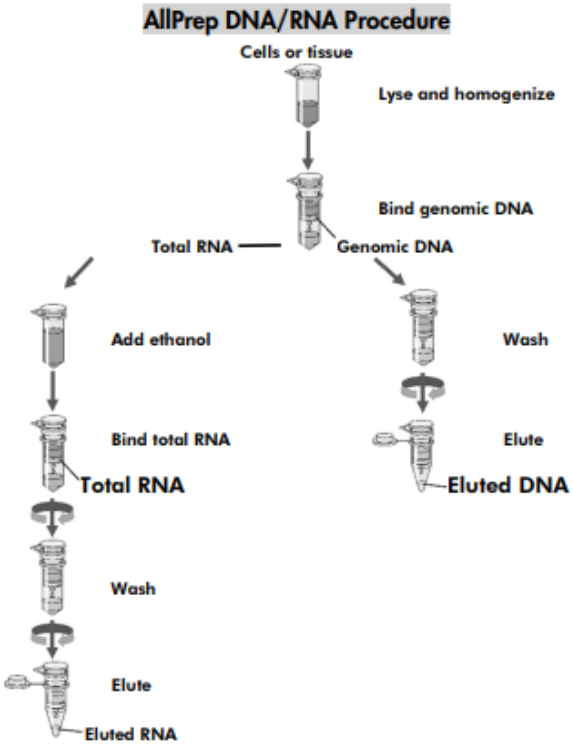

Figure 1. Workflow of RNA extraction

Reverse-Transcription (RT)

RT-PCR was performed to synthetize cDNA using Precision nanoScript™ Reverse Transcription kit (PrimerDesign, Cat # RT-NanoScript2-150).

Firstly, the RT primers were annealed to the denatured RNA strand (annealing step). Secondly, annealed RNA was incubated with appropriate buffer enabling the reverse transcription into cDNA (extension step). Briefly, during the annealing step each sample was incubated with a primer mix of oligo-dT primers and Random primers at 65°C for 5

min. The former binds to the polyA tail of mRNAs avoiding the RT and amplification of ribosomal RNA, the latter primes on all RNA species including partially degraded RNA without polyA tail. During the extension step, RNA samples were incubated with a mix of dNTPs and RT enzyme at 25°C for 5 min, followed by 42°C for 20 min. Finally, the reaction was heat-inactivated by incubation at 75°C for 10 min and cDNA samples were stored at -20°C.

Droplet digital PCR (ddPCR)

cDNA samples were loaded into single reaction tubes of the DG8^{TM} Cartridge for droplet generation (Biorad). The ddPCR reagents, including ddPCR^{TM} supermix for probes (no dUTP, Biorad, Cat #1863024), the house keeping *Hprt* primer/probe mix (Biorad, Cat #, dMmuCPE5095492) and the gene target *Hmox1* primer/probe mix (Biorad, Cat #, dMmuCPE5124493) were thawed RT, mixed by vortexing to ensure homogeneity and centrifuged briefly to collect contents at the bottom of the tubes. The mix was prepared as detailed in Table 1 and dispensed into each reaction tube of the DG8^{TM} Cartridge to a final volume of 22 µl/each tube. The cartridge was centrifuged for 5 min and transferred to the Automated Droplet Generator QX200 (Biorad). After droplet generation, the cartridge was sealed and placed in the Thermocycler to perform the PCR reaction, as described in Table 2. After amplification, positive droplets, defined as droplets containing HEX and FAM signals, were read in a QX200 Droplet Reader (Biorad). To discriminate between positive and negative droplets, we set a threshold and QuantaSoft^{TM} software (Biorad) was used to quantify the number of positive and negative droplets for each fluorophore in each sample. The software fits the fraction of positive droplets to a Poisson algorithm to determine the starting concentration of the target DNA molecules in units of copies/µl.

Table 1.

	Volume per reaction (µl)
2x ddPCR Supermix for Probes (no dUTP)	11

20x target primers/probe mix (HEX)	1.1
20x reference primers/probe mix (FAM)	1.1
cDNA	variable
RNase/DNase-free water	variable
Total Volume	22

Table 2.

Cycling step	**Temperature (°C)**	**Time**	**Ramp rate**	**n° of cycles**
Enzyme activation	95	10 min	2°C/second	1
Denaturation	94	30 s		40
Annealing/extension	55	1 min		
Enzyme deactivation	98	10 min		1
Hold	4	infinite		1

RNA-seq analysis

Total RNA was isolated from sorted SLAM HSCs as described above. Ovation SoLo RNA-seq kit (Illumina) has been used for library preparation following the manufacturer's instructions, starting with 1 ng of RNA as input. Samples were quantified by using the Qubit 2.0 Fluorometer (Invitrogen) and/or quality tested by Agilent 2100 Bioanalyzer RNA assay (Agilent technologies) depending on sufficient amount of starting material. Libraries were then processed with Illumina cBot for cluster generation on the flowcell, following the manufacturer's instructions and sequenced on paired-end 125 bp mode on HiSeq2500 (Illumina). The CASAVA 1.8.2 version of the Illumina pipeline was used to process raw data for both format conversion and de-multiplexing. FPKM read count files containing the estimated gene-level expression values were generated and statistically analysed. The quality of the input reads was determined using the FastQC software and low-quality sequences were trimmed using Trimmomatic.

RNA-seq data were aligned to the *Mus musculus* reference genome (GRCm38/mm10) using STAR with standard input parameters. Alignments were then filtered with the

MarkDuplicates tool of Picard, considering the Unique Molecular Identifiers (UMI) tags (--BARCODE_TAG option) added before cDNA amplification, as specified in the library manufacturer's instructions, and gene UMI counts were produced using Subread featureCounts against the Genecode (v17) reference annotation.

UMIs are a type of molecular barcoding that uniquely tag each molecule in a sample library, thus providing error correction and resulting in a more accurate quantification of the transcript count (Chen *et al*, 2018). Since UMIs are incorporated on each original RNA fragment before any PCR amplification, true variants present in the original sample can be distinguished from errors introduced during library preparation, PCR and sequencing. To quantify the transcript count, the UMI count of mitochondrial genes were normalized to *hprt* housekeeping gene.

Transcript UMI counts with values > 3 were processed using DESeq2 (normalizing for library size using Relative Log Expression and correcting by sex) using standard protocols as reported in the respective manuals, and differential expression was determined considering *p* values corrected by FDR. To determine whether some specific gene sets were significantly different between wt and *th3* mice, we performed Gene Set Enrichment Analysis (GSEA) employing the Reactome Pathway database and the biological process (BP) branch of the gene ontology (GO) database on genes ranked by log2 fold change values.

We tested a list of antioxidant genes (*Gpx7, Txn2, Ccs, Prdx2, Prdx3, Gpx1, Gsr, Rps19bp1, Txn1, Prdx6, Fkbp4, Cat, Sod2*) and we represented the enrichment score (ES) and the position of gene set members on the rank-ordered list using GSEA enrichment plot.

The expression levels of specific genes of interest (rows) in the considered samples (columns) were visualized as heatmap and, to highlight gene and/or condition patterns, unsupervised clustering was performed on rows and/or columns, respectively. The colour and the intensity of the boxes in the heatmaps reflects changes of gene expression calculated using the z-score.

Gene expression RNA-seq data for this study have been deposited in European Nucleotide Archive database with accession numbers PRJEB31882 and PRJEB31937 (http://www.ebi.ac.uk/ena/data/view/PRJEB31882; http://www.ebi.ac.uk/ena/data/view/PRJEB31937).

Statistical analyses

Analyses were performed by using GraphPad prism v8.0 software (La Jolla, CA, USA). All data are presented as single values and mean±SEM. Mann-Whitney test was used for comparisons between two independent groups, Wilcoxon test was performed for comparison between dependent groups. Kruskal-Wallis test was performed for comparison among more than two independent groups. Bonferroni correction was applied for comparison among more than 2 groups.

Statistical significance is reported as follows: * $p < 0.05$, ** $p < 0.01$, *** $p < 0.001$, **** $p < 0.0001$.

REFERENCES

Adamiak M, Moore JBt, Zhao J, Abdelbaset-Ismail A, Grubczak K, Rzeszotek S, Wysoczynski M, Ratajczak MZ (2016) Downregulation of Heme Oxygenase 1 (HO-1) Activity in Hematopoietic Cells Enhances Their Engraftment After Transplantation. *Cell Transplant* 25: 1265-1276

Adams GB, Scadden DT (2006) The hematopoietic stem cell in its place. *Nat Immunol* 7: 333-337

Akashi K, Traver D, Miyamoto T, Weissman IL (2000) A clonogenic common myeloid progenitor that gives rise to all myeloid lineages. *Nature* 404: 193-197

Ali M. ASA, Mansoori H. (2020) Extensive iron overload in bone marrow: A cause of pancytopenia in a thalassemia major patient – A case report. *Ajts*

Angelopoulos NG, Goula A, Rombopoulos G, Kaltzidou V, Katounda E, Kaltsas D, Tolis G (2006) Hypoparathyroidism in transfusion-dependent patients with beta-thalassemia. *J Bone Miner Metab* 24: 138-145

Angelucci E, Matthes-Martin S, Baronciani D, Bernaudin F, Bonanomi S, Cappellini MD, Dalle JH, Di Bartolomeo P, de Heredia CD, Dickerhoff R *et al* (2014) Hematopoietic stem cell transplantation in thalassemia major and sickle cell disease: indications and management recommendations from an international expert panel. *Haematologica* 99: 811-820

Angelucci E, Pilo F (2016) Management of iron overload before, during, and after hematopoietic stem cell transplantation for thalassemia major. *Ann N Y Acad Sci* 1368: 115-121

Anso E, Weinberg SE, Diebold LP, Thompson BJ, Malinge S, Schumacker PT, Liu X, Zhang Y, Shao Z, Steadman M *et al* (2017) The mitochondrial respiratory chain is essential for haematopoietic stem cell function. *Nat Cell Biol* 19: 614-625

Antoniani C, Meneghini V, Lattanzi A, Felix T, Romano O, Magrin E, Weber L, Pavani G, El Hoss S, Kurita R *et al* (2018) Induction of fetal hemoglobin synthesis by CRISPR/Cas9-mediated editing of the human beta-globin locus. *Blood* 131: 1960-1973

Aprile A, Gulino A, Storto M, Villa I, Beretta S, Merelli I, Rubinacci A, Ponzoni M, Marktel S, Tripodo C *et al* (2020) Hematopoietic stem cell function in beta-thalassemia is impaired and is rescued by targeting the bone marrow niche. *Blood* 136: 610-622

Aprile A, Sighinolfi S, Raggi L, Ferrari G (2022) Targeting the Hematopoietic Stem Cell Niche in beta-Thalassemia and Sickle Cell Disease. *Pharmaceuticals (Basel)* 15

Argüello RJ, Combes AJ, Char R, Gigan J-P, Baaziz AI, Bousiquot E, Camosseto V, Samad B, Tsui J, Yan P, Boissonneau, Figarella-Branger D *et al* (2020) SCENITH: A Flow Cytometry-Based Method to Functionally Profile Energy Metabolism with Single-Cell Resolution. *Cell Stem Cell* 32(6):1063-1075.e7

Baldwin JE, Krebs H (1981) The evolution of metabolic cycles. *Nature* 291: 381-382

Bartram J, Filippi MD (2022) The new metabolic needs of hematopoietic stem cells. *Curr Opin Hematol* 29: 188-193

Batandier C, Fontaine E, Keriel C, Leverve XM (2002) Determination of mitochondrial reactive oxygen species: methodological aspects. *J Cell Mol Med* 6: 175-187

Batsivari A, Haltalli MLR, Passaro D, Pospori C, Lo Celso C, Bonnet D (2020) Dynamic responses of the haematopoietic stem cell niche to diverse stresses. *Nat Cell Biol* 22: 7-17

Beerman I, Bhattacharya D, Zandi S, Sigvardsson M, Weissman IL, Bryder D, Rossi DJ (2010) Functionally distinct hematopoietic stem cells modulate hematopoietic lineage potential during aging by a mechanism of clonal expansion. *Proc Natl Acad Sci U S A* 107: 5465-5470

Berg J. M. SL, Tymoczko J. L., Gatto G. J. (2015) *Biochemistry*

Bianco P, Cao X, Frenette PS, Mao JJ, Robey PG, Simmons PJ, Wang CY (2013) The meaning, the sense and the significance: translating the science of mesenchymal stem cells into medicine. *Nat Med* 19: 35-42

Bigarella CL, Liang R, Ghaffari S (2014) Stem cells and the impact of ROS signaling. *Development* 141: 4206-4218

Bingol B, Sheng M (2016) Mechanisms of mitophagy: PINK1, Parkin, USP30 and beyond. *Free Radic Biol Med* 100: 210-222

Bord S, Frith E, Ireland DC, Scott MA, Craig JI, Compston JE (2005) Megakaryocytes modulate osteoblast synthesis of type-l collagen, osteoprotegerin, and RANKL. *Bone* 36: 812-819

Bozza MT, Jeney V (2020) Pro-inflammatory Actions of Heme and Other Hemoglobin-Derived DAMPs. *Front Immunol* 11: 1323

Bruns I, Lucas D, Pinho S, Ahmed J, Lambert MP, Kunisaki Y, Scheiermann C, Schiff L, Poncz M, Bergman A *et al* (2014) Megakaryocytes regulate hematopoietic stem cell quiescence through CXCL4 secretion. *Nat Med* 20: 1315-1320

Burt R, Dey A, Aref S, Aguiar M, Akarca A, Bailey K, Day W, Hooper S, Kirkwood A, Kirschner K *et al* (2019) Activated stromal cells transfer mitochondria to rescue acute lymphoblastic leukemia cells from oxidative stress. *Blood* 134: 1415-1429

Calvi LM, Adams GB, Weibrecht KW, Weber JM, Olson DP, Knight MC, Martin RP, Schipani E, Divieti P, Bringhurst FR *et al* (2003) Osteoblastic cells regulate the haematopoietic stem cell niche. *Nature* 425: 841-846

Caocci G, Orofino MG, Vacca A, Piroddi A, Piras E, Addari MC, Caria R, Pilia MP, Origa R, Moi P *et al* (2017) Long-term survival of beta thalassemia major patients treated with hematopoietic stem cell transplantation compared with survival with conventional treatment. *Am J Hematol* 92: 1303-1310

Cappellini MD, Viprakasit V, Taher AT, Georgiev P, Kuo KHM, Coates T, Voskaridou E, Liew HK, Pazgal-Kobrowski I, Forni GL *et al* (2020) A Phase 3 Trial of Luspatercept in Patients with Transfusion-Dependent beta-Thalassemia. *N Engl J Med* 382: 1219-1231

Casanova-Acebes M, Pitaval C, Weiss LA, Nombela-Arrieta C, Chevre R, N AG, Kunisaki Y, Zhang D, van Rooijen N, Silberstein LE *et al* (2013) Rhythmic modulation of the hematopoietic niche through neutrophil clearance. *Cell* 153: 1025-1035

Casu C, Chessa R, Liu A, Gupta R, Drakesmith H, Fleming R, Ginzburg YZ, MacDonald B, Rivella S (2020) Minihepcidins improve ineffective erythropoiesis and splenomegaly in a new mouse model of adult beta-thalassemia major. *Haematologica* 105: 1835-1844

Casu C, Oikonomidou PR, Chen H, Nandi V, Ginzburg Y, Prasad P, Fleming RE, Shah YM, Valore EV, Nemeth E *et al* (2016) Minihepcidin peptides as disease modifiers in mice affected by beta-thalassemia and polycythemia vera. *Blood* 128: 265-276

Chai X, Li D, Cao X, Zhang Y, Mu J, Lu W, Xiao X, Li C, Meng J, Chen J *et al* (2015) ROS-mediated iron overload injures the hematopoiesis of bone marrow by damaging hematopoietic stem/progenitor cells in mice. *Sci Rep* 5: 10181

Chan DC (2012) Fusion and fission: interlinked processes critical for mitochondrial health. *Annu Rev Genet* 46: 265-287

Chandel NS, Jasper H, Ho TT, Passegue E (2016) Metabolic regulation of stem cell function in tissue homeostasis and organismal ageing. *Nat Cell Biol* 18: 823-832

Chandel NS, Maltepe E, Goldwasser E, Mathieu CE, Simon MC, Schumacker PT (1998) Mitochondrial reactive oxygen species trigger hypoxia-induced transcription. *Proc Natl Acad Sci U S A* 95: 11715-11720

Chen C, Liu Y, Liu R, Ikenoue T, Guan KL, Liu Y, Zheng P (2008) TSC-mTOR maintains quiescence and function of hematopoietic stem cells by repressing mitochondrial biogenesis and reactive oxygen species. *J Exp Med* 205: 2397-2408

Chen W, Li Y, Easton J, Finkelstein D, Wu G, Chen X (2018) UMI-count modeling and differential expression analysis for single-cell RNA sequencing. *Genome Biol* 19: 70

Cheung YF, Chan GC, Ha SY (2002) Arterial stiffness and endothelial function in patients with beta-thalassemia major. *Circulation* 106: 2561-2566

Chiabrando D, Vinchi F, Fiorito V, Mercurio S, Tolosano E (2014) Heme in pathophysiology: a matter of scavenging, metabolism and trafficking across cell membranes. *Front Pharmacol* 5: 61

Chow A, Lucas D, Hidalgo A, Mendez-Ferrer S, Hashimoto D, Scheiermann C, Battista M, Leboeuf M, Prophete C, van Rooijen N *et al* (2011) Bone marrow CD169+ macrophages promote the retention of hematopoietic stem and progenitor cells in the mesenchymal stem cell niche. *J Exp Med* 208: 261-271

Chow DC, Wenning LA, Miller WM, Papoutsakis ET (2001) Modeling pO(2) distributions in the bone marrow hematopoietic compartment. II. Modified Kroghian models. *Biophys J* 81: 685-696

Christodoulou C, Spencer JA, Yeh SA, Turcotte R, Kokkaliaris KD, Panero R, Ramos A, Guo G, Seyedhassantehrani N, Esipova TV *et al* (2020) Live-animal imaging of native haematopoietic stem and progenitor cells. *Nature* 578: 278-283

Cilibrizzi A, Pourzand C, Abbate V, Reelfs O, Versari L, Floresta G, Hider R (2022) The synthesis and properties of mitochondrial targeted iron chelators. *Biometals*

Coffey R, Ganz T (2018) Erythroferrone: An Erythroid Regulator of Hepcidin and Iron Metabolism. *Hemasphere* 2: e35

Crippa S, Rossella V, Aprile A, Silvestri L, Rivis S, Scaramuzza S, Pirroni S, Avanzini MA, Basso-Ricci L, Hernandez RJ *et al* (2019) Bone marrow stromal cells from β-thalassemia patients have impaired hematopoietic supportive capacity. *Journal of Clinical Investigation* 130

de Almeida MJ, Luchsinger LL, Corrigan DJ, Williams LJ, Snoeck HW (2017) Dye-Independent Methods Reveal Elevated Mitochondrial Mass in Hematopoietic Stem Cells. *Cell Stem Cell* 21: 725-729 e724

Decker M, Leslie J, Liu Q, Ding L (2018) Hepatic thrombopoietin is required for bone marrow hematopoietic stem cell maintenance. *Science* 360: 106-110

Dikalov SI, Harrison DG (2014) Methods for detection of mitochondrial and cellular reactive oxygen species. *Antioxid Redox Signal* 20: 372-382

Ding L, Morrison SJ (2013) Haematopoietic stem cells and early lymphoid progenitors occupy distinct bone marrow niches. *Nature* 495: 231-235

Ding L, Saunders TL, Enikolopov G, Morrison SJ (2012) Endothelial and perivascular cells maintain haematopoietic stem cells. *Nature* 481: 457-462

Dixon SJ, Lemberg KM, Lamprecht MR, Skouta R, Zaitsev EM, Gleason CE, Patel DN, Bauer AJ, Cantley AM, Yang WS *et al* (2012) Ferroptosis: an iron-dependent form of nonapoptotic cell death. *Cell* 149: 1060-1072

Doan PL, Russell JL, Himburg HA, Helms K, Harris JR, Lucas J, Holshausen KC, Meadows SK, Daher P, Jeffords LB *et al* (2013) Tie2(+) bone marrow endothelial cells regulate hematopoietic stem cell regeneration following radiation injury. *Stem Cells* 31: 327-337

Donegan RK, Moore CM, Hanna DA, Reddi AR (2019) Handling heme: The mechanisms underlying the movement of heme within and between cells. *Free Radic Biol Med* 133: 88-100

Dykstra B, Kent D, Bowie M, McCaffrey L, Hamilton M, Lyons K, Lee SJ, Brinkman R, Eaves C (2007) Long-term propagation of distinct hematopoietic differentiation programs in vivo. *Cell Stem Cell* 1: 218-229

El-Badri NS, Wang BY, Cherry, Good RA (1998) Osteoblasts promote engraftment of allogeneic hematopoietic stem cells. *Exp Hematol* 26: 110-116

Fan Y, Hanai JI, Le PT, Bi R, Maridas D, DeMambro V, Figueroa CA, Kir S, Zhou X, Mannstadt M *et al* (2017) Parathyroid Hormone Directs Bone Marrow Mesenchymal Cell Fate. *Cell Metab* 25: 661-672

Ferrari G, Thrasher AJ, Aiuti A (2021) Gene therapy using haematopoietic stem and progenitor cells. *Nat Rev Genet* 22: 216-234

Fibach E, Dana M (2019) Oxidative Stress in beta-Thalassemia. *Mol Diagn Ther* 23: 245-261

Filippi MD (2021) Hematopoietic stem cell (HSC) divisional memory: The journey of mitochondrial metabolism through HSC division. *Exp Hematol* 96: 27-34

Filippi MD, Ghaffari S (2019) Mitochondria in the maintenance of hematopoietic stem cells: new perspectives and opportunities. *Blood* 133: 1943-1952

Fujisaki J, Wu J, Carlson AL, Silberstein L, Putheti P, Larocca R, Gao W, Saito TI, Lo Celso C, Tsuyuzaki H *et al* (2011) In vivo imaging of Treg cells providing immune privilege to the haematopoietic stem-cell niche. *Nature* 474: 216-219

Gane EJ, Weilert F, Orr DW, Keogh GF, Gibson M, Lockhart MM, Frampton CM, Taylor KM, Smith RA, Murphy MP (2010) The mitochondria-targeted anti-oxidant mitoquinone decreases liver damage in a phase II study of hepatitis C patients. *Liver Int* 30: 1019-1026

Ganz T (2012) Macrophages and systemic iron homeostasis. *J Innate Immun* 4: 446-453

Gao G, Li J, Zhang Y, Chang YZ (2019) Cellular Iron Metabolism and Regulation. *Adv Exp Med Biol* 1173: 21-32

Garcia-Santos D, Hamdi A, Saxova Z, Fillebeen C, Pantopoulos K, Horvathova M, Ponka P (2018) Inhibition of heme oxygenase ameliorates anemia and reduces iron overload in a beta-thalassemia mouse model. *Blood* 131: 236-246

Gardenghi S, Marongiu MF, Ramos P, Guy E, Breda L, Chadburn A, Liu Y, Amariglio N, Rechavi G, Rachmilewitz EA *et al* (2007) Ineffective erythropoiesis in beta-thalassemia is characterized by increased iron absorption mediated by down-regulation of hepcidin and up-regulation of ferroportin. *Blood* 109: 5027-5035

Geiger H, de Haan G, Florian MC (2013) The ageing haematopoietic stem cell compartment. *Nat Rev Immunol* 13: 376-389

Gekas C, Graf T (2013) CD41 expression marks myeloid-biased adult hematopoietic stem cells and increases with age. *Blood* 121: 4463-4472

Gleyzer N, Vercauteren K, Scarpulla RC (2005) Control of mitochondrial transcription specificity factors (TFB1M and TFB2M) by nuclear respiratory factors (NRF-1 and NRF-2) and PGC-1 family coactivators. *Mol Cell Biol* 25: 1354-1366

Gomzikova MO, James V, Rizvanov AA (2021) Mitochondria Donation by Mesenchymal Stem Cells: Current Understanding and Mitochondria Transplantation Strategies. *Front Cell Dev Biol* 9: 653322

Greenbaum A, Hsu YM, Day RB, Schuettpelz LG, Christopher MJ, Borgerding JN, Nagasawa T, Link DC (2013) CXCL12 in early mesenchymal progenitors is required for haematopoietic stem-cell maintenance. *Nature* 495: 227-230

Gursel O, Tapan S, Sertoglu E, Tascilar E, Eker I, Ileri T, Uysal Z, Kurekci AE (2018) Elevated plasma asymmetric dimethylarginine levels in children with beta-thalassemia major may be an early marker for endothelial dysfunction. *Hematology* 23: 304-308

Halestrap AP, Price NT (1999) The proton-linked monocarboxylate transporter (MCT) family: structure, function and regulation. *Biochem J* 343 Pt 2: 281-299

Hampton MB, Kettle AJ, Winterbourn CC (1998) Inside the neutrophil phagosome: oxidants, myeloperoxidase, and bacterial killing. *Blood* 92: 3007-3017

Hashimoto M, Umemoto T, Nakamura-Ishizu A, Matsumura T, Yokomizo T, Sezaki M, Takizawa H, Suda T (2021) Autophagy is dispensable for the maintenance of hematopoietic stem cells in neonates. *Blood Adv* 5: 1594-1604

Hennrich ML, Romanov N, Horn P, Jaeger S, Eckstein V, Steeples V, Ye F, Ding X, Poisa-Beiro L, Lai MC *et al* (2018) Cell-specific proteome analyses of human bone marrow reveal molecular features of age-dependent functional decline. *Nat Commun* 9: 4004

Hentze MW, Muckenthaler MU, Galy B, Camaschella C (2010) Two to tango: regulation of Mammalian iron metabolism. *Cell* 142: 24-38

Hinge A, He J, Bartram J, Javier J, Xu J, Fjellman E, Sesaki H, Li T, Yu J, Wunderlich M *et al* (2020) Asymmetrically Segregated Mitochondria Provide Cellular Memory of Hematopoietic Stem Cell Replicative History and Drive HSC Attrition. *Cell Stem Cell* 26: 420-430 e426

Hirata Y, Furuhashi K, Ishii H, Li HW, Pinho S, Ding L, Robson SC, Frenette PS, Fujisaki J (2018) CD150(high) Bone Marrow Tregs Maintain Hematopoietic Stem Cell Quiescence and Immune Privilege via Adenosine. *Cell Stem Cell* 22: 445-453 e445

Hirayama T, Kadota S, Niwa M, Nagasawa H (2018) A mitochondria-targeted fluorescent probe for selective detection of mitochondrial labile Fe(ii). *Metallomics* 10: 794-801

Ho TT, Warr MR, Adelman ER, Lansinger OM, Flach J, Verovskaya EV, Figueroa ME, Passegue E (2017) Autophagy maintains the metabolism and function of young and old stem cells. *Nature* 543: 205-210

Holmstrom KM, Finkel T (2014) Cellular mechanisms and physiological consequences of redox-dependent signalling. *Nat Rev Mol Cell Biol* 15: 411-421

Hu M, Zeng H, Chen S, Xu Y, Wang S, Tang Y, Wang X, Du C, Shen M, Chen F *et al* (2018) SRC-3 is involved in maintaining hematopoietic stem cell quiescence by regulation of mitochondrial metabolism in mice. *Blood* 132: 911-923

Huang M, Wu Q, Jiang ZH (2022) Epigenetic Alterations under Oxidative Stress in Stem Cells. *Oxid Med Cell Longev* 2022: 6439097

Hur J, Choi JI, Lee H, Nham P, Kim TW, Chae CW, Yun JY, Kang JA, Kang J, Lee SE *et al* (2016) CD82/KAI1 Maintains the Dormancy of Long-Term Hematopoietic Stem Cells through Interaction with DARC-Expressing Macrophages. *Cell Stem Cell* 18: 508-521

Iezzoni JC (2018) Diagnostic histochemistry in hepatic pathology. *Semin Diagn Pathol* 35: 381-389

Itkin T, Gur-Cohen S, Spencer JA, Schajnovitz A, Ramasamy SK, Kusumbe AP, Ledergor G, Jung Y, Milo I, Poulos MG *et al* (2016) Distinct bone marrow blood vessels differentially regulate haematopoiesis. *Nature* 532: 323-328

Ito K, Carracedo A, Weiss D, Arai F, Ala U, Avigan DE, Schafer ZT, Evans RM, Suda T, Lee CH *et al* (2012) A PML-PPAR-delta pathway for fatty acid oxidation regulates hematopoietic stem cell maintenance. *Nat Med* 18: 1350-1358

Ito K, Hirao A, Arai F, Takubo K, Matsuoka S, Miyamoto K, Ohmura M, Naka K, Hosokawa K, Ikeda Y *et al* (2006) Reactive oxygen species act through p38 MAPK to limit the lifespan of hematopoietic stem cells. *Nat Med* 12: 446-451

Ito K, Turcotte R, Cui J, Zimmerman SE, Pinho S, Mizoguchi T, Arai F, Runnels JM, Alt C, Teruya-Feldstein J *et al* (2016) Self-renewal of a purified Tie2+ hematopoietic stem cell population relies on mitochondrial clearance. *Science* 354: 1156-1160

Jacobsen RN, Forristal CE, Raggatt LJ, Nowlan B, Barbier V, Kaur S, van Rooijen N, Winkler IG, Pettit AR, Levesque JP (2014) Mobilization with granulocyte colony-stimulating factor blocks medullar erythropoiesis by depleting F4/80(+)VCAM1(+)CD169(+)ER-HR3(+)Ly6G(+) erythroid island macrophages in the mouse. *Exp Hematol* 42: 547-561 e544

Jang YY, Sharkis SJ (2007) A low level of reactive oxygen species selects for primitive hematopoietic stem cells that may reside in the low-oxygenic niche. *Blood* 110: 3056-3063

Jiang X, Stockwell BR, Conrad M (2021) Ferroptosis: mechanisms, biology and role in disease. *Nat Rev Mol Cell Biol* 22: 266-282

Jin G, Xu C, Zhang X, Long J, Rezaeian AH, Liu C, Furth ME, Kridel S, Pasche B, Bian XW *et al* (2018) Atad3a suppresses Pink1-dependent mitophagy to maintain homeostasis of hematopoietic progenitor cells. *Nat Immunol* 19: 29-40

Juntilla MM, Patil VD, Calamito M, Joshi RP, Birnbaum MJ, Koretzky GA (2010) AKT1 and AKT2 maintain hematopoietic stem cell function by regulating reactive oxygen species. *Blood* 115: 4030-4038

Kajarabille N, Latunde-Dada GO (2019) Programmed Cell-Death by Ferroptosis: Antioxidants as Mitigators. *Int J Mol Sci* 20

Kakhlon O, Cabantchik ZI (2002) The labile iron pool: characterization, measurement, and participation in cellular processes(1). *Free Radic Biol Med* 33: 1037-1046

Kalish Y, Malyutin Z, Shai E, Dana M, Avraham L, Jahshan N, Rachmilewitz E, Fibach E, Varon D (2015) A mouse model to study thrombotic complications of thalassemia. *Thromb Res* 135: 521-525

Kao Y-R CJ, Kumari R., Tatiparthy M., Ma Y., Aivalioti MM., Zintiridou A., Thiruthuvanathan V., Reisz JA., Stranski S., Sidoli S., Steidl U., D'Alessandro A., Will B. (2021) Cytoplasmic labile iron accumulates in aging stem cells perturbing a key rheostat for identity control. *BioRxiv https://doiorg/101101/20210803454947 [PREPRINT]*

Kattamis A, Kwiatkowski JL, Aydinok Y (2022) Thalassaemia. *Lancet* 399: 2310-2324

Kauffman ME, Kauffman MK, Traore K, Zhu H, Trush MA, Jia Z, Li YR (2016) MitoSOX-Based Flow Cytometry for Detecting Mitochondrial ROS. *React Oxyg Species (Apex)* 2: 361-370

Kawano Y, Fukui C, Shinohara M, Wakahashi K, Ishii S, Suzuki T, Sato M, Asada N, Kawano H, Minagawa K *et al* (2017) G-CSF-induced sympathetic tone provokes fever and primes antimobilizing functions of neutrophils via PGE2. *Blood* 129: 587-597

Kiel MJ, Yilmaz OH, Iwashita T, Yilmaz OH, Terhorst C, Morrison SJ (2005) SLAM family receptors distinguish hematopoietic stem and progenitor cells and reveal endothelial niches for stem cells. *Cell* 121: 1109-1121

King KY, Goodell MA (2011) Inflammatory modulation of HSCs: viewing the HSC as a foundation for the immune response. *Nat Rev Immunol* 11: 685-692

Kobayashi H, Morikawa T, Okinaga A, Hamano F, Hashidate-Yoshida T, Watanuki S, Hishikawa D, Shindou H, Arai F, Kabe Y *et al* (2019) Environmental Optimization Enables Maintenance of Quiescent Hematopoietic Stem Cells Ex Vivo. *Cell Rep* 28: 145-158 e149

Kocabas F, Zheng J, Thet S, Copeland NG, Jenkins NA, DeBerardinis RJ, Zhang C, Sadek HA (2012) Meis1 regulates the metabolic phenotype and oxidant defense of hematopoietic stem cells. *Blood* 120: 4963-4972

Kohler A, Schmithorst V, Filippi MD, Ryan MA, Daria D, Gunzer M, Geiger H (2009) Altered cellular dynamics and endosteal location of aged early hematopoietic progenitor cells revealed by time-lapse intravital imaging in long bones. *Blood* 114: 290-298

Kohli L, Passegue E (2014) Surviving change: the metabolic journey of hematopoietic stem cells. *Trends Cell Biol* 24: 479-487

Kontoghiorghes GJ, Kontoghiorghe CN (2020) Iron and Chelation in Biochemistry and Medicine: New Approaches to Controlling Iron Metabolism and Treating Related Diseases. *Cells* 9(6):1456

Korolnek T, Hamza I (2015) Macrophages and iron trafficking at the birth and death of red cells. *Blood* 125: 2893-2897

Kumar S, Filippi MD (2016) An Alternative Approach for Sample Preparation with Low Cell Number for TEM Analysis. *J Vis Exp*

Kumar S, Geiger H (2017) HSC Niche Biology and HSC Expansion Ex Vivo. *Trends Mol Med* 23: 799-819

Kusumbe AP, Ramasamy SK, Itkin T, Mae MA, Langen UH, Betsholtz C, Lapidot T, Adams RH (2016) Age-dependent modulation of vascular niches for haematopoietic stem cells. *Nature* 532(7599):380-4

Laurenti E, Gottgens B (2018) From haematopoietic stem cells to complex differentiation landscapes. *Nature* 553: 418-426

Lemieux JM, Horowitz MC, Kacena MA (2010) Involvement of integrins alpha(3)beta(1) and alpha(5)beta(1) and glycoprotein IIb in megakaryocyte-induced osteoblast proliferation. *J Cell Biochem* 109: 927-932

Li H, Choesang T, Bao W, Chen H, Feola M, Garcia-Santos D, Li J, Sun S, Follenzi A, Pham P *et al* (2017) Decreasing TfR1 expression reverses anemia and hepcidin suppression in b-thalassemic mice. *Blood* 129(11):1514-1526

Liang R, Arif T, Kalmykova S, Kasianov A, Lin M, Menon V, Qiu J, Bernitz JM, Moore K, Lin F *et al* (2020) Restraining Lysosomal Activity Preserves Hematopoietic Stem Cell Quiescence and Potency. *Cell Stem Cell* 26: 359-376 e357

Lidonnici M.R. CG, Tiboni F., Barcella M., Merelli I., Scaramuzza S., Rossi C., Crippa S., Storto M., Bernardo M.E., Ciceri F., Aiuti A., Marktel S., Ferrari G. (2021) S269 TGF-BETA SIGNALING CONTROLS THE LINEAGE CELL FATE OF HEMATOPOIETIC STEM CELLS TOWARDS ERYTHROID BRANCHING IN BETA-THALASSEMIA. *HemaSphere* 5: e566

Lidonnici MR, Ferrari G (2018) Gene therapy and gene editing strategies for hemoglobinopathies. *Blood Cells Mol Dis* 70: 87-101

Locatelli F. FH, Corbacioglu S., de la Fuente J., Wall D., Capellini M.D., de Montalembert M., Kattamis A., Lobitz S., Rondelli D., Sheth S., Steinberg M., Walters M.C., Bobruff Y., Simard C., Song Y., Zhang L., Sharma A., Imren S., Hobbs B., Grupp S. (2022) EFFICACY AND SAFETY OF A SINGLE DOSE OF CTX001 FOR TRANSFUSION-DEPENDENT BETA-THALASSEMIA AND SEVERE SICKLE CELL DISEASE. *HemaSphere*

Lu W, Zhao M, Rajbhandary S, Xie F, Chai X, Mu J, Meng J, Liu Y, Jiang Y, Xu X *et al* (2013) Free iron catalyzes oxidative damage to hematopoietic cells/mesenchymal stem cells in vitro and suppresses hematopoiesis in iron overload patients. *Eur J Haematol* 91: 249-261

Lucarelli G, Clift RA, Galimberti M, Polchi P, Angelucci E, Baronciani D, Giardini C, Andreani M, Manna M, Nesci S *et al* (1996) Marrow transplantation for patients with thalassemia: results in class 3 patients. *Blood* 87: 2082-2088

Lucarelli G, Isgro A, Sodani P, Gaziev J (2012) Hematopoietic stem cell transplantation in thalassemia and sickle cell anemia. *Cold Spring Harb Perspect Med* 2: a011825

Luchsinger LL, de Almeida MJ, Corrigan DJ, Mumau M, Snoeck HW (2016) Mitofusin 2 maintains haematopoietic stem cells with extensive lymphoid potential. *Nature* 529: 528-531

Ludin A, Itkin T, Gur-Cohen S, Mildner A, Shezen E, Golan K, Kollet O, Kalinkovich A, Porat Z, D'Uva G *et al* (2012) Monocytes-macrophages that express alpha-smooth muscle actin preserve primitive hematopoietic cells in the bone marrow. *Nat Immunol* 13: 1072-1082

Luo Y, Shao L, Chang J, Feng W, Liu YL, Cottler-Fox MH, Emanuel PD, Hauer-Jensen M, Bernstein ID, Liu L *et al* (2018) M1 and M2 macrophages differentially regulate hematopoietic stem cell self-renewal and ex vivo expansion. *Blood Adv* 2: 859-870

Ma Y, Abbate V, Hider RC (2015) Iron-sensitive fluorescent probes: monitoring intracellular iron pools. *Metallomics* 7: 212-222

Mahachoklertwattana P, Sirikulchayanonta V, Chuansumrit A, Karnsombat P, Choubtum L, Sriphrapradang A, Domrongkitchaiporn S, Sirisriro R, Rajatanavin R (2003) Bone histomorphometry in children and adolescents with beta-thalassemia disease: iron-associated focal osteomalacia. *J Clin Endocrinol Metab* 88: 3966-3972

Mansell E, Sigurdsson V, Deltcheva E, Brown J, James C, Miharada K, Soneji S, Larsson J, Enver T (2021) Mitochondrial Potentiation Ameliorates Age-Related Heterogeneity in Hematopoietic Stem Cell Function. *Cell Stem Cell* 28: 241-256 e246

Mantel CR, O'Leary HA, Chitteti BR, Huang X, Cooper S, Hangoc G, Brustovetsky N, Srour EF, Lee MR, Messina-Graham S *et al* (2015) Enhancing Hematopoietic Stem Cell Transplantation Efficacy by Mitigating Oxygen Shock. *Cell* 161: 1553-1565

Marktel S, Scaramuzza S, Cicalese MP, Giglio F, Galimberti S, Lidonnici MR, Calbi V, Assanelli A, Bernardo ME, Rossi C *et al* (2019) Intrabone hematopoietic stem cell gene therapy for adult and pediatric patients affected by transfusion-dependent ss-thalassemia. *Nat Med* 25: 234-241

Maryanovich M, Zaltsman Y, Ruggiero A, Goldman A, Shachnai L, Zaidman SL, Porat Z, Golan K, Lapidot T, Gross A (2015) An MTCH2 pathway repressing mitochondria metabolism regulates haematopoietic stem cell fate. *Nat Commun* 6: 7901

Matte A, Federti E, Kung C, Kosinski PA, Narayanaswamy R, Russo R, Federico G, Carlomagno F, Desbats MA, Salviati M *et al* (2021) The pyruvate kinase activator mitapivat reduces hemolysis and improves anemia in a β-thalassemia mouse model. *Journal of Clinical Investigation* 131:e144206

McColl B, Vadolas J (2016) Animal models of beta-hemoglobinopathies: utility and limitations. *J Blood Med* 7: 263-274

Mendelson A, Frenette PS (2014) Hematopoietic stem cell niche maintenance during homeostasis and regeneration. *Nat Med* 20: 833-846

Mendez-Ferrer S, Lucas D, Battista M, Frenette PS (2008) Haematopoietic stem cell release is regulated by circadian oscillations. *Nature* 452: 442-447

Mendez-Ferrer S, Michurina TV, Ferraro F, Mazloom AR, Macarthur BD, Lira SA, Scadden DT, Ma'ayan A, Enikolopov GN, Frenette PS (2010) Mesenchymal and haematopoietic stem cells form a unique bone marrow niche. *Nature* 466: 829-834

Mendonca R, Silveira AA, Conran N (2016) Red cell DAMPs and inflammation. *Inflamm Res* 65: 665-678

Miccio A, Cesari R, Lotti F, Rossi C, Sanvito F, Ponzoni M, Routledge SJ, Chow CM, Antoniou MN, Ferrari G (2008) In vivo selection of genetically modified erythroblastic progenitors leads to long-term correction of beta-thalassemia. *Proc Natl Acad Sci U S A* 105: 10547-10552

Mishra P, Chan DC (2014) Mitochondrial dynamics and inheritance during cell division, development and disease. *Nat Rev Mol Cell Biol* 15: 634-646

Mistry JJ, Marlein CR, Moore JA, Hellmich C, Wojtowicz EE, Smith JGW, Macaulay I, Sun Y, Morfakis A, Patterson A *et al* (2019) ROS-mediated PI3K activation drives mitochondrial transfer from stromal cells to hematopoietic stem cells in response to infection. *Proc Natl Acad Sci U S A* 116: 24610-24619

Mittal M, Siddiqui MR, Tran K, Reddy SP, Malik AB (2014) Reactive oxygen species in inflammation and tissue injury. *Antioxid Redox Signal* 20: 1126-1167

Miyamoto K, Araki KY, Naka K, Arai F, Takubo K, Yamazaki S, Matsuoka S, Miyamoto T, Ito K, Ohmura M *et al* (2007) Foxo3a is essential for maintenance of the hematopoietic stem cell pool. *Cell Stem Cell* 1: 101-112

Morganti C, Bonora M, Ito K, Ito K (2019) Electron transport chain complex II sustains high mitochondrial membrane potential in hematopoietic stem and progenitor cells. *Stem Cell Res* 40: 101573

Morganti C, Cabezas-Wallscheid N, Ito K (2022) Metabolic Regulation of Hematopoietic Stem Cells. *Hemasphere* 6: e740

Morganti C, Ito K (2021) Mitochondrial Contributions to Hematopoietic Stem Cell Aging. *Int J Mol Sci* 22

Morikawa S, Mabuchi Y, Kubota Y, Nagai Y, Niibe K, Hiratsu E, Suzuki S, Miyauchi-Hara C, Nagoshi N, Sunabori T *et al* (2009) Prospective identification, isolation, and systemic transplantation of multipotent mesenchymal stem cells in murine bone marrow. *J Exp Med* 206: 2483-2496

Moroishi T, Nishiyama M, Takeda Y, Iwai K, Nakayama KI (2011) The FBXL5-IRP2 axis is integral to control of iron metabolism in vivo. *Cell Metab* 14: 339-351

Morrison SJ, Scadden DT (2014) The bone marrow niche for haematopoietic stem cells. *Nature* 505: 327-334

Muckenthaler MU, Rivella S, Hentze MW, Galy B (2017) A Red Carpet for Iron Metabolism. *Cell* 168: 344-361

Muhlenhoff U, Hoffmann B, Richter N, Rietzschel N, Spantgar F, Stehling O, Uzarska MA, Lill R (2015) Compartmentalization of iron between mitochondria and the cytosol and its regulation. *Eur J Cell Biol* 94: 292-308

Murphy MP (2009) How mitochondria produce reactive oxygen species. *Biochem J* 417: 1-13

Murphy MP (2012) Mitochondrial thiols in antioxidant protection and redox signaling: distinct roles for glutathionylation and other thiol modifications. *Antioxid Redox Signal* 16: 476-495

Murphy MP, Smith RA (2007) Targeting antioxidants to mitochondria by conjugation to lipophilic cations. *Annu Rev Pharmacol Toxicol* 47: 629-656

Muto Y, Nishiyama M, Nita A, Moroishi T, Nakayama KI (2017) Essential role of FBXL5-mediated cellular iron homeostasis in maintenance of hematopoietic stem cells. *Nat Commun* 8: 16114

Nai A, Pagani A, Mandelli G, Lidonnici MR, Silvestri L, Ferrari G, Camaschella C (2012) Deletion of TMPRSS6 attenuates the phenotype in a mouse model of beta-thalassemia. *Blood* 119: 5021-5029

Nakamura-Ishizu A, Ito K, Suda T (2020) Hematopoietic Stem Cell Metabolism during Development and Aging. *Dev Cell* 54: 239-255

Nakamura-Ishizu A, Matsumura T, Stumpf PS, Umemoto T, Takizawa H, Takihara Y, O'Neil A, Majeed A, MacArthur BD, Suda T (2018) Thrombopoietin Metabolically Primes Hematopoietic Stem Cells to Megakaryocyte-Lineage Differentiation. *Cell Rep* 25: 1772-1785 e1776

Naveiras O, Nardi V, Wenzel PL, Hauschka PV, Fahey F, Daley GQ (2009) Bone-marrow adipocytes as negative regulators of the haematopoietic microenvironment. *Nature* 460: 259-263

Notta F, Doulatov S, Laurenti E, Poeppl A, Jurisica I, Dick JE (2011) Isolation of single human hematopoietic stem cells capable of long-term multilineage engraftment. *Science* 333: 218-221

Nyffenegger N, Flace A, Doucerain C, Durrenberger F, Manolova V (2021) The Oral Ferroportin Inhibitor VIT-2763 Improves Erythropoiesis without Interfering with Iron Chelation Therapy in a Mouse Model of beta-Thalassemia. *Int J Mol Sci* 22

Oguro H, Ding L, Morrison SJ (2013) SLAM family markers resolve functionally distinct subpopulations of hematopoietic stem cells and multipotent progenitors. *Cell Stem Cell* 13: 102-116

Okabe H, Suzuki T, Uehara E, Ueda M, Nagai T, Ozawa K (2014) The bone marrow hematopoietic microenvironment is impaired in iron-overloaded mice. *Eur J Haematol* 93: 118-128

Oliveira GL, Coelho AR, Marques R, Oliveira PJ (2021) Cancer cell metabolism: Rewiring the mitochondrial hub. *Biochim Biophys Acta Mol Basis Dis* 1867: 166016

Origa R, Galanello R, Ganz T, Giagu N, Maccioni L, Faa G, Nemeth E (2007) Liver iron concentrations and urinary hepcidin in beta-thalassemia. *Haematologica* 92: 583-588

Pani G, Koch OR, Galeotti T (2009) The p53-p66shc-Manganese Superoxide Dismutase (MnSOD) network: a mitochondrial intrigue to generate reactive oxygen species. *Int J Biochem Cell Biol* 41: 1002-1005

Park MH, Jin HK, Min WK, Lee WW, Lee JE, Akiyama H, Herzog H, Enikolopov GN, Schuchman EH, Bae JS (2015) Neuropeptide Y regulates the hematopoietic stem cell microenvironment and prevents nerve injury in the bone marrow. *EMBO J* 34: 1648-1660

Parmar K, Mauch P, Vergilio JA, Sackstein R, Down JD (2007) Distribution of hematopoietic stem cells in the bone marrow according to regional hypoxia. *Proc Natl Acad Sci U S A* 104: 5431-5436

Paul BT, Manz DH, Torti FM, Torti SV (2017) Mitochondria and Iron: current questions. *Expert Rev Hematol* 10: 65-79

Perry SW, Norman JP, Barbieri J, Brown EB, Gelbard HA (2011) Mitochondrial membrane potential probes and the proton gradient: a practical usage guide. *Biotechniques* 50: 98-115

Pietras EM (2017) Inflammation: a key regulator of hematopoietic stem cell fate in health and disease. *Blood* 130: 1693-1698

Pietras EM, Mirantes-Barbeito C, Fong S, Loeffler D, Kovtonyuk LV, Zhang S, Lakshminarasimhan R, Chin CP, Techner JM, Will B *et al* (2016) Chronic interleukin-1 exposure drives haematopoietic stem cells towards precocious myeloid differentiation at the expense of self-renewal. *Nat Cell Biol* 18: 607-618

Pietras EM, Reynaud D, Kang YA, Carlin D, Calero-Nieto FJ, Leavitt AD, Stuart JM, Gottgens B, Passegue E (2015) Functionally Distinct Subsets of Lineage-Biased Multipotent Progenitors Control Blood Production in Normal and Regenerative Conditions. *Cell Stem Cell* 17: 35-46

Pilo F, Angelucci E (2019) Iron Toxicity and Hemopoietic Cell Transplantation: Time to Change the Paradigm. *Mediterr J Hematol Infect Dis* 11: e2019030

Pinho S, Frenette PS (2019) Haematopoietic stem cell activity and interactions with the niche. *Nat Rev Mol Cell Biol* 20: 303-320

Poli A, Schmitt C, Moulouel B, Mirmiran A, Puy H, Lefebvre T, Gouya L (2021) Iron, Heme Synthesis and Erythropoietic Porphyrias: A Complex Interplay. *Metabolites* 11

Presley AD, Fuller KM, Arriaga EA (2003) MitoTracker Green labeling of mitochondrial proteins and their subsequent analysis by capillary electrophoresis with laser-induced fluorescence detection. *J Chromatogr B Analyt Technol Biomed Life Sci* 793: 141-150

Qiu J, Gjini J, Arif T, Moore K, Lin M, Ghaffari S (2021) Using mitochondrial activity to select for potent human hematopoietic stem cells. *Blood Adv* 5: 1605-1616

Ramasamy SK, Kusumbe AP, Wang L, Adams HR (2014) Endothelial Notch activity promotes angiogenesis and osteogenesis in bone. *Nature* 507(7492):376-380

Rimmele P, Bigarella CL, Liang R, Izac B, Dieguez-Gonzalez R, Barbet G, Donovan M, Brugnara C, Blander JM, Sinclair DA *et al* (2014) Aging-like phenotype and defective lineage specification in SIRT1-deleted hematopoietic stem and progenitor cells. *Stem Cell Reports* 3: 44-59

Rimmele P, Liang R, Bigarella CL, Kocabas F, Xie J, Serasinghe MN, Chipuk J, Sadek H, Zhang CC, Ghaffari S (2015) Mitochondrial metabolism in hematopoietic stem cells requires functional FOXO3. *EMBO Rep* 16: 1164-1176

Rossman MJ, Santos-Parker JR, Steward CAC, Bispham NZ, Cuevas LM, Rosenberg HL, Woodward KA, Chonchol M, Gioscia-Ryan RA, Murphy MP *et al* (2018) Chronic Supplementation With a Mitochondrial Antioxidant (MitoQ) Improves Vascular Function in Healthy Older Adults. *Hypertension* 71: 1056-1063

Sacchetti B, Funari A, Michienzi S, Di Cesare S, Piersanti S, Saggio I, Tagliafico E, Ferrari S, Robey PG, Riminucci M *et al* (2007) Self-renewing osteoprogenitors in bone marrow sinusoids can organize a hematopoietic microenvironment. *Cell* 131: 324-336

Sangkhae V, Nemeth E (2017) Regulation of the Iron Homeostatic Hormone Hepcidin. *Adv Nutr* 8: 126-136

Sanjuan-Pla A, Macaulay IC, Jensen CT, Woll PS, Luis TC, Mead A, Moore S, Carella C, Matsuoka S, Bouriez Jones T *et al* (2013) Platelet-biased stem cells reside at the apex of the haematopoietic stem-cell hierarchy. *Nature* 502: 232-236

Scala S, Aiuti A (2019) In vivo dynamics of human hematopoietic stem cells: novel concepts and future directions. *Blood Adv* 3: 1916-1924

Scapin G, Goulard MC, Dharampuriya PR, Cillis JL, Shah DI (2019) Analysis of Hematopoietic Stem Progenitor Cell Metabolism. *J Vis Exp* (153):10.3791/60234

Schindelin J, Arganda-Carreras I, Frise E, Kaynig V, Longair M, Pietzsch T, Preibisch S, Rueden C, Saalfeld S, Schmid B *et al* (2012) Fiji: an open-source platform for biological-image analysis. *Nat Methods* 9: 676-682

Schonberger K, Obier N, Romero-Mulero MC, Cauchy P, Mess J, Pavlovich PV, Zhang YW, Mitterer M, Rettkowski J, Lalioti ME *et al* (2022) Multilayer omics analysis reveals a non-classical retinoic acid signaling axis that regulates hematopoietic stem cell identity. *Cell Stem Cell* 29: 131-148 e110

Sena JA, Galotto G, Devitt NP, Connick MC, Jacobi JL, Umale PE, Vidali L, Bell CJ (2018) Unique Molecular Identifiers reveal a novel sequencing artefact with implications for RNA-Seq based gene expression analysis. *Sci Rep* 8: 13121

Seyfried AN, Maloney JM, MacNamara KC (2020a) Macrophages Orchestrate Hematopoietic Programs and Regulate HSC Function During Inflammatory Stress. *Front Immunol* 11: 1499

Seyfried TN, Arismendi-Morillo G, Mukherjee P, Chinopoulos C (2020b) On the Origin of ATP Synthesis in Cancer. *iScience* 23: 101761

Shehee WR, Oliver P, Smithies O (1993) Lethal thalassemia after insertional disruption of the mouse major adult beta-globin gene. *Proc Natl Acad Sci U S A* 90: 3177-3181

Simsek T, Kocabas F, Zheng J, Deberardinis RJ, Mahmoud AI, Olson EN, Schneider JW, Zhang CC, Sadek HA (2010) The distinct metabolic profile of hematopoietic stem cells reflects their location in a hypoxic niche. *Cell Stem Cell* 7: 380-390

Skow LC, Burkhart BA, Johnson FM, Popp RA, Popp DM, Goldberg SZ, Anderson WF, Barnett LB, Lewis SE (1983) A mouse model for beta-thalassemia. *Cell* 34: 1043-1052

Snow BJ, Rolfe FL, Lockhart MM, Frampton CM, O'Sullivan JD, Fung V, Smith RA, Murphy MP, Taylor KM, Protect Study G (2010) A double-blind, placebo-controlled study to assess the mitochondria-targeted antioxidant MitoQ as a disease-modifying therapy in Parkinson's disease. *Mov Disord* 25: 1670-1674

Sookoian S, Pirola CJ (2015) Liver enzymes, metabolomics and genome-wide association studies: from systems biology to the personalized medicine. *World J Gastroenterol* 21: 711-725

Spinelli JB, Haigis MC (2018) The multifaceted contributions of mitochondria to cellular metabolism. *Nat Cell Biol* 20: 745-754

Stanga S, Caretto A, Boido M, Vercelli A (2020) Mitochondrial Dysfunctions: A Red Thread across Neurodegenerative Diseases. *Int J Mol Sci* 21

Sugiyama T, Kohara H, Noda M, Nagasawa T (2006) Maintenance of the hematopoietic stem cell pool by CXCL12-CXCR4 chemokine signaling in bone marrow stromal cell niches. *Immunity* 25: 977-988

Sun X, Cao B, Naval-Sanchez M, Pham T, Sun YBY, Williams B, Heazlewood SY, Deshpande N, Li J, Kraus F *et al* (2021) Nicotinamide riboside attenuates age-associated metabolic and functional changes in hematopoietic stem cells. *Nat Commun* 12: 2665

Taher AK-S, A.; Tantiworawit, A; Wong, P.; Szecsödy, P. (2022) S272: SAFETY AND PRELIMINARY PHARMACODYNAMIC EFFECTS OF THE FERROPORTIN INHIBITOR VAMIFEPORT (VIT-2763) IN PATIENTS WITH NON-TRANSFUSION-DEPENDENT BETA THALASSEMIA (NTDT): RESULTS FROM A PHASE 2A STUDY. *Hemasphere* 6

Taher AT, Musallam KM, Cappellini MD (2021) beta-Thalassemias. *N Engl J Med* 384: 727-743

Taher AT, Musallam KM, Wood JC, Cappellini MD (2010) Magnetic resonance evaluation of hepatic and myocardial iron deposition in transfusion-independent thalassemia intermedia compared to regularly transfused thalassemia major patients. *Am J Hematol* 85: 288-290

Taher AT, Otrock ZK, Uthman I, Cappellini MD (2008) Thalassemia and hypercoagulability. *Blood Rev* 22: 283-292

Taher AT, Saliba AN (2017) Iron overload in thalassemia: different organs at different rates. *Hematology Am Soc Hematol Educ Program* 2017: 265-271

Taher AT, Weatherall DJ, Cappellini MD (2018) Thalassaemia. *Lancet* 391: 155-167

Taichman RS, Emerson SG (1994) Human osteoblasts support hematopoiesis through the production of granulocyte colony-stimulating factor. *J Exp Med* 179: 1677-1682

Takihara Y, Nakamura-Ishizu A, Tan DQ, Fukuda M, Matsumura T, Endoh M, Arima Y, Chin DWL, Umemoto T, Hashimoto M *et al* (2019) High mitochondrial mass is associated with reconstitution capacity and quiescence of hematopoietic stem cells. *Blood Adv* 3: 2323-2327

Takubo K, Goda N, Yamada W, Iriuchishima H, Ikeda E, Kubota Y, Shima H, Johnson RS, Hirao A, Suematsu M *et al* (2010) Regulation of the HIF-1alpha level is essential for hematopoietic stem cells. *Cell Stem Cell* 7: 391-402

Takubo K, Nagamatsu G, Kobayashi CI, Nakamura-Ishizu A, Kobayashi H, Ikeda E, Goda N, Rahimi Y, Johnson RS, Soga T *et al* (2013) Regulation of glycolysis by Pdk functions as a metabolic checkpoint for cell cycle quiescence in hematopoietic stem cells. *Cell Stem Cell* 12: 49-61

Tan DQ, Suda T (2018) Reactive Oxygen Species and Mitochondrial Homeostasis as Regulators of Stem Cell Fate and Function. *Antioxid Redox Signal* 29: 149-168

Tang A, Strat AN, Rahman M, Zhang H, Bao W, Liu Y, Shi D, An X, Manwani D, Shi P, Yazdanbakhsh K, Mendelson A (2021) Murine bone marrow mesenchymal stromal cells have reduced hematopoietic maintenance ability in sickle cell disease. *Blood* 138(24):2570-2582.

Tanaka H, Espinoza JL, Fujiwara R, Rai S, Morita Y, Ashida T, Kanakura Y, Matsumura I (2019) Excessive Reactive Iron Impairs Hematopoiesis by Affecting Both Immature Hematopoietic Cells and Stromal Cells. *Cells* 8

Taniguchi Ishikawa E, Gonzalez-Nieto D, Ghiaur G, Dunn SK, Ficker AM, Murali B, Madhu M, Gutstein DE, Fishman GI, Barrio LC *et al* (2012) Connexin-43 prevents hematopoietic stem cell senescence through transfer of reactive oxygen species to bone marrow stromal cells. *Proc Natl Acad Sci U S A* 109: 9071-9076

Terpos E, Voskaridou E (2010) Treatment options for thalassemia patients with osteoporosis. *Ann N Y Acad Sci* 1202: 237-243

Thompson AA, Walters MC, Kwiatkowski J, Rasko JEJ, Ribeil JA, Hongeng S, Magrin E, Schiller GJ, Payen E, Semeraro M *et al* (2018) Gene Therapy in Patients with Transfusion-Dependent beta-Thalassemia. *N Engl J Med* 378: 1479-1493

Till JE, Mc CE (1961) A direct measurement of the radiation sensitivity of normal mouse bone marrow cells. *Radiat Res* 14: 213-222

Vander Heiden MG, Cantley LC, Thompson CB (2009) Understanding the Warburg effect: the metabolic requirements of cell proliferation. *Science* 324: 1029-1033

Vannini N, Girotra M, Naveiras O, Nikitin G, Campos V, Giger S, Roch A, Auwerx J, Lutolf MP (2016) Specification of haematopoietic stem cell fate via modulation of mitochondrial activity. *Nat Commun* 7: 13125

Vinchi F, Costa da Silva M, Ingoglia G, Petrillo S, Brinkman N, Zuercher A, Cerwenka A, Tolosano E, Muckenthaler MU (2016) Hemopexin therapy reverts heme-induced proinflammatory phenotypic switching of macrophages in a mouse model of sickle cell disease. *Blood* 127: 473-486

Vinchi F, Sparla R, Passos ST, Sharma R, Vance SZ, Zreid HS, Juaidi H, Manwani D, Yazdanbakhsh K, Nandi V *et al* (2021) Vasculo-toxic and pro-inflammatory action of unbound haemoglobin, haem and iron in transfusion-dependent patients with haemolytic anaemias. *Br J Haematol* 193: 637-658

Vogiatzi MG, Tsay J, Verdelis K, Rivella S, Grady RW, Doty S, Giardina PJ, Boskey AL (2010) Changes in bone microarchitecture and biomechanical properties in the th3 thalassemia mouse are associated with decreased bone turnover and occur during the period of bone accrual. *Calcif Tissue Int* 86: 484-494

Voskaridou E, Terpos E (2004) New insights into the pathophysiology and management of osteoporosis in patients with beta thalassaemia. *Br J Haematol* 127: 127-139

Voskou S, Aslan M, Fanis P, Phylactides M, Kleanthous M (2015) Oxidative stress in beta-thalassaemia and sickle cell disease. *Redox Biol* 6: 226-239

Walter D, Lier A, Geiselhart A, Thalheimer FB, Huntscha S, Sobotta MC, Moehrle B, Brocks D, Bayindir I, Kaschutnig P *et al* (2015) Exit from dormancy provokes DNA-damage-induced attrition in haematopoietic stem cells. *Nature* 520: 549-552

Wang CY, Babitt JL (2019) Liver iron sensing and body iron homeostasis. *Blood* 133: 18-29

Wang S, He X, Wu Q, Jiang L, Chen L, Yu Y, Zhang P, Huang X, Wang J, Ju Z *et al* (2020) Transferrin receptor 1-mediated iron uptake plays an essential role in hematopoiesis. *Haematologica* 105: 2071-2082

Waypa GB, Schumacker PT (2002) O(2) sensing in hypoxic pulmonary vasoconstriction: the mitochondrial door re-opens. *Respir Physiol Neurobiol* 132: 81-91

Wein F, Pietsch L, Saffrich R, Wuchter P, Walenda T, Bork S, Horn P, Diehlmann A, Eckstein V, Ho AD *et al* (2010) N-cadherin is expressed on human hematopoietic progenitor cells and mediates interaction with human mesenchymal stromal cells. *Stem Cell Res* 4: 129-139

Whitelaw E, Tsai SF, Hogben P, Orkin SH (1990) Regulated expression of globin chains and the erythroid transcription factor GATA-1 during erythropoiesis in the developing mouse. *Mol Cell Biol* 10: 6596-6606

Winkler IG, Barbier V, Nowlan B, Jacobsen RN, Forristal CE, Patton JT, Magnani JL, Levesque JP (2012) Vascular niche E-selectin regulates hematopoietic stem cell dormancy, self renewal and chemoresistance. *Nat Med* 18: 1651-1657

Yalcin S, Zhang X, Luciano JP, Mungamuri SK, Marinkovic D, Vercherat C, Sarkar A, Grisotto M, Taneja R, Ghaffari S (2008) Foxo3 is essential for the regulation of ataxia telangiectasia mutated and oxidative stress-mediated homeostasis of hematopoietic stem cells. *J Biol Chem* 283: 25692-25705

Yamazaki S, Ema H, Karlsson G, Yamaguchi T, Miyoshi H, Shioda S, Taketo MM, Karlsson S, Iwama A, Nakauchi H (2011) Nonmyelinating Schwann cells maintain hematopoietic stem cell hibernation in the bone marrow niche. *Cell* 147: 1146-1158

Yang B, Kirby S, Lewis J, Detloff PJ, Maeda N, Smithies O (1995) A mouse model for beta 0-thalassemia. *Proc Natl Acad Sci U S A* 92: 11608-11612

Youle RJ, van der Bliek AM (2012) Mitochondrial fission, fusion, and stress. *Science* 337: 1062-1065

Yu WM, Liu X, Shen J, Jovanovic O, Pohl EE, Gerson SL, Finkel T, Broxmeyer HE, Qu CK (2013) Metabolic regulation by the mitochondrial phosphatase PTPMT1 is required for hematopoietic stem cell differentiation. *Cell Stem Cell* 12: 62-74

Zhang D, Gao X, Li H, Borger DK, Wei Q, Yang E, Xu C, Pinho S, Frenette PS (2022) The microbiota regulates hematopoietic stem cell fate decisions by controlling iron availability in bone marrow. *Cell Stem Cell* 29: 232-247 e237

Zhang J, Wu Q, Johnson CB, Pham G, Kinder JM, Olsson A, Slaughter A, May M, Weinhaus B, D'Alessandro A *et al* (2021) In situ mapping identifies distinct vascular niches for myelopoiesis. *Nature* 590: 457-462

Zhao J, Jia Y, Mahmut D, Deik AA, Jeanfavre S, Clish CB, Sankaran VG (2022) Human hematopoietic stem cell vulnerability to ferroptosis BioRxiv https://doi.org/10.1101/2022.06.03.494357

Zhao M, Perry JM, Marshall H, Venkatraman A, Qian P, He XC, Ahamed J, Li L (2014) Megakaryocytes maintain homeostatic quiescence and promote post-injury regeneration of hematopoietic stem cells. *Nat Med* 20: 1321-1326

Zhou BO, Ding L, Morrison SJ (2015) Hematopoietic stem and progenitor cells regulate the regeneration of their niche by secreting Angiopoietin-1. *Elife* 4: e05521

Zhou X, Huang L, Wu J, Qu Y, Jiang H, Zhang J, Qiu S, Liao C, Xu X, Xia J *et al* (2022) Impaired bone marrow microenvironment and stem cells in transfusion-dependent beta-thalassemia. *Biomed Pharmacother* 146: 112548

Zou C, Wang Y, Shen Z (2005) 2-NBDG as a fluorescent indicator for direct glucose uptake measurement. *J Biochem Biophys Methods* 64: 207-215

Silvia Sighinolfi